Development of Optical Sensors ("Optodes") for Carbon Dioxide and their Application to Modified Atmosphere Packaging (MAP)

Dissertation

zur Erlangung des Doktorgrades der Naturwissenschaften (Dr. rer. nat.)
an der Naturwissenschaftlichen Fakultät IV – Chemie und Pharmazie
der Universität Regensburg

vorgelegt von
Christoph Alexander Johannes von Bültzingslöwen
aus Regensburg
2003

Diese Arbeit wurde angeleitet von Prof. Dr. Otto Wolfbeis

Promotionsgesuch eingereicht am:
Tag des Kolloquiums:

Prüfungsausschuss:	Prof. Dr. O. Reiser (Vorsitzender)
	Prof. Dr. O. Wolfbeis
	Prof. Dr. B. McCraith
	N. N.

Contents

Abbreviations and Symbols

CTA-OH	Cetyl-trimethylammonium hydroxide
D^-	Deprotonated pH-indicator dye
DH	Protonated pH-indicator dye
DLR	Dual Luminophore Referencing
dm	Demodulation
E_A	Activation energy
EtCell	Ethyl cellulose
ETEOS	Ethyltriethoxysilane
f	Modulation frequency
FRET	Fluorescence resonance energy transfer
HPTS	1-Hydroxypyrene-3,6,8-trisulfonate
I	Luminescence intensity
J	Spectral overlap integral
J_0	Spectral overlap integral when dye is completely protonated
K	Equilibrium constant
K_{SV}	Stern-Volmer constant
LED	Light emitting diode
LOD	Limit of detection
MAP	Modified atmosphere packaging
MTEOS	Methyltriethoxysilane
Ormosil	Organically modified silica glass
PAN	Poly(acrylonitrile)
pCO_2	Partial pressure of carbon dioxide
PET	Photo-induced electron transfer
pO_2	Partial pressure of oxygen
poly(HEMA)	Hydrophilic polymer poly(hydroxyethyl methacrylate)
Q^+OH^-	Quaternary ammonium hydroxide
r	Correlation coefficient
R	Universal gas constant
R_d	Ratio of protonated to deprotonated pH-indicator dye
$Ru(dpp)_3^{2+}$	Ru^{II}-tris(4,7-diphenyl-1,10-phenantroline)]$^{2+}$
TBA-OH	Tetrabutylammonium hydroxide

TDA-OH	Tetra-decylammonium hydroxide
TDTA-OH	Tetradecyl-trimethylammonium hydroxide
TEOS	Tetraethoxysilane
TMOS	Tetramethoxysilane
TOA-OH	Tetraoctylammonium hydroxide
TSPS	3-(Trimethylsilyl)-1-propane-sulfonate
ϕ	Phase angle
λ	Wavelength
σ	Standard deviation
τ	Fluorescence lifetime
τ_0	Fluorescence lifetime measured in absence of carbon dioxide
τ_{max}	Fluorescence lifetime in absence of any quenching molecules

1. Introduction

1.1. Modified Atmosphere Packaging

In the last fifteen years, there has been a rapid increase in the use of modified atmosphere packaging (MAP) as a method for extending the shelf life of many food products. MAP is a way of preserving quality by controlling the gas atmosphere in food packages in order to increase safety, expand the shelf life and sometimes enhance the visual appearance of the food products.

The three gases which are most widely used to replace air in the packages are nitrogen (N_2), carbon dioxide(CO_2) and oxygen(O_2). Often, but not always, the exclusion of oxygen is preferred in order to inhibit growth of aerobic spoilage organisms, whereas carbon dioxide is typically used in food packs to decrease bacterial growth rates, and because of its comparatively low price. The composition of the protective atmosphere, however, depends on the type of food and the delivery stage of the food item. Package integrity must therefore be one of the most essential parts of the food packaging process, because leaking may cause substantial problems for consumers and the food packaging industry [1].

Presently MAP packages are only tested at random, using destructive methods in the food packaging plant. These involve extraction of the gas atmosphere from the package using a needle probe, followed by an electrochemical fuel cell for oxygen analysis and infrared absorption spectrometry for carbon dioxide measurement [2]. In the event of one package failing such a MAP test, a very large number of packages before and after the tested one will have to be destroyed and the food items re-packed [3]. This kind of quality control requires a trained technician, the use of expensive analytical machinery and is destructive and time consuming. It not only leads to large financial losses every year, but it also only allows for random sampling of the food packages, so that 100% quality control is not possible.

In order to overcome these problems, a measurement technology should be developed which can provide visual or instrumentally measurable information about the gas atmosphere in the packages, and therefore about the quality of the packaged food. In particular, optical indicator materials incorporated on or in the pack can be used to monitor the package integrity. For such a solution it is necessary to find optical sensor membranes for oxygen and carbon dioxide that can be used in these sensor strips. They should be capable of detecting changes over the whole range of encountered concentrations (0 – 100%) with sufficient resolution (±1%).

In the past, some approaches for both oxygen and carbon dioxide sensors have been used in food packaging technology, but these have generally been in the form of tablets or sachets, mostly relying on colourimetric leak indicators [2]. An approach which is more compatible with industrial demands would consist of sensor membranes that are printed on the packaging material and provide an exact measure of both analyte gases at any given stage in the packaging and delivery process. Most food packaging companies would prefer a membrane type which is not visible to the eye of the normal customers. These membranes would enable only the staff in the packaging industry and the sales personnel in the supermarket to test package integrity. Similarly they would enable the food industry to perform 100% testing in a non-destructive manner and would significantly reduce costs compared to destructive random testing of samples.

1.2. Oxygen Optodes for MAP Analysis

Optical oxygen sensors are very often more attractive than typical amperometric devices because they offer faster responses, do not consume the analyte and lack electrical connections. Most of the oxygen indicators in MAP technology reported to date are absorption-based and change their colour according to the O_2 concentration [4,5]. An alternative approach to purely visual oxygen indicators is luminescence-based, and it has many attractive features even if it makes external equipment necessary. Sensors based on luminescence detection can be used for accurate, quantitative measurement of oxygen concentrations and they usually result in higher sensitivity than those based on absorption or reflectance [6,7].

Thin films doped with luminescent indicators are very suitable for this approach, and have often been used for the design of oxygen optodes. Although both luminescence intensity and its lifetime are modified by the presence of molecular oxygen, sensing based on luminescence lifetime can provide certain benefits. This approach can overcome problems such as photobleaching or leaching of the dye, drift of the light source and the photodetector and displacement or even delamination of the sensing layer, which all can affect luminescence intensity readings [8]. The relationship between fluorescence lifetime τ and oxygen partial pressure pO_2 is described for an ideal single-exponential decay by the Stern-Volmer equation:

$$pO_2 = \frac{1}{K_{SV}} \cdot \left(\frac{\tau_{max}}{\tau} - 1 \right) \qquad (1\text{-}1)$$

where K_{SV} is the diffusion-dependent bimolecular quenching constant (Stern-Volmer constant) and τ_{max} is the luminescence lifetime in the absence of oxygen.

Although static quenching, inhomogeneous systems and short lifetimes can pose significant barriers, many sensors are based on this scheme. Because K_{SV} is proportional to τ_{max}, materials with long lifetimes will, in general, be more easily quenched by oxygen [9]. Thus, organic fluorophores with short τ_{max} values in the ns range are rarely used for fluorometric oxygen sensors, because of their poor response. Although fluorescent organics with longer lifetimes have been used [10,11], the most successful oxygen probes are based on luminescent transition metal complexes.

Ruthenium polypyridyl complexes have often been employed for oxygen sensors based on luminescence quenching [12-14]. These fluorophores have lifetimes in the range of microseconds and offer the possibility for phase-fluorometric decay time analysis. This is a robust and accurate measurement technology, which is already well established and compatible with low-cost LEDs and photodiodes [14-16]. Many sensors are based on [Ru^{II}-tris(4,7-diphenyl-1,10-phenantroline)]$^{2+}$ ($Ru(dpp)_3^{2+}$), which is chosen because of its highly emissive metal-to-ligand charge transfer state, long lifetime, and strong absorption in the blue/green region of the spectrum, which is compatible with blue light emitting diodes. An example of a calibration plot for such a lifetime-based oxygen sensor is depicted in Fig. 1-1.

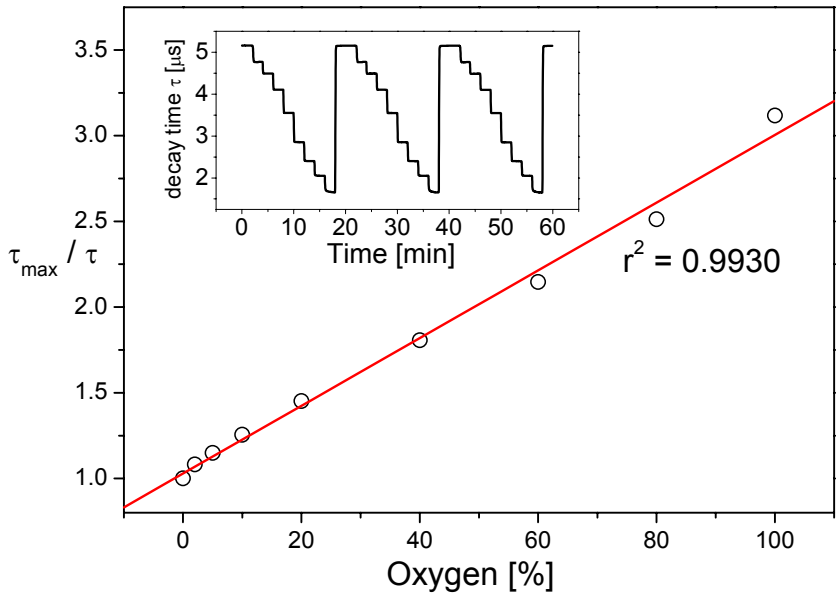

Fig. 1-1 *Response and Stern-Volmer plot of a $Ru(dpp)_3^{2+}$-based optode*

This well-established optical method can easily be used for accurate, quantitative measurement of oxygen concentrations inside of MAP packages in a non-destructive manner.

1.3. Carbon Dioxide Optodes

Carbon dioxide is a key parameter in many clinical, biochemical and industrial processes, and it draws this important status mainly from its important role in animal and plant metabolism. Quantitative and qualitative analysis of CO_2 is very often carried out using infra-red spectroscopy. However, this technique suffers from a series of drawbacks: Instruments are often expensive, bulky, not particularly robust, they require long pathlengths, are prone to interference and lack mechanical stability [17].

Routine analysis of dissolved carbon dioxide has long been performed using the Severinghaus electrode, which makes use of a pH-electrode, placed in contact with a thin layer of an aqueous sodium bicarbonate solution, trapped behind a gas permeable, but ion impermeable membrane [18]. Carbon dioxide can diffuse through this membrane and change the pH in the aqueous solution by forming carbonic acid,

which is then measured by the pH-electrode. When carbon dioxide is entering water, the following equilibria are quickly established:

$$CO_2(g) \rightleftharpoons CO_2(aq) \qquad k_1 = 3.4 \times 10^{-2} \text{ mol } l^{-1} \text{ atm}^{-1} \qquad (1\text{-}2)$$

$$CO_2(aq) + H_2O \rightleftharpoons H_2CO_3 \qquad k_2 = 2.6 \times 10^{-3} \qquad (1\text{-}3)$$

$$H_2CO_3 \rightleftharpoons H^+ + HCO_3^- \qquad k_3 = 1.7 \times 10^{-4} \text{ mol } l^{-1} \qquad (1\text{-}4)$$

$$HCO_3^- \rightleftharpoons H^+ + CO_3^{2-} \qquad k_4 = 5.6 \times 10^{-11} \text{ mol } l^{-1} \qquad (1\text{-}5)$$

The Severinghaus electrode takes advantage of this acidic nature of carbon dioxide and monitors the partial pressure of CO_2 via the pH change it induces in the trapped sodium bicarbonate layer. However, it has a number of disadvantages. It is bulky, quite expensive and prone to electrical and chemical interference. Because of these disadvantages, there has been a growing interest in the development of optical sensors for carbon dioxide over the last twenty years. Such sensors are usually sensitive, robust, fast, cheap and easily miniaturised.

1.3.1. Wet Sensors

The pH changes in buffered aqueous media caused by carbon dioxide in the Severinghaus electrode, have also been used for the development of optical carbon dioxide sensors, this time using pH sensitive dyes rather than a pH electrode to determine the pH variations.

In the early optical sensors for carbon dioxide, the pH sensitive dye was dissolved in a sodium bicarbonate solution and trapped behind a gas-permeable, ion-impermeable membrane. This membrane was designed mainly to prevent leaching of the indicator and interference from ionic species when used to measure dissolved carbon dioxide levels in water [19]. This arrangement is still very similar in many ways to that used in the Severinghaus electrode. However, there were early variations of this theme, including gels or sponge materials soaked in sodium bicarbonate solution, with the pH indicator attached to them [20,21]. Later examples of this technique focused on the development of sensors in single membranes which either relied on the formation of water droplets emulsified in hydrophobic

membranes, or the use of hydrophilic membranes like poly(ethylene glycol) [22,23]. The latter approach obviously cannot be used for measuring carbon dioxide levels in water because of the water soluble matrix material.

The response features of these 'wet sensors' are influenced by either water pressure (gas phase measurements) or osmotic pressure (dissolved carbon dioxide) of the test system. In these circumstances, hydration or dehydration can seriously interfere with the sensor performance, and therefore the use of these sensors is limited.

1.3.2. Solid Sensors

A real breakthrough in the development of solid carbon dioxide sensor optodes was published in 1992 by A. Mills and his co-workers [24]. In this report, a phase transfer agent was used to solubilise the pH-indicator dye into the relatively hydrophobic medium of a polymer, such as ethyl cellulose or poly (vinyl butyral). These solid-type carbon dioxide sensors do not contain a classic aqueous buffer system, but they contain a quaternary ammonium hydroxide, mostly tetraoctyl-ammonium hydroxide (TOA-OH), in a hydrophobic membrane.

The preparation involves reaction of the protonable moiety of the dye (DH) with the quaternary ammonium base (TOA^+OH^-) to form a hydrated ion-pair ($TOA^+D^- \cdot H_2O$) [17,25-27]. This acts as an ion-pairing agent for the polar pH indicator in the non-polar gas-permeable membrane. It also acts as an internal buffer and provides the sensing chemistry with the necessary water of crystallisation [26]. The sensing mechanism is summarised by eq. 1-6, where $\{TOA^+D^- \cdot x\ H_2O\}$ is the complex of the deprotonated pH-indicator dye ion-paired with the quaternary ammonium cation and a number x of chemisorbed water molecules.

$$\left\{TOA^+D^- \cdot x\,H_2O\right\} + CO_2 \xrightarrow{k} \left\{TOA^+HCO_3^- \cdot (x-1)H_2O \cdot HD\right\} \quad (1\text{-}6)$$

These solid sensor membranes are capable of determining carbon dioxide levels in gases of different humidity as well as in aqueous solutions with different osmotic pressures. In a dry gas environment, it might be expected that such a solid sensor would eventually dry out and cease to function. However, the water of

crystallisation associated with the ion-pair appears to be very tightly bound, and many of these films can be used in very dry conditions without any loss in performance. The excess base in the thin solid carbon dioxide sensor acts as a lipophilic bicarbonate buffer system and therefore exists in the form of $TOA^+HCO_3^- \cdot x\ H_2O$ [17]. Therefore, increasing the background concentration of the excess base should shift the sensitivity of the sensor to higher carbon dioxide concentrations.

1.3.3. MAP-Sensing Strategies

As was mentioned above, the optoelectronic technology required to interrogate oxygen and carbon dioxide sensing films inside of the MAP packages should ideally be the same, consequently there is a need for fluorescence lifetime-based CO_2 optodes. However, most of the luminescent pH-indicator dyes, such as 1-hydroxypyrene-3,6,8-trisulfonate (HPTS) and fluorescein, which have been used in optical CO_2 sensors, have lifetimes which are largely independent from pCO_2 [17]. In 1995 G. Orellana and his co-workers reported a lifetime-based optical carbon dioxide sensor, based on $[Ru^{II}$-tris(2-(2-pyrazinyl)thiazole$)]^{2+}$ immobilised in CM-Sephadex [28,29]. Unfortunately the decay time of this dye is about ten times shorter than that of the $Ru(dpp)^{2+}$ complex. Moreover, this sensor is made with an aqueous hydrogen phthalate buffer and therefore retains the disadvantages of conventional wet sensor membranes.

A new approach, which was recently described by Lakowicz and his co-workers, is the use of fluorophores containing amines and photo-induced electron transfer (PET) quenching [30]. Although this technique demonstrates a novel direct approach for fluorescence detection of carbon dioxide, the decay times in the range of nano-seconds necessitate relatively complicated and high-priced instrumentation.

The Fluorescence Resonance Energy Transfer (FRET) technique has produced carbon dioxide sensors which are capable of converting colour changes into decay time information. However, the first generation of these sensors again had to use complex and expensive instrumentation in order to measure the very short lifetimes involved in this technique [31,32]. Recently, Klimant and his co-workers have reported a long-lifetime ruthenium complex as a donor for this type of FRET-based carbon dioxide sensors [33-35]. This sensor, which utilises the ion-pair concept and therefore offers all the advantages of the solid sensor approach, was used for the

detection of dissolved carbon dioxide levels between 0 and 3% in a marine environment.

Recently, Klimant introduced another novel sensing scheme, which offers the possibility to overcome some of the problems normally associated with luminescence intensity-based sensors [36-40]. Dual Luminophore Referencing (DLR) is an internal ratiometric method whereby an analyte-sensitive fluorescence intensity signal is converted into the phase domain by co-immobilising an inert long-lifetime reference luminophore with similar spectral characteristics. The reported DLR-based sensor makes use of the HPTS pH indicator dye and the $Ru(dpp)^{2+}$ referencing dye to create a lifetime-based CO_2 sensor in a marine environment [39,40].

This sensor, as well as most other carbon dioxide sensors used plasticised ethyl cellulose (EtCell) as a matrix material. Unfortunately, almost all published CO_2 optodes are using matrix materials which are not particularly suited to food packaging technologies. Silicone rubber, plasticised ethyl cellulose and polyvinyl butyral are all not very resistant to the high degree of mechanical and chemical interactions which are present in modern day food packages. One material, which has been used for carbon dioxide sensing [41] and which is very resistant against these influences, is an *or*ganically *mo*dified *sil*ica glass (ormosil).

1.4. Sol-Gel Material

The rugged and often very moist conditions that are encountered inside food packages impose serious preconditions for the immobilisation matrix of the sensors. Many polymers that have previously been employed for oxygen or carbon dioxide sensing do not offer sufficient chemical and mechanical stability under these conditions. Sol-gel-derived materials, however, are not only chemically robust and mechanically very resistant, but properties such as polarity and porosity can be tailored to the specific needs of the application [12,42,43]. Furthermore they are optically transparent and they can be printed or patterned using industrial scale processes.

The sol-gel process may be defined rather broadly as the preparation of ceramic materials by preparation of a sol, gelation of the sol, and removal of the solvent [44]. A sol is a colloidal suspension of solid particles in a liquid which may

consist of dense oxide particles or polymeric clusters produced from inorganic or organic precursors [45]. A gel is formed when the clusters aggregate to form a continuous solid skeleton enclosing a continuous liquid phase. The exact gel point is not easy to determine [44]. The sol-gel process can be divided in four steps: Hydrolysis and condensation, gelation, aging and drying.

1.4.1. Hydrolysis and Condensation

As this work deals only with sol-gel the production of glasses from silicon alkoxides, the description of the various steps will be restricted to this special system. The most common representatives of silicon alkoxides are tetraethoxysilane (TEOS) and methyltriethoxysilane (MTEOS), which can be represented by the formula $Si(OR)_4$ and $RSi(OR)_3$. Hydrolysis and condensation of these compounds can be described by eqs. 1-7 to 1-9.

$$\equiv Si{-}OR + H_2O \underset{\text{esterification}}{\overset{\text{hydrolysis}}{\rightleftharpoons}} \equiv Si{-}OH + R{-}OH \qquad (1\text{-}7)$$

$$\equiv Si{-}OR + HO{-}Si\equiv \underset{\text{alcoholysis}}{\overset{\text{alcohol condensation}}{\rightleftharpoons}} \equiv Si{-}O{-}Si\equiv + R{-}OH \qquad (1\text{-}8)$$

$$\equiv Si{-}OH + HO{-}Si\equiv \underset{\text{hydrolysis}}{\overset{\text{water condensation}}{\rightleftharpoons}} \equiv Si{-}O{-}Si\equiv + H_2O \qquad (1\text{-}9)$$

These reactions occur on mixing of the alkoxide with water or exposure to moist atmosphere, and the colloidal particles produced by them form the sol. The two reactions cannot be separated from one another as condensation and polycondensation commence when hydrolysis is not complete, and both reactions continue to occur even during the later stages of gelation and aging of the gel. There is a variety of factors that can influence the reaction rates, such as pH, temperature, concentration of water, solvent (generally ethanol), and alkoxide, all of which greatly affect the structure and properties of the resulting glass [46-50]. Both hydrolysis and condensation can be either base or acid catalysed, and the glasses formed by them will have a different structure with different pore sizes [44].

1.4.2. Gelation

During gelation, the clusters grow by condensation of polymers or aggregation of particles until the clusters collide and form links between them to form bigger clusters. The result is the above mentioned 'super-cluster' which spans throughout the reaction vessel, and the solution suddenly loses its fluidity and takes on the behaviour of an elastic solid. The gel consists now of a solid skeleton enclosing a liquid phase. Despite the fact that the gel shows the properties of a solid, it should not be forgotten that this is only a macroscopic effect, and the mobility of the liquid phase and hence of the dissolved species is still as in a normal solution. Reaction rates remain virtually unchanged in the early stages of gelation. Again, the above mentioned process parameters play a crucial role in the timing of gelation and the properties of the resulting glass.

1.4.3. Aging

The process of aging a sol-gel can be decisive when it comes to the production of uncracked glass monoliths, as it is often necessary for optical applications [44]. It is characterised by further polymerisation, syneresis, coarsening and sometimes phase transformations. Polymerisation strengthens and stiffens the network by further condensation of Si-OH bonds as indicated in Fig. 1-2, and it can continue for months if the reaction vessel is kept closed. As a natural consequence, the liquid still present in the pores gets expelled due to contraction of the pores, and subsequently the gel shrinks and loses liquid, a process which is called syneresis. Coarsening or ripening is a process of dissolution and condensation driven by differences in solubility between surfaces with different radii of curvature

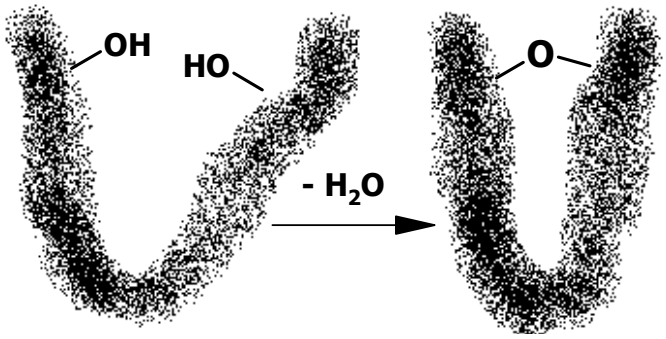

Fig. 1-2 *Pore contraction due to polymerisation during aging*

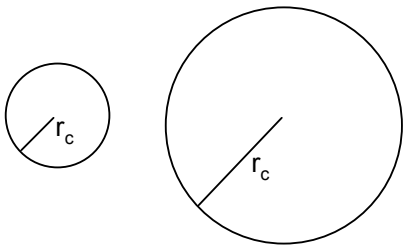

Fig. 1-3 *Small and big radii of curvature*

(Fig. 1-3). The solubility, s, of a surface is related to its radius of curvature r_c by the relation

$$s \propto \exp\left(\frac{1}{r_c}\right) \qquad (1\text{-}10)$$

so the bigger the particle, the worse its solubility. This has two consequences, the first being a general increase in particle size by dissolution of smaller particles and subsequent reprecipitation on the surface of the bigger ones. The second consequence is a further stiffening of the network due to the formation of necks between different particles. As necks have negative radii of curvature (because their centre of curvature lies outside of the particle), their solubility is particularly small, and dissolved material tends to precipitate on them, thus enlarging the connection between the particles [51]. (see Fig. 1-4). This results not only in the above mentioned increase in particle size, but also in an enlargement of the average pore size, because small pores disappear as well as small particles.

There are several types of phase transformations that can occur during aging. If the polymerisation is accompanied by coagulation there is a phase separation on a microscopic scale between the particles and the surrounding liquid. Another kind of phase separation which occurs more frequently in sol-gels from alkoxy-precursors is the segregation of the liquid phase into two. Especially during base-catalysed hydrolysis of silicon alkoxides, there may remain isolated regions of unreacted alkoxide which segregate and make the glass turn opaque when it is soaked in pure water. There are also some types of sol-gels which recrystallize on aging, leaving behind areas with amorphous structure separated from the crystalline regions. The structural changes during aging have an important effect on the quality of the resulting glass, because only if the structure has been strengthened and the solid-liquid interfacial area has been decreased sufficiently, will the network be able to withstand the capillary pressure that occurs while drying.

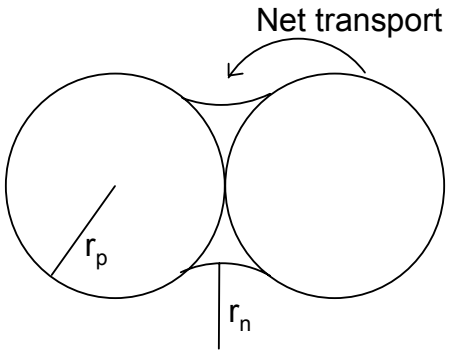

Fig. 1-4 *Growth of necks between particles*

1.4.4. Drying

The last stage in the formation of a sol-gel is the removal of the solvent by evaporation. That process can be divided into three periods (Fig. 1-5). The first one is called the constant rate period (CRP), because the rate of evaporation is independent of time, similar to that of an open glass of liquid. The liquid evaporates from the pores near the surface, and capillary tension develops as liquid flows to prevent exposure of the solid phase, so the network is drawn back into the liquid. During that period, the amount of shrinkage of the gel corresponds exactly to the volume of liquid evaporated. At the critical point, where cracking is most likely to occur, the network gets too stiff to follow the capillary stress easily, and the liquid starts to recede into the interior of the glass body. After the critical point the evaporation rate decreases, so this period is referred to as first falling rate period (FRP1). The pores of the surface area are filled with air, but the pore walls are still covered with a thin layer of liquid, which flows from the interior of the glass to the outside and evaporates there.

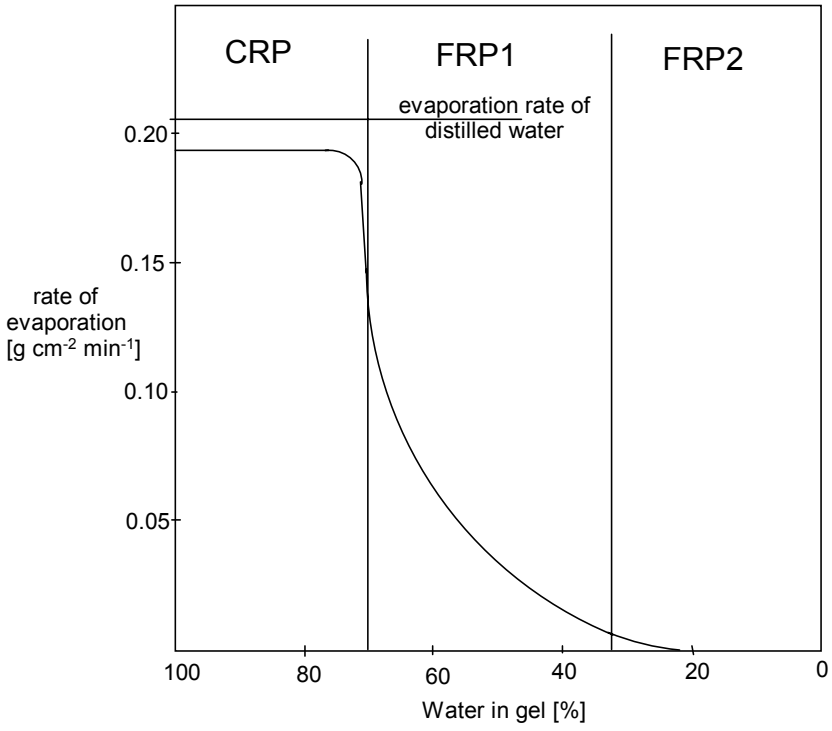

Fig. 1-5 *The three periods of evaporation rates of a sol-gel [52]*

The gel now shrinks less than the volume of the lost liquid, as pores are filled up with air. The final stage of drying is called the second falling rate period (FRP2), during which the flow of liquid through the pores finally stops, and further drying is

only possible by evaporation inside of the gel, and subsequent diffusion of the vapour through the matrix. This process finally comes to an end or at least reaches an equilibrium between diffusion into the glass and out of it. At this stage, the glass still contains water in the inner parts of the sol-gel, and it is this water content, which is desired for the application as a matrix for colourimetric reactions, which normally are done in aqueous solution.

The partial hydrolysis of silicon alkoxides, such as TEOS or TMOS, results in the retention of a proportion of Si-OH linkages on the surface of the pores. These conventional sol-gels are well suited for sensing ions, but the silanol groups can have a pronounced effect on pH indicators and render them insensitive to analytes such as carbon dioxide. In ormosil glasses such as MTEOS or ETEOS, an unreactive alkyl group covers most of the outside and inside pore surfaces, and therefore a more hydrophobic material is obtained, and the sensitivity of pH indicators is not reduced [36]. These ormosil sol-gels have been used in the past for sensor membranes for oxygen, ammonia, pH and carbon dioxide [12,14,41, 53-57].

1.5. Objectives

The principal objective of this work was the development of new carbon dioxide sensor materials for modified atmosphere food packaging applications. In this context, the developed materials should possess the following critical properties:

- Operational range from LOD to 100% CO_2 as required for the food packaging application.
- Spectral and instrumental compatibility with the existing lifetime-based oxygen sensor materials so that a single scanner instrument could be employed for interrogation of both O_2 and CO_2 sensor films.
- Zero cross-sensitivity of the CO_2 sensor to O_2 and other relevant interferents.
- Long-term stability and reversibility.
- Printability of sensor formulation onto flexible packaging material using standard industrial printing techniques.

1.6. References

1 Church, N. *Trends Food Sci. Technol.*, **1994**, *5*, 345

2 Smolander, M.; Hurme, E.; Ahvenainen, R. *Trends in Food Sci. and Technol.*, **1997**, *8*, 101

3 Mills, A. *International Symposium on Printing and Coating Technology*, Conference Proceedings, Swansea, UK, **1998**, 12-1

4 Mattila-Sandholm, T.; Ahvenainen, R.; Hurme, E.; Järvi-Kääriäinen, T. *EU Pat.*, EP 0666977B1, **1998**

5 Ahvenainen, R.; Hurme, E.; Randell, K.; Eilamo, M. *Technical Research Centre of Finland (VTT)*, **1995**, VTT Research Notes 1683

6 Wolfbeis, O.; Leiner, M.; Posch, H. *Microchim. Acta*, **1986**, *3*, 359

7 MacCraith, B.; McDonagh, C.; O'Keefe, G.; Keyes, E.; Vos, J.; O'Kelly, B.; McGilp, J. *Analyst*, **1993**, *118*, 385

8 McEvoy, A.; McDonagh, C.; MacCraith, B. *Analyst*, **1996**, *121*, 785

9 Demas, J.; DeGraff, B.; Coleman, P. *Anal. Chem. News & Features*, **1999**, *A*, 793

10 Ramasamy, S.; Hurtubise, R. *Talanta*, **1998**, *47*, 971

11 Campo, J.; Pérez, M.; González, M.; Ferrero, F. *Proc. IEEE Instr. Measurement Tech. Conf.*, **1998**, *2*, 1162

12 McDonagh, C.; MacCraith, B.; McEvoy, A. *Anal. Chem.*, **1998**, *70*, 45

13 Wolfbeis, O.; Klimant, I.; Werner, T.; Huber, C.; Kosch, U.; Krause, C.; Neurauter, G.; Dürkop, A. *Sens. Actuators B*, **1998**, *51*, 17

14 McDonagh, C.; Kolle, C.; McEvoy, A.; Dowling, D.; Cafolla, A.; Cullen, S.; MacCraith, B. *Sens. Actuators B*, **2001**, *74*, 124

15 Lippitsch, M.; Draxler, S. *Sens. Actuators B*, **1993**, *11*, 97

16 Holst, G.; Köster, T.; Voges, E.; Lübbers, D. *Sens. Actuators B*, **1995**, *29*, 231

17 Mills, A.; Eaton, K. *Química Analítica*, **2000**, *19*, 75

18 Severinghaus, J.; Bradley, A. *J. Appl. Physiol.*, **1958**, *13*, 515

19 Lübbers, D.; Opitz, N. *Z. Naturforsch.*, **1975**, *30c*, 532

20 Wolfbeis, O.; Weis, L.; Leiner, M.; Ziegler, W. *Anal. Chem.*, **1988**, *60*, 2028

21 Uttamlal, M.; Walt, D. *Bio/Technology*, **1995**, *13*, 597

22 Leiner, M. *Anal. Chim. Acta*, **1991**, *255*, 209

23 Kawabata, Y.; Kamichika, T.; Imasaka, T.; Ishibashi, N. *Anal. Chim. Acta*, **1989**, *219*, 223

24 Mills, A.; Chang, Q.; McMurray, N. *Anal. Chem.*, **1992**, *64*, 1383

25 Mills, A.; Chang, Q. *Analyst*, **1993**, *118*, 839

26 Mills, A.; Chang, Q. *Anal. Chim. Acta*, **1994**, *285*, 113

27 Chang, Q.; Randers-Eichhorn, L.; Lakowicz, J.; Rao, G. *Biotechnol. Prog.*, **1998**, *14*, 326

28 Marazuela, M.; Moreno-Bondi, M.; Orellana, G. *Sens. Actuators B*, **1995**, *29*, 126

29 Marazuela, M.; Moreno-Bondi, M.; Orellana, G. *Appl. Spectrosc.*, **1998**, *52*, 1314

30 Herman, P.; Murtaza, Z.; Lakowicz, J. *Anal. Biochem.*, **1999**, *272*, 87

31 Sipior, J.; Randers-Eichhorn, L.; Lakowicz, J.; Carter, G.; Rao, G. *Biotechnol. Prog.*, **1996**, *12*, 266

32 Chang, Q.; Randers-Eichhorn, L.; Lakowicz, J.; Rao, G. *Biotechnol. Prog.*, **1998**, *14*, 326

33 Wolfbeis, O.; Klimant, I.; Werner, T.; Huber, C.; Kosch, U.; Krause, C.; Neurauter, G.; Dürkop, A. *Sens. Actuators B*, **1998**, *51*, 17

34 Neurauter, G.; Klimant, I.; Wolfbeis, O. *Anal. Chim. Acta*, **1999**, *382*, 67

35 Neurauter, G.; Klimant, I.; Wolfbeis, O. *Fresenius J. Anal. Chem.*, **2000**, *366*, 481

36 Klimant, I. *Ger. Pat. Appl.*, **1997**, DE 198.29.657

37 Lakowicz, J.; Castellano, F.; Dattelbaum, J.; Tolosa, L.; Rao, G.; Gryczynski, I. *Anal. Chem.*, **1998**, *70*, 5115

38 Huber, C.; Klimant, I.; Krause, C.; Werner, T.; Mayr, T.; Wolfbeis, O. *Fresenius J. Anal. Chem.*, **2000**, *368*, 196

39 Klimant, I.; Huber, C.; Liebsch, G.; Neurauter, G.; Stangelmayer, A.; Wolfbeis, O. In: Valeur, B.; Brochon, C. (Eds), *Fluorescence Spectroscopy: New Methods and Applications*, **2001**, Springer, Berlin

40 Neurauter, G. *Dissertation*, Univ. Regensburg, **2000**, 40

41 Malins, C.; MacCraith, B. *Analyst*, **1998**, *123*, 2373

42 Lin, J.; Brown, C. *Trends in Anal. Chem.*, **1997**, *16*, 200

43 Collinson, M. *Crit. Rev. Anal. Chem.*, **1999**, *29*, 289

44 Brinker, C.; Scherer, G. *Sol-Gel Science*, **1990**, Academic Press Ltd., London

45 Hollemann, A.; Wiberg, N. *Lehrbuch der Anorganischen Chemie*, **1985**, de Gruyter, Berlin

46 Pope, E.; Mackenzie, J. *J. Non-Cryst. Solids*, **1986**, *87*, 185

47 Chen, K.; Tsuchiya, T.; Mackenzie, J. *J. Non-Cryst. Solids*, **1986**, *81*, 227

48 Kamiya, K.; Yoko, T. *J. Mat. Sci.*, **1986**, *21*, 842

49 Sheunfain, R.; Stas, O.; Makovskaya, T. *Kolloid Zeitung*, **1972**, *34*, 869

50 Shukla, B.; Johari, G. *J. Non-Cryst. Solids*, **1988**, *101*, 263

51 Iler, R. *Chemistry of Silica*, **1979**, Wiley, New York

52 Dwivedi, R. *J. Mater. Sci. Lett.* **1986**, *5*, 373

53 Liu, H.; Switalski, S.; Coltrain, B.; Merkel, P. *Appl. Spectrosc.*, **1992**, *46*, 1266

54 Malins, C.; Butler, T.; MacCraith, B. *Thin Solid Films*, **2000**, *368*, 105

55 Butler, T.; MacCraith, B.; McDonagh, C. *J. Non-Cryst. Solids*, **1998**, *224*, 249

56 Makote, R.; Collinson, M. *Anal. Chim. Acta*, **1999**, *394*, 195

57 Ismail, F.; Malins, C.; Goddard, N. *Analyst*, **2002**, *127*, 253

2. Energy Transfer

2.1. Introduction

2.1.1. Phase-Domain Lifetime Measurement

The average time molecules remain in the excited state before returning to the ground state is termed the luminescence lifetime [1]. In the case of a single exponential decay, the lifetime (decay time) τ is defined as the time after which the fraction 1/e of the excited molecules still exists in excited state. Lifetime measurements are frequently used in modern fluorescence spectroscopy in order to eliminate various drawbacks associated with intensity measurements. Luminescence lifetime signals generally are independent of signal fluctuations caused by light sources and photodetectors, and effects like photobleaching, photodecomposition and leaching have a negligible effect.

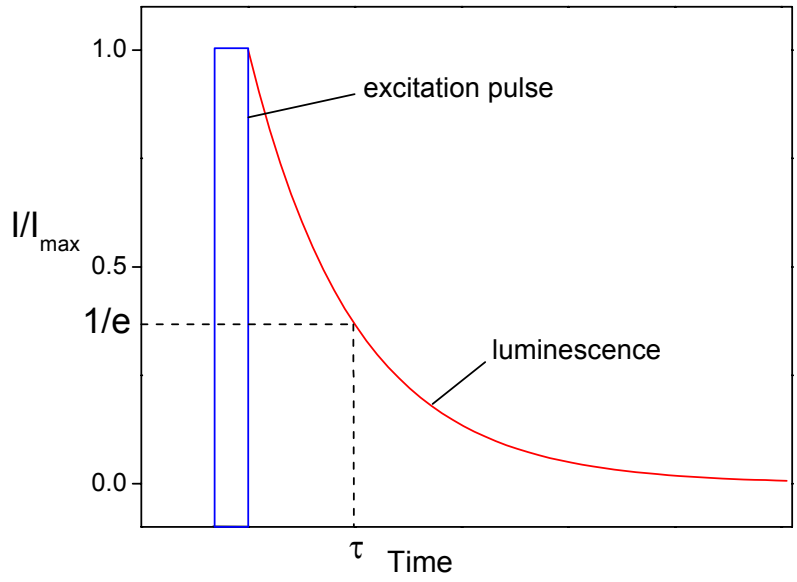

Fig. 2-1 *Description of time domain decay time measurement. The time it takes for the intensity to achieve 1/e of its original amount is defined as the luminescence lifetime, τ.*

If the signal-to-noise ratio is sufficiently high, changes in the indicator dye concentrations (e.g. by leaching) of lifetime-based sensors do not influence lifetime measurements [2-4].

Fundamentally there are two widely used techniques to determine luminescence lifetimes: the direct pulse method (time-domain), which evaluates the decay profile of the monitored lifetime, and the indirect phase modulation method (frequency-domain), which uses the phase shift of a modulated luminescence signal to calculate the lifetime [1]. The direct pulse lifetime determination requires short pulse excitation sources (e.g. lasers) and wide bandwidth and high-speed detectors in combination with fast signal processing systems. After excitation of the sensor with a short light pulse, the time it takes fluorescence intensity to descend to 1/e of its original level is called the luminescence lifetime τ (Fig. 2-1).

In the phase-modulation technique, where the luminophore is excited using sinusoidally modulated light at frequency f, the emitted sinusoidal sensor luminescence is modulated at the same frequency. However, the luminescence signal is time delayed with respect to the excitation signal and therefore exhibits a phase shift (Fig. 2-2).

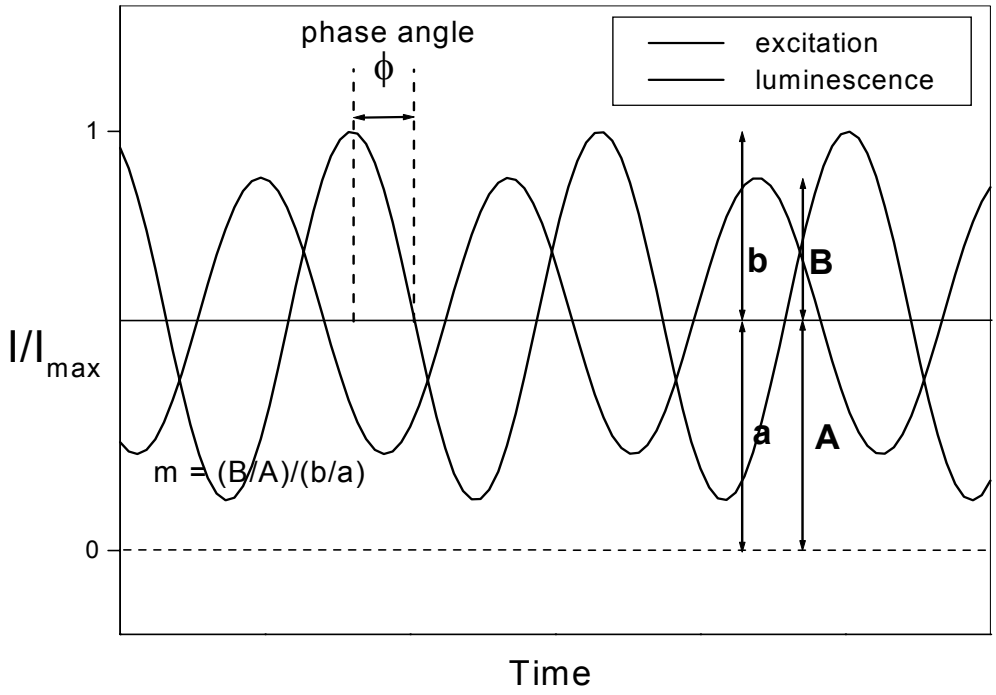

Fig. 2-2 *Schematic representation of the phase domain decay time measurement. Luminescence emission is delayed in phase angle ϕ and demodulated relative to excitation (m).*

This phase shift (ϕ) is associated with the decrease in emission intensity relative to the incident light. This reduction in emission intensity compared to excitation is described by the demodulation (m). The emission amplitude (B/A) is smaller than the compared excitation amplitude (b/a). The lifetime of the measured fluorophore can be calculated from both phase shift ϕ and demodulation m according to eqs. 2-1 and 2-2 [1].

$$\tau_\phi = \frac{\tan\phi}{2\cdot\pi\cdot f} \qquad (2\text{-}1)$$

$$\tau_m = \frac{\sqrt{m^{-2}-1}}{2\cdot\pi\cdot f} \qquad (2\text{-}2)$$

However, the assumption that τ_ϕ and τ_m are equal to τ is only valid for single exponential decays. Otherwise, the calculated lifetimes are only apparent values, and the measurement of lifetime τ is more complicated.

Phase modulation-based lifetime technology has been used as a very attractive analytical tool for many applications. Absorption and luminescence intensity-based techniques are not as accurate techniques as fluorescence lifetime technology. The instrumentation which is used in phase fluorometry is rather simple. Excitation light sources are light emitting diodes (LED) and photomultiplier tubes or even photodiodes are used as light detectors. Light sources and detectors both need suitable excitation and emission filters, and the fluorescent signal is processed in a lock-in amplifier. This lifetime detection can be independent of electronic cross-talk signals and ambient light interference. Many frequency-domain decay time based sensors in the past have used dyes with lifetimes in the ps and ns range [5,6]. However, short lifetimes such as these require very high modulation frequencies in the range of 100 MHz or above, and therefore require rather expensive equipment. Therefore, indicators with decay times in the range of μs are needed in order to allow low modulation frequencies in the order of kHz. One promising way to overcome the lack of suitable long lifetime indicators is the use of fluorescence resonance energy transfer (FRET) technology.

2.1.2. Fluorescence Resonance Energy Transfer

The detection of luminescence lifetime, rather than intensity, can overcome many of the problems associated with intensity-based systems [5]. However, there is only a limited number of luminescent pH-indicators which have long enough decay times and suitable pK_A-values for CO_2 detection using low cost instrumentation. An alternative approach, which enables the use of colourimetric pH-indicators in lifetime-based sensors, is Fluorescence Resonance Energy Transfer (FRET). This technique overcomes the problem of the lack of suitable luminescent pH-indicators by converting the colour change of a colourimetric pH-indicator into lifetime information [6]. An inert fluorescent dye, whose emission band overlaps with the absorption band of the pH-indicator, is co-immobilised in the sensor film. When radiationless energy transfer occurs, the intensity and decay time of the fluorophore are modulated [1].

FRET is a distance-dependent interaction between the electronic excited states of two dye molecules in which excitation is transferred using dipole-dipole interactions from a donor molecule to an acceptor molecule without emission or absorption of a photon. Similar energy transfers which involve photon emission and absorption processes are called radiative transfer or inner filter effect [1]. The rate of FRET (k_T) depends on the following conditions:

- Donor and acceptor molecules must be in close proximity (typically between 20Å and 60Å).
- The absorption spectrum of the acceptor must overlap the fluorescence emission spectrum of the donor (Fig. 2-2).
- Donor fluorescence quantum yield must be high enough.

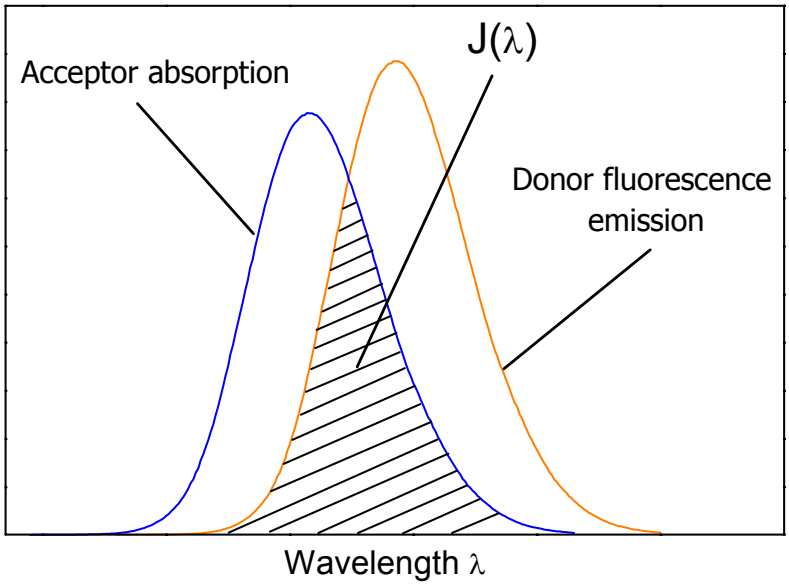

Fig. 2-3 *Schematic representation of the FRET spectral overlap integral J(λ).*

Theory developed by Förster [7], leads to a quantitative expression for this rate of energy transfer between a donor and acceptor pair as a function of the intermolecular separation distance r:

$$k_T = \frac{8.71 \cdot 10^{23} \cdot \kappa^2 \cdot \phi_D}{r^6 \cdot n^4 \cdot \tau_D} \cdot J(\lambda) \qquad (2\text{-}3)$$

where κ^2 is the dipole orientation factor, which can range between 0 and 4, but for randomly oriented donors and acceptors κ^2 equals to 2/3. The refractive index of the medium is given by n and ϕ_D and τ_D are respectively the fluorescence quantum yield and lifetime of the donor in absence of the acceptor. $J(\lambda)$ is the spectral overlap integral between donor and acceptor (Fig. 2-3), with

$$J(\lambda) = \int_0^\infty \varepsilon_A(\lambda) \cdot F_D(\lambda) \cdot \lambda^4 \, d\lambda \qquad (2\text{-}4)$$

where ε_A is the extinction coefficient of the acceptor dye, and F_D is the fluorescence emission intensity of the donor as a fraction of the total integrated intensity. The distance at which 50% of the excited donors are deactivated by energy transfer is defined by the Förster radius (R_0), and the magnitude of R_0 is dependent on the spectral properties of the donor and acceptor dyes:

$$R_0 = \left[8.71 \cdot 10^{23} \cdot \kappa^2 \cdot n^{-4} \cdot \phi_D \cdot J(\lambda)\right]^{1/6} \qquad (2\text{-}5)$$

The efficiency of FRET is dependent on the inverse sixth power of the intermolecular separation, and therefore FRET can be a tool for monitoring distances between donor and acceptor labelled targets [8].

Acceptors with an analyte dependent absorbance that spectrally overlap the donor fluorescence can be used to design a FRET-based sensor. For this purpose the luminescent donor should not be influenced by the analyte, and the acceptor dye does not have to be fluorescent, and is preferably not. The main advantage of such an energy transfer system is the conversion of an absorbance-based signal into a fluorescence decay time signal. Higher sensitivity, selectivity and compatibility with cheap excitation sources generally results from fluorescence, rather than absorption. For this reason it is possible to transform absorption-based sensors into lifetime-based sensors by co-immobilising suitable analyte insensitive donors. The first series of FRET based sensors, however, was based on fluorescent dyes which have very short lifetimes in the order of only a few nanoseconds. In order to measure such short lifetimes, pulsed light source techniques or phase modulation methods with

frequencies close to 100 MHz have to be employed, thereby leading to expensive and complex instrumentation [6, 9-12].

However, there are some organic complex compounds using transition metals like ruthenium, iridium, osmium which are very promising long-lifetime reference luminophores. Several ruthenium bipyridyl and phenantroline complexes offer very promising donor properties, such as high lifetimes ($\leq 5\mu s$), high quantum yields, high colouration (molar extinction coefficients ≥ 30000) and good photochemical stability. Ruthenium metal-ligand complexes can easily be prepared and they allow many different combinations with ligands and counter ions. These Ru-complexes have recently been used for the development of lifetime-based sensors for pH [13], ions [14-16], ammonia [17], urea & glucose [16] and carbon dioxide [16,18]. However, all published optical CO_2 sensors only offer good sensitivities in low concentration ranges. Therefore this work focused on the development of a long lifetime FRET-based carbon dioxide sensor with a measurement concentration range 0-100% CO_2. The work is presented in this chapter.

2.2. Experimental

2.2.1. pH-Indicator

The dynamic range of a carbon dioxide sensor depends on the type of buffer system used and on the pK_A-value of the pH-indicator. The development of a FRET-based carbon dioxide sensor, using a long-lifetime ruthenium complex and having a dynamic range up to 100% CO_2, requires a pH-indicator with an absorption band around 600 nm (matching the emission peak of ruthenium polypyridyl complexes) and a just over neutral pK_A-value. Unfortunately, the broad range of conventional pH-indicators does not offer a suitable candidate with these qualities. Cresol purple, thymol blue, xylenol blue, phenol red, cresol red and α-naphtholphthalein were evaluated and found to be too sensitive to extend the dynamic range to 100% CO_2, whereas bromothymol blue, bromoxylenol blue and nitrazine yellow did not show any response to carbon dioxide in a solid matrix.

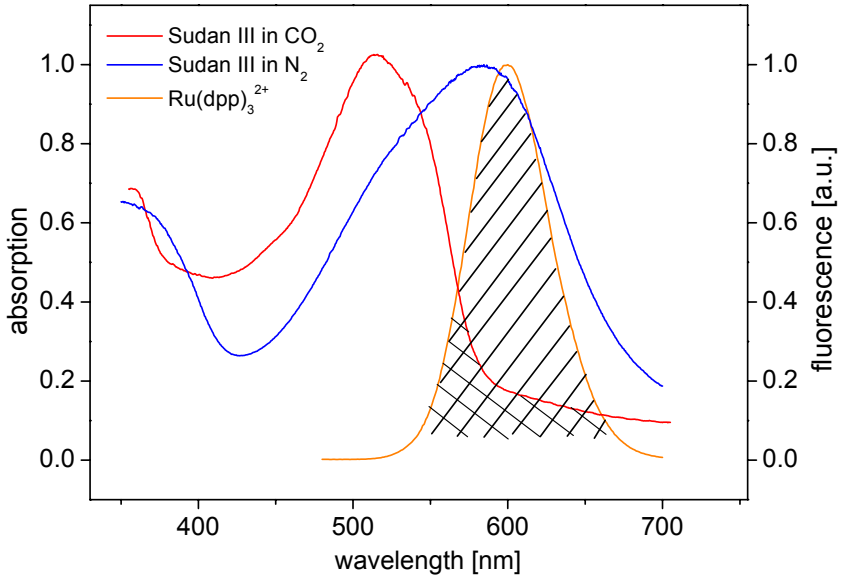

Fig. 2-4 *Fluorescence emission spectrum of the $Ru(dpp)_3^{2+}$ complex and absorption spectra of sudan III in 100% nitrogen and carbon dioxide. The striped area demonstrates the overlap of donor and deprotonated acceptor spectra. The crossed area shows the remaining overlap after complete protonation of the acceptor dye.*

It was therefore necessary to extend the search for a suitable indicator dye into areas that normally are not connected to conventional colourimetric analytical chemistry. The suitability of sudan III as a candidate for a FRET-based pCO_2 sensor is reported here (Fig. 2-4). Its spectral properties satisfy the requirements of such a sensor. This dye has so far only been used as a fat stain in histological research, and as a colorant for oils, waxes, hydrocarbons, polishes and cosmetics [19]. Sudan III is a red disazo dye that is neither acidic nor basic, but it contains one protonable hydroxy group which is responsible for its CO_2 sensitivity (Fig. 2-5). This highly lipophilic compound cannot be used in aqueous environments, and therefore it is impossible to determine a formal pK_A-value for the dye. The good solubility in non-polar solvents and polymers, however, allows its use in solid carbon dioxide sensors, an application which commonly relies on ion-pairing techniques to solubilise the polar

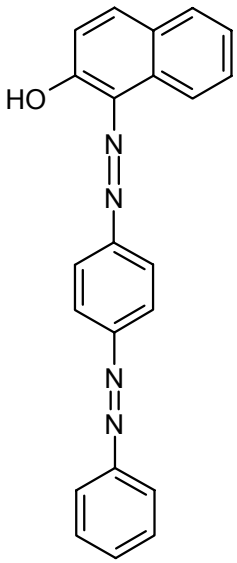

Fig. 2-5 *Sudan III*

pH-indicators in the non-polar matrix materials [20]. The preparation of solid non-aqueous pCO_2 sensors involves reaction of the protonable moiety of the pH-indicator dye (DH) with a quaternary ammonium base (Q^+OH^-) to form a hydrated ion-pair ($D^- Q^+ \times H_2O$) [9,16,18,20-23,25].

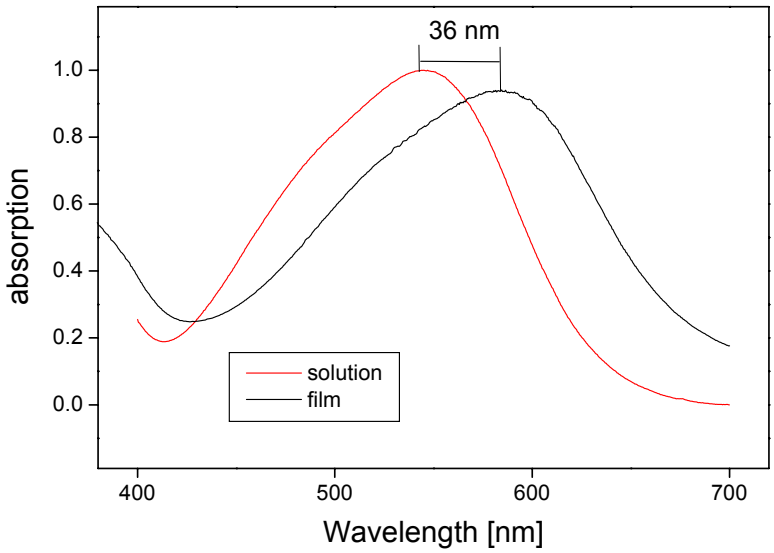

Fig. 2-6 *The bathochromic shift of λ_{max} for the ion-paired sudan III dye in a film of ethyl cellulose as opposed to its solution in toluene. This strong shift of 36 nm provides evidence for ion-pairs between sudan III and TOA-OH.*

The lipophilic base, in most cases tetraoctylammonium hydroxide (TOA-OH), stabilises the deprotonated form of the dye in the matrix and provides the sensing chemistry with the necessary water of crystallisation [22]. Mills et al. found bathochromic shifts in absorption spectra of the deprotonated forms of immobilised pH-indicators, compared with what is measured in solution [20-22]. This provides supporting evidence for a close association between the dye and organic base in the form of ion-pairs. The absorption spectrum recorded in a film of ethyl cellulose, using TOA-OH as a lipophilic base, exhibited a bathochromic shift of 36 nm compared to what is measured in toluene solution (Fig. 2-6). This shift verifies the formation of closely associated ion-pairs between sudan III and TOA-OH [21].

The response of such an ion-paired film to CO_2 in the range 0 to 100% is shown in Fig. 2-7. This figure illustrates the observed change in the absorption spectrum of the sudan III dye immobilised in an ethyl cellulose film as a function of

the carbon dioxide concentration in the surrounding gas phase. This film exhibits a completely reversible and hyperbolic response, with higher sensitivity at low carbon dioxide concentrations, which is typical for this type of pCO_2 sensors. Although the sensitivity exhibited under these conditions is clearly too low between 50% and 100% CO_2, the use of the ormosil matrix, the lipophilic base and the use of FRET technology was expected to extend the sensitivity to a higher range.

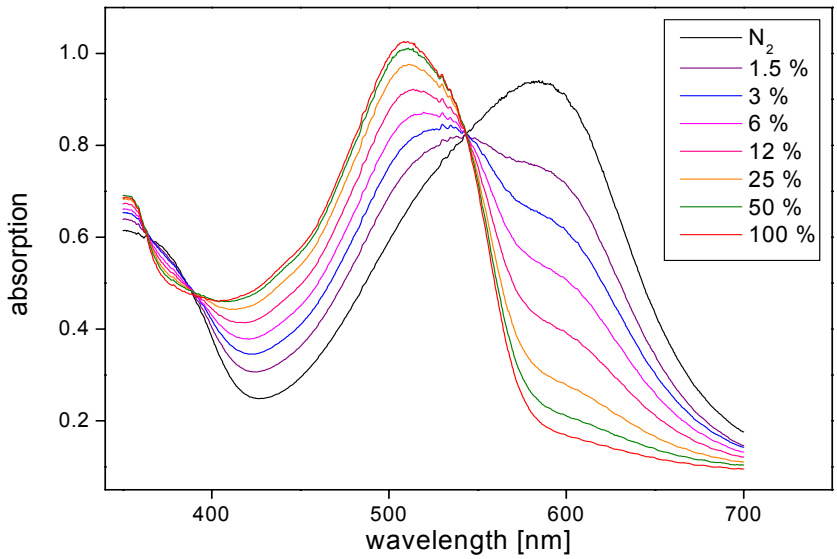

Fig. 2-7 *Absorption spectra of sudan III immobilised in EtCell when exposed to 0, 1.5, 3, 6, 12, 25, 50 and 100% CO_2 in top to bottom order at 584 nm.*

2.2.2. Donor

The change in the absorption spectrum of an analyte-sensitive acceptor dye is converted into lifetime information by co-immobilising a luminescent donor with an overlapping emission spectrum. A substantial spectral overlap between donor emission and acceptor absorption is essential for the performance of the sensor. The pH-indicator used in this study is the lipophilic disazo dye sudan III.

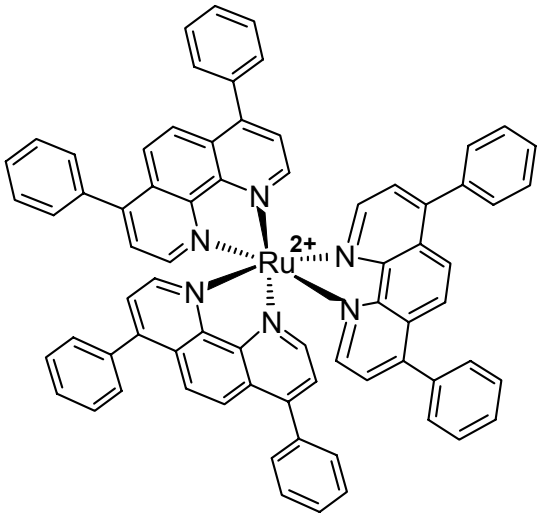

Fig. 2-8 *Chemical Structure of ruthenium (II) tris(4,7-diphenyl-1,10-phenanthroline)*

The subject of this work was to design a pCO_2 sensor with luminescence lifetimes in the range of microseconds. Therefore a luminescent ruthenium complex was selected as the most promising candidate for a donor (Fig. 2-8). The well-known ruthenium(II) tris(4,7-diphenyl-1,10-phenanthroline) complex ($Ru(dpp)_3^{2+}$) seems to be an almost perfect donor because of its decay time of ~5μs, its high quantum yield (~0.5) and its spectral compatibility with blue LED's. It is ion-paired with a lipophilic counterion to adapt its solubility in the matrix to the non-polar sudan III. Fig. 2-4 shows the spectral properties of this donor / acceptor pair in the absence and presence of carbon dioxide (100%). There is sufficient spectral overlap between the deprotonated form of sudan III (λ_{max} = 582 nm) and the donor (λ_{max} = 600 nm) to guarantee an efficient rate of energy transfer. However, there clearly remains some overlap in the presence of 100% carbon dioxide, and this will limit the sensitivity to some extent.

2.2.3. Base

A precondition for a carbon dioxide sensor for application in food packaging technology is that it provides sufficient sensitivity over the complete range of CO_2

concentrations that are encountered in MAP gases (0–100%). The majority of reported optical chemical carbon dioxide sensors, however, only provide sufficient sensitivity up to ca. 10% CO_2 [9,16,18,20-25]. The sensitivity of a carbon dioxide sensor is linked to the equilibrium constant of the pH indicator used (pK_A) and to the nature of the buffer that surrounds it. . The first generation of optical carbon dioxide sensors, which contained an aqueous hydrogen carbonate buffer, was later replaced by solid sensor membranes. Solid-type carbon dioxide sensors do not contain a classic aqueous buffer system, but they contain a quaternary ammonium hydroxide in a hydrophobic membrane. The preparation, as discussed in Section 2.2.1, involves reaction of the protonable moiety of the dye (DH) with the quaternary ammonium base (Q^+OH^-) to form a hydrated ion-pair (D^-Q^+ x H_2O). This acts as an ion-pairing agent for the polar pH indicator in the non-polar gas-permeable membrane, as well as an internal buffer and provides the sensing chemistry with the necessary water of crystallisation [22]. The excess amount of the base is neutralised by atmospheric carbon dioxide to form a lipophilic hydrogen carbonate buffer in the solid matrix, which can tune the sensitivity and improve the storage stability of the sensor [18, 22].

In order to ensure a FRET-based CO_2 sensor with a high enough sensitivity, a range of five different available quaternary ammonium hydroxides was tested for the application in sudan III based sensors.

Tetraoctylammonium hydroxide (TOA-OH) is the quaternary ammonium base, which was successfully used in almost all published solid carbon dioxide sensors [9,16,18,20-23]. Next to TOA-OH, cetyl-trimethylammonium hydroxide (CTA-OH) is, to our knowledge, the only other quaternary ammonium base that has been reported for solid carbon dioxide sensors [25]. Tetrabutylammonium hydroxide (TBA-OH) has been used as a phase transfer agent in an early example of optical carbon dioxide sensors [26]. It represents a readily available candidate for a smaller, but still spherical quaternary ammonium base. In order to increase the chance for a high enough sensitivity for the FRET-based sensor, two more easily accessible quaternary ammonium hydroxides, tetradecyl-trimethylammonium hydroxide (TDTA-OH) and tetra-decylammonium hydroxide (TDA-OH), were included in this analysis (Fig. 2-9).

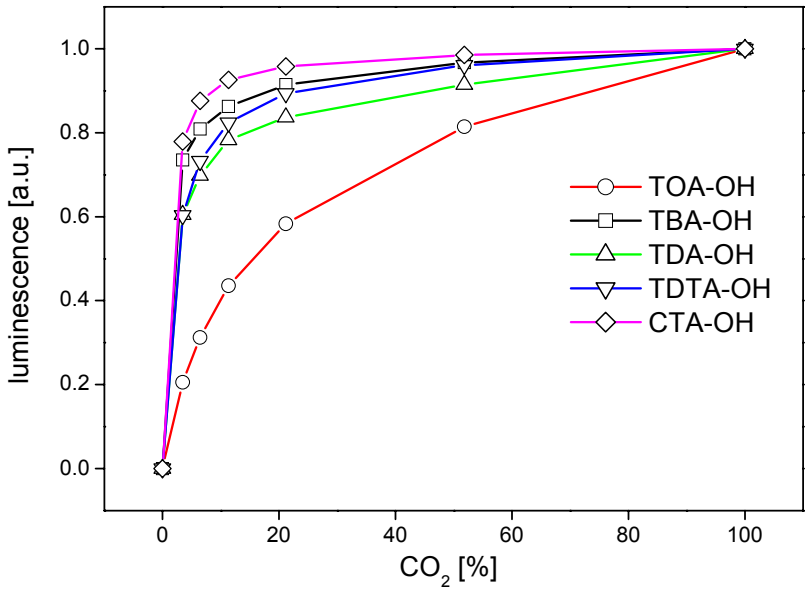

Fig. 2-9 *Normalised phase calibration plots for FRET-based carbon dioxide sensor films using the five tested quaternary ammonium bases and the pH-indicator sudan III.*

As can be seen in Fig. 2-9, there is clearly only one of these ammonium bases which provides a high enough carbon dioxide sensitivity for this sensor. The other option for increasing the sensitivity range of this sensor is to use a higher concentration of this ammonium base. Most sensors use TOA-OH at the industrially available concentration of 20% w/w.

This base concentration was increased to 30% and 40 % w/w in order to achieve a better sensitivity range at high CO_2 concentrations (Fig. 2-10). Although this sensitivity increase for higher concentrations seems to be a positive step, it is important to limit the base concentration in the sol-gel matrix. If there is too much base present, the sol-gel material will lose much of its stability and chemical neutrality. Therefore it was decided to compromise between good chemical matrix stability and high enough sensitivity by choosing a base concentration of 30% w/w for the TOA-OH solution.

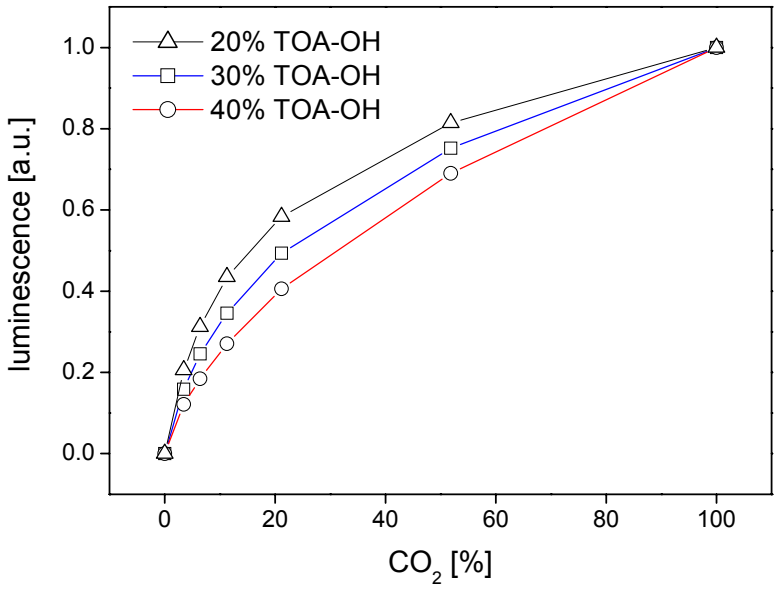

Fig. 2-10 *Normalised phase calibration plots for FRET-based sensors using sudan III acceptor dye and tetraoctylammonium hydroxide base in three different concentrations.*

2.2.4. Preparation

Ethyl cellulose (5.0 g) was dissolved in 100 ml of a toluene/ethanol mixture (80/20 v/v). Sol-gel solutions were prepared by adding 1.45 ml of 0.1 N hydrochloric acid to 4.0 ml of MTEOS while stirring rapidly until the two phases mix, and hydrolysis and condensation starts. The sol-gel was then stirred for a further two hours before mixing into the sensor cocktails. Stock solution I was prepared by dissolving 58.0 mg of the $Ru(dpp)_3(TSPS)_2$ ion-pair in 20.0 ml of the methanolic TOA-OH solution. Stock solution II was prepared by dissolving 60.0 mg Sudan III in 10.0 ml of the TOA-OH solution.

Cocktails for making films with different quantities of Sudan III (**S0** – **S6**) were made by mixing different quantities of stock solution I and II, the methanolic base solution, the ethyl cellulose solution and the sol-gel solution (Table 2-1). The cocktails were saturated with carbon dioxide before spin coating at 700 RPM onto dust free polymer substrates. The resulting membranes were dried at 70ºC for 22 hours and then stored in sealed plastic bags under ambient conditions.

Table 2-1 *Composition of sensor membranes **S0** to **S6***

membrane	S0	S1	S2	S3	S4	S5	S6
sol-gel [ml]	3.365	3.365	3.365	3.365	3.365	3.365	3.365
ethyl cellulose [ml]	1.360	1.360	1.360	1.360	1.360	1.360	1.360
TOA-OH [ml]	1.0	0.875	0.750	0.625	0.50	0.250	-
solution I [ml]	1.0	1.0	1.0	1.0	1.0	1.0	1.0
solution II [ml]	-	0.125	0.250	0.375	0.500	0.750	1.0
Sudan III in the matrix [mmol kg^{-1}]	0	2.34	4.69	7.03	9.38	14.06	18.76

2.2.5. Instrumentation

Fluorescence emission spectra were recorded with a Spex FluoroMax 2 spectrofluorometer (Jobin Yvon Inc., Edison, NJ, USA), and absorption spectra were acquired with a Cary 50 Scan UV-vis spectrometer (Varian Inc, USA). The flow cell used for the phase fluorometric measurements is described in Fig. 2-11. A digital dual-phase lock-in amplifier (DSP 7225 Perkin Elmer Instruments, USA) was used for sinusoidal modulation of the LED (20 kHz / 5.0 V) and for phase-shift detection of the photodiode output signal. The optical set-up consisted of a blue LED (l_{max} = 470 nm, NSPB 500 Nichia, Germany) with a blue band-pass filter (BG-12, Schott, Mainz, Germany) and an integrated photodiode amplifier (IPL 10530 DAL, IPL Inc, Dorset, UK) with an orange long-pass filter (LEE 135, LEE Filters, Hampshire, UK).

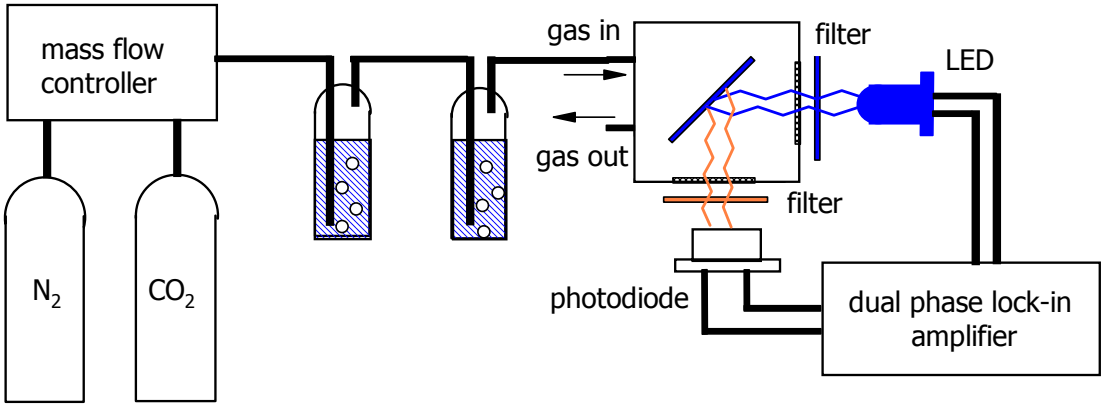

Fig. 2-11 *Experimental set-up for carbon dioxide measurements.*

The desired concentrations of carbon dioxide were adjusted by mixing pure nitrogen and carbon dioxide using computer-controlled mass flow controllers (UNIT Instruments, Dublin, Ireland). Gas mixtures of different humidity were made using different combinations of two midget impingers with a constant flow rate of 500 $cm^3 \cdot min^{-1}$. The humidity of the sample gas stream was measured using a relative humidity meter (TH210, Eirelec, Dundalk, Ireland).

2.3. Theory

It was described in early literature that linear calibration plots can be obtained for solid carbon dioxide sensors by plotting the ratio of protonated and deprotonated pH-indicator against pCO_2 [21]. Either absorption or fluorescence intensity does correlate with protonation levels of pH-indicators in a solid matrix. The linearisation of FRET-based carbon dioxide sensors was presented in a very similar manner [18]. However, the theory used in these cases always relied on pH-indicators which had no spectral overlap with the donor when they were completely protonated. The absorption spectrum of fully protonated sudan III still overlaps the emission of the $Ru(dpp)_3^{2+}$ dye to some extent (Fig.2-4). Therefore, an important change to the present theory has to be introduced in order to convert the measured phase angles into a parameter which can linearly reflect the concentration of deprotonated sudan III in these FRET-based sensors. This important change is based on the fact that the overlap integral J presented in Fig. 2-3 can not be equal to zero when the dye is completely protonated. This change is presented in the following development of theory.

The ratio of the lifetimes τ_{max}/τ can be expressed as:

$$\frac{\tau_{\max}}{\tau} = \frac{K_F + K_{ET}}{K_F} \qquad (2\text{-}6)$$

where K_{ET} is the rate of energy transfer and K_F is the rate of all other deactivations, including luminescence. The lifetime τ_{max} cannot reflect the measured lifetime on complete protonation of the dye, because there still remains some energy transfer. However, it does reflect the donor lifetime measured if there is no sudan III co-immobilised in the membrane and therefore no energy transfer occurs. From Förster equations 2-3 to 2-5 it is known that the rate of energy transfer is proportional to the spectral overlap integral between donor emission and acceptor absorption ($K_{ET} \propto J$). Since the spectrum of protonated sudan III still overlaps the emission of ion-paired $Ru(dpp)_3^{2+}$ dye, the overlap integral J is proportional to the level of deprotonated pH-indicator plus a constant J_0 (Eq. 2-7). A sensor of defined and constant composition has a constant deactivation rate K_F which is not dependent on carbon dioxide levels.

$$\frac{\tau_{\max}}{\tau} - 1 = \frac{K_{ET}}{K_F} \approx J \approx \left[D^-\right] + J_0 \qquad (2\text{-}7)$$

This equation corresponds to the situation of dynamic quenching of luminescence as described by the Stern-Volmer equation. The constant J_0 which was necessary here is nothing else but the remaining overlap integral J between donor and acceptor when all of the pH-indicator dye is protonated. As mentioned above, the ratio of protonated to deprotonated pH-indicator dye (R_d) is linear to carbon dioxide partial pressure pCO_2:

$$R_d = \frac{[HD]}{\left[D^-\right]} = \frac{\left[HD_0\right] - \left[D^-\right]}{\left[D^-\right]} = K \cdot pCO_2 \qquad (2\text{-}8)$$

$[HD_0]$ corresponds to the total amount of sudan III in the sensing membrane, [HD] reflects the protonated and $[D^-]$ the deprotonated form of it. The combination of equations 2-7 and 2-8 leads to a linear correlation of the lifetime data and the corresponding pCO_2:

$$\frac{\left(\frac{\tau_{max}}{\tau_0}-1-J_0\right)-\left(\frac{\tau_{max}}{\tau}-1-J_0\right)}{\left(\frac{\tau_{max}}{\tau}-1-J_0\right)}=K\cdot pCO_2 \qquad (2\text{-}9)$$

where τ_0 is the very short decay time measured in absence of carbon dioxide. This equation can be changed and simplified using equation 2-1 in order to represent the measured phase angles of these lifetimes. Equation 2-10 represents this final version of theory for FRET-based pCO_2 sensors using sudan III:

$$R_d = K\cdot pCO_2 = \frac{\cot\phi_0 - \cot\phi}{\cot\phi - \cot\phi_{max}\cdot(1+J_0)} \qquad (2\text{-}10)$$

where ϕ_0 is the phase angle measured in absence of carbon dioxide, and ϕ_{max} is the phase angle measured when there is no sudan III dye co-immobilised with the $Ru(dpp)_3^{2+}$ donor.

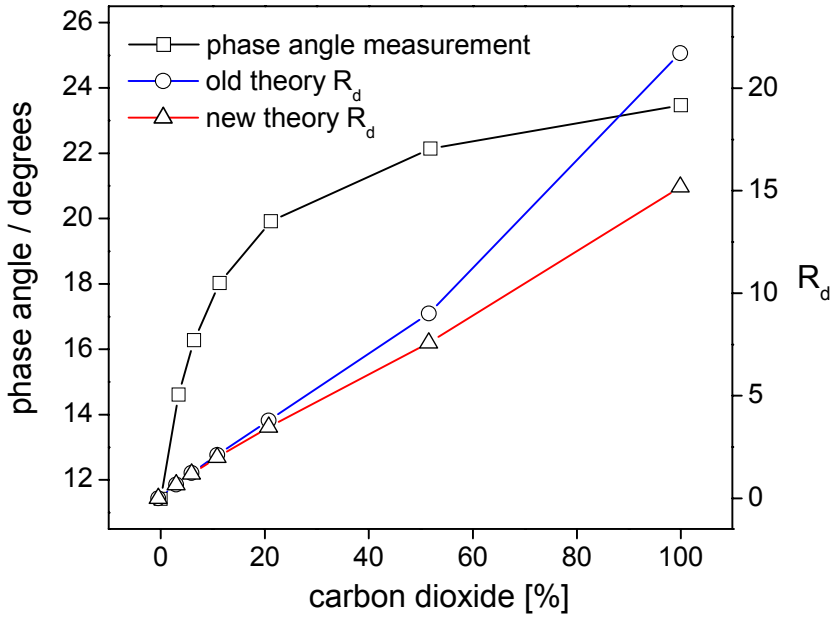

Fig. 2-12 *Example of sudan III sensor calibration plot in the phase domain (black). Phase angles were linearised using the published old theory (blue) and the newly developed theory (red) of calculating the ratio of protonated to deprotonated pH-indicator dye (R_d).*

The new theory was tested and compared to the old theory. Fig. 2-12 illustrates in black the phase response of a sensor from zero to 100% carbon dioxide. The old theory presents the linearised calibration plot (blue) with a bad correlation factor (r^2=0.9896). The new corrected theory (red) strongly improved this linearisation which achieved a better correlation factor of r^2=0.9990.

2.4. Characterisation

2.4.1. Sensitivity

It has been reported that the concentration of the donor in the matrix has almost no effect on the sensor calibration [18]. The only effect that a concentration increase of the donor offers is the improvement of the signal-to-noise ratio by increasing the fluorescence signal intensity. However, the concentration of the pH-indicator was reported to have a strong influence on the energy transfer rate between the donor and acceptor. For these reasons, the influence of the sudan III concentration in the membrane on the sensitivity of the sensor was investigated. Fig. 2-13 shows the relation between the acceptor concentration in the matrix and the absolute phase signal change between 100% nitrogen and 100% carbon dioxide (membranes **S0** – **S6**). The total phase difference reaches its maximum of about 11.2 degrees at a sudan III concentration of 7.03 mmol kg^{-1}, after which it remains constant. A further increase of the concentration does not extend the total phase difference, but it shifts the useful measurement range of the sensor towards higher carbon dioxide concentrations.

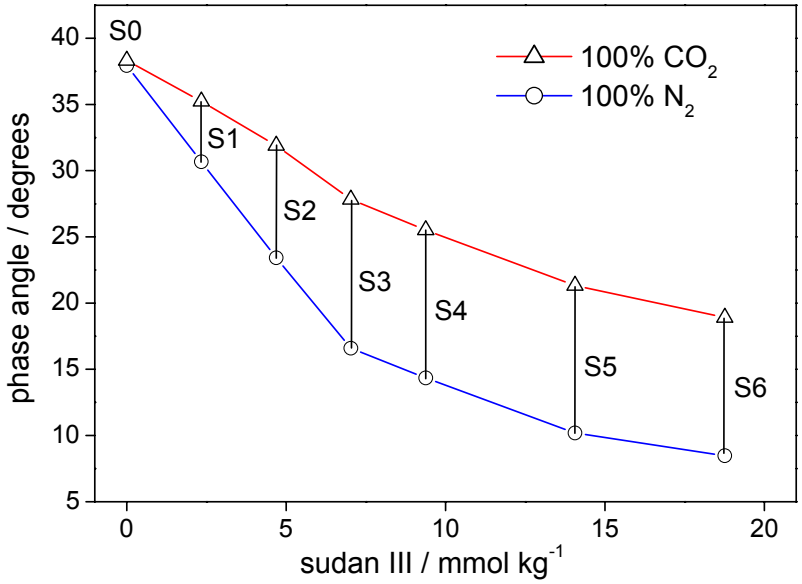

Fig. 2-13 *Absolute phase response of sensor membranes **S0** – **S6** in the absence (blue) and presence (red) of carbon dioxide (100%).*

Unfortunately, the increase in acceptor concentration also results in a higher inner filter effect, thereby decreasing the detected luminescence intensity and the signal-to-noise ratio [18]. Bearing in mind the above points, a concentration of 14.06 mmol kg^{-1} was found to be optimal (membrane **S5**). A further effect visible in Fig. 2-13 is the strong decrease of the phase signal in 100% carbon dioxide with increasing acceptor concentration, indicating that there still is a considerable rate of energy transfer at 100% carbon dioxide. This can be explained by the partial overlap with the $Ru(dpp)_3(TSPS)_2$ emission spectrum, which the protonated form of sudan III displays in Fig. 2-4.

The sensor performance of the membranes with the fixed concentrations of donors, acceptors and TOA-OH was then tested. Fig. 2-14 displays the phase response and recovery behaviour of sensor membrane **S5**. The resulting phase calibration plot was linearised using equation 2-10 and this is shown in Fig. 2-15.

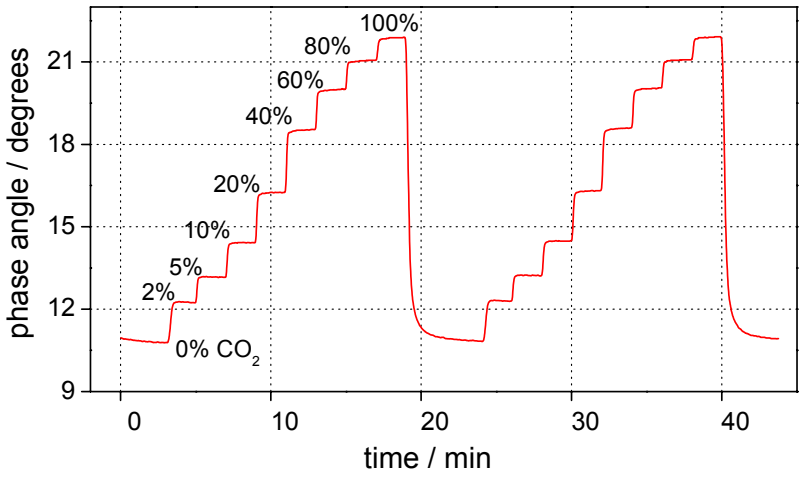

Fig. 2-14 *The phase response of sensor membrane **S5** to 0, 2, 5, 10, 20, 40, 60, 80 and 100% carbon dioxide.*

The sensor displays a fast response and a fully reversible phase difference of 11.2 degrees between 100% N_2 and 100% CO_2. The measured response time, which lies in the order of 20 – 30 seconds, is determined by the equilibration time of the midget impingers and the dead volume of the gas tubes, rather than the true response time of the sensor membrane.

The dynamic range is sufficiently high to guarantee a resolution of ± 1% up to 50% CO_2 and ± 2% above that level. A conservative estimate for the limit of detection (LOD) was found to be 0.06% CO_2, calculated as three times the standard deviation (3σ).

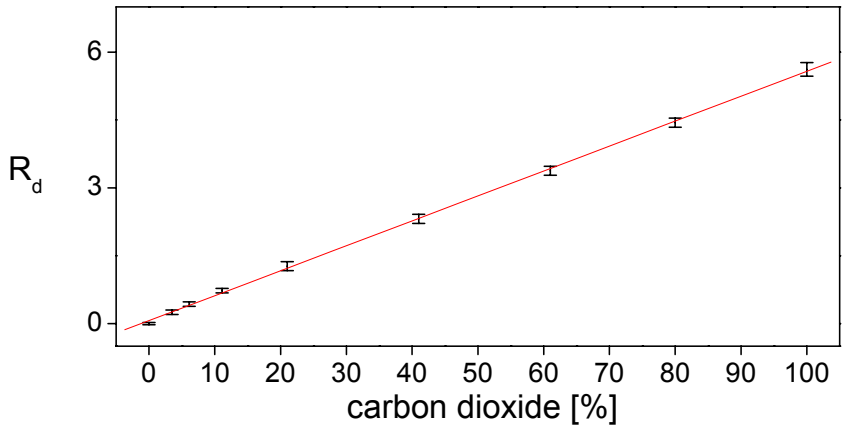

Fig. 2-15 *Linearised phase calibration plot for the **S5** membrane.*

A preliminary spot reproducibility test for the spin-coated sensor membrane yielded a maximum standard deviation of ±1.6% of the total phase signal (n=10). The shelf life of the membranes, if kept in ambient conditions, in the dark, and away from detrimental influences like SO_2 or HCl, is longer than three months, during which a slight drift in sensitivity was observed (< 5%). However, there is no need for the presence of sodium carbonate or similar sinks for volatile acidic compounds in the storage bags, as was reported for previous FRET-based pCO_2 sensors [18].

2.4.2. Temperature Dependence

It is well known that temperature can influence the sensitivity of solid-type carbon dioxide sensors [20,21]. It was therefore necessary to establish how strongly the sensor reported here is influenced by this parameter. Phase calibration curves were recorded between 10ºC and 35ºC in steps of five degrees. These data were linearised according to equation 2-10 in order to obtain a set of straight lines, from which the equilibrium constants K of the sensing reaction could be determined.

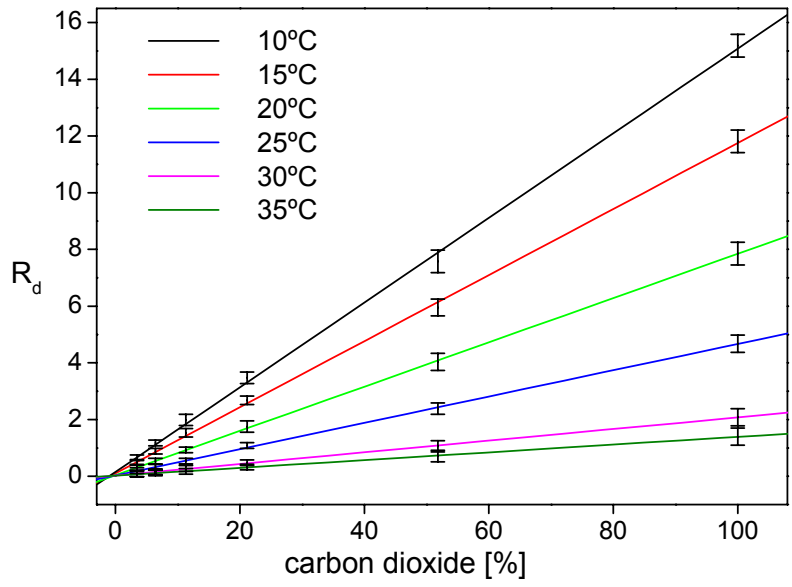

Fig. 2-16 *Calibration plots for membrane **S5** showing its behaviour over a range of different temperatures between 10ºC and 35ºC in steps of five degrees.*

Fig. 2-16 shows the phase angle pCO_2 calibration curves at different temperatures. As expected the sensitivity decreases with increasing temperature caused by the decrease of carbon dioxide solubility in the sensor film.

According to the temperature dependence of equilibrium constant K given by Arrhenius equation (Eq. 2-11), a plot can be generated where calibration curve gradients versus temperature result in a straight line.

$$\ln K = \ln A - \frac{E_A}{R \cdot T} \qquad (2\text{-}11)$$

Therefore, a plot of ln K versus 1/T should be linear and yield ln A from the intercept and $-E_A/R$ from the gradient, where A is the pre-exponential factor, R is the universal gas constant and E_A is the activation energy of the sensing reaction [27]. According to activated complex theory, the activation enthalpy ΔH is equal to E_A in this case, and if data is plotted in the per cent scale, the activation entropy ΔS can be calculated from ln A as follows:

$$\Delta S = R \cdot \left(\ln A + \ln 100\right) \qquad (2\text{-}12)$$

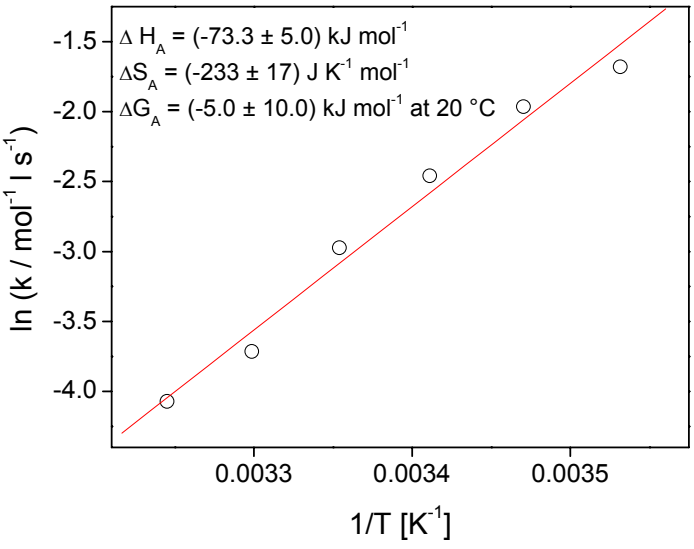

Fig. 2-17 *Arrhenius plot for the **S5** membrane with fitting parameters.*

The Gibbs energy ΔG, which is expected to be negative, is calculated from activation enthalpy ΔH and activation entropy ΔS using equation 2-13:

$$\Delta G = \Delta H - T \cdot \Delta S \qquad (2\text{-}13)$$

A linear correlation was found between 1/T and ln K (r=0.99024), and the analysis according to the Arrhenius equation yielded an activation enthalpy ΔH = -73.3±5.0 kJ mol^{-1} and an entropy term of -233±17 J K^{-1} mol^{-1}. As expected, both are large negative values [27]. Gibbs entropy at 20°C was calculated as –5.0±10.0 kJ mol^{-1}. The negative value for ΔH indicates that the sensitivity of the membranes is greater at lower temperatures, which is apparent from Fig. 2-16 as well. This fact has been explained previously by the higher solubility of carbon dioxide in the matrix at lower temperatures [18].

2.4.3. Humidity Dependence

Humidity can have a pronounced influence on the sensitivity of some solid-type carbon dioxide sensors, especially when immobilised in un-plasticised ethyl cellulose or sol-gel material [20,23]. Fig. 2-18 shows linearised phase calibration functions which were recorded at three different humidity levels.

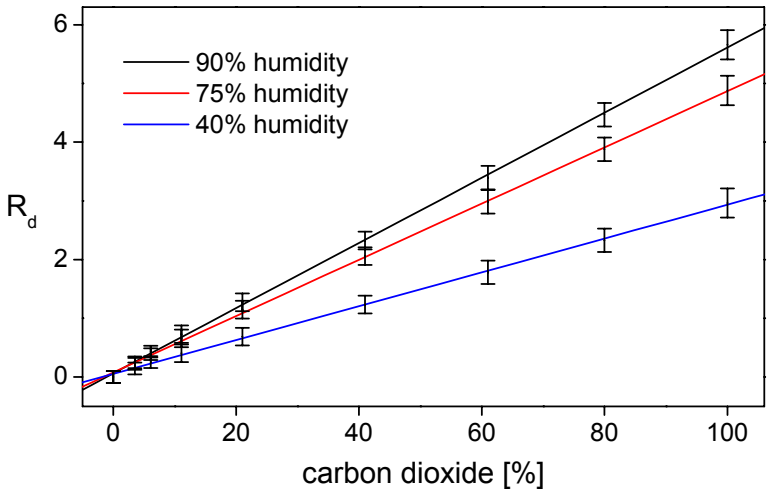

Fig. 2-18 *Linearised phase calibration plots for membrane **S5** at three different humidity levels.*

The sensor membrane shows an increase in sensitivity with increasing humidity levels of the gas. However, this sensor shows no sensible response at zero percent humidity. This strong humidity dependence, which is absent from plastic carbon dioxide sensors in very hydrophobic polymers, appears to be a disadvantage, and indicates that the sensor would be best employed in atmospheres of high and fixed relative humidity (e.g. food packaging technology).

2.4.4. Oxygen Cross-Sensitivity

The spectral compatibility of $Ru(dpp)_3(TSPS)_2$ with sudan III, as well as its long lifetime (~ 5 μs) and high quantum yield make it an excellent candidate for use as a donor luminophore in the carbon dioxide sensor. In common with many ruthenium polypyridyl complexes, however, its fluorescence intensity and decay time are strongly quenched by molecular oxygen [4,28]. Neurauter et al. used a ruthenium polypyridyl complex with a shorter decay time (~2.0 μs) [18] to reduce oxygen cross-sensitivity to 1.3 degrees quenching in 18% oxygen at a modulation frequency 45 kHz. Furthermore, they encountered a dramatically increased rate of photobleaching in the presence of oxygen. The reason for this enhanced photobleaching effect is the oxidative destruction of the thymol blue acceptor dye by reactive singlet oxygen.

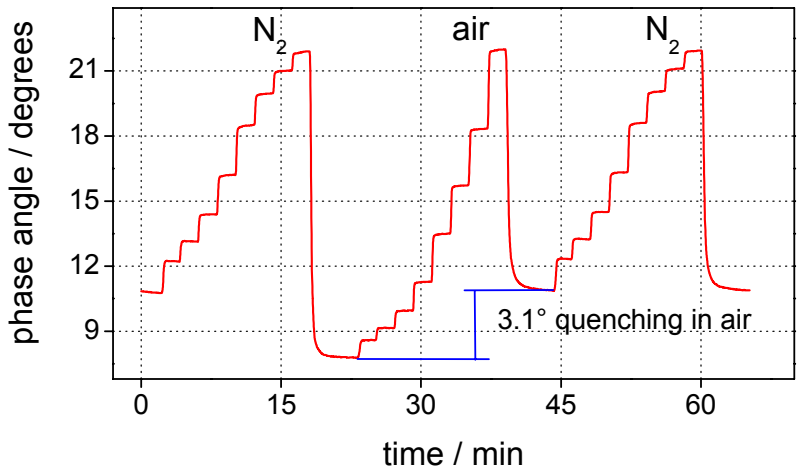

Fig. 2-19 *The phase response of sensor membrane **S5** using nitrogen and air (21% O_2) as carrier gases for carbon dioxide experiments.*

In order to test the oxygen cross-sensitivity for the membranes reported here, a comparison was made between calibration cycles, which were recorded with nitrogen and air, respectively, as carrier gases (Fig. 2-19). The sensor membrane **S5** displayed oxygen quenching of 3.1 degrees in 100% air (21% O_2) as compared to 100% nitrogen. This higher oxygen cross-sensitivity is caused by the longer lifetime of the donor complex. Strategies to minimise oxygen cross-sensitivity may include the use of gas-impermeable nano-particles doped with the reference luminophore [29], or application of oxygen-impermeable sol-gel materials [30]. However, no measurable photobleaching was encountered during the calibration experiments with the alternating carrier gases (>2h). This result suggests that the sudan III dye offers a far better photostability than the commonly used sulphonephthaleine indicator dyes.

2.4.5. Results

A lifetime-based pCO_2 sensor is presented which exploits radiationless energy transfer from a ruthenium complex to the new pH-indicator sudan III. The decay time in the range of 5 μs allows frequency domain sensing at a low modulation frequency (20 kHz), using an inexpensive light source (LED) and photodiode.

The sensor presented exhibits a fast and reversible response to carbon dioxide over a wide range of concentrations. The use of the pH-sensitive disazo dye sudan III has dramatically increased the dynamic range up to 100% CO_2 with a resolution of ±2%. However, it is capable of detecting concentrations as low as 0.06% CO_2. The use of Fluorescence Resonance Energy Transfer has enabled the sensor to gain some of the advantages of lifetime-based sensor technology, and to be interrogated using the low-cost phase fluorometric measurement technique.

The maximum phase signal detected between 0 and 100% carbon dioxide is 11.2 degrees (20ºC) at a modulation frequency of 20 kHz. The optimum sudan III concentration in the matrix was found to be 14.05 mmol kg^{-1}. Photostability and shelf life of the sensor membranes have improved compared to previous FRET-based carbon dioxide sensors. Limiting factors to the application of the sensor presented here are an elevated cross-sensitivity to molecular oxygen and a strong dependence on changes in the humidity and temperature levels.

2.5. Improvement Strategies

While adequate performance has been demonstrated by the sensor presented here, it exhibits only moderate sensitivity at higher concentrations and is strongly quenched by molecular oxygen. These issues could be addressed through a number of improvement strategies and these are detailed here.

One strategy to further improve the sensitivity may be the replacement of Sudan III acceptor dye using other organic dyes from the same dye family. There are several dyes available which all contain methyl-groups in various positions around the Sudan III basic structure. However, these methyl groups push pH-indicators to higher sensitivity, which leads to CO_2 sensors with a more narrow detection range (Fig. 2-20). Therefore, the Sudan III dye already represents the pH-indicator of that family with the lowest pK_A value available.

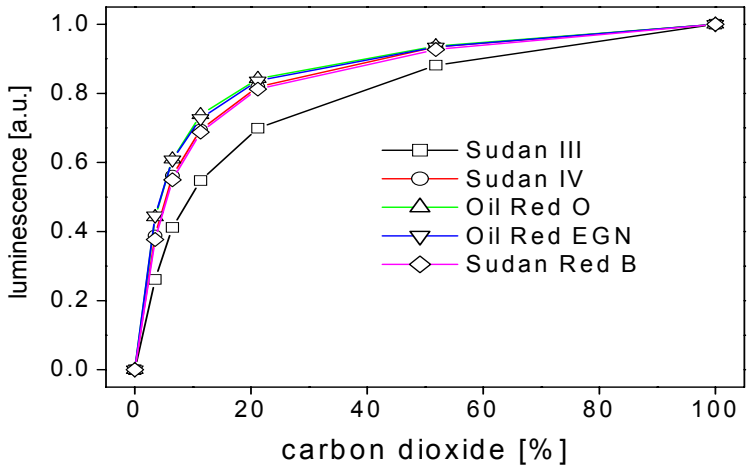

Fig. 2-20 *Normalised phase calibration plots for FRET-based carbon dioxide sensor films using the sudan III and four different members of this family of dyes in an ethyl cellulose membrane.*

Cross-sensitivity by molecular oxygen might be removed by using doped nano-particles which realise a sufficient distance to allow energy transfer. The $Ru(dpp)_3^{2+}$ donor is encapsulated in PAN-nanospheres SPR-1 with an average diameter of 50 nm still realising a sufficient distance to allow energy transfer [31]. Although the 28% cross sensitivity for oxygen can be reduced to 11%, the signal available from this set-up is not as good as seen previously (Fig. 2-21).

This new sensor membrane only offers 42% of the signal achieved by the membrane using $Ru(dpp)_3(TSPS)_2$ outside of particles. Although this approach removes some of the oxygen cross sensitivity problem, it reduces the sensor signal far too low to be considered for an application in modified atmosphere packaging.

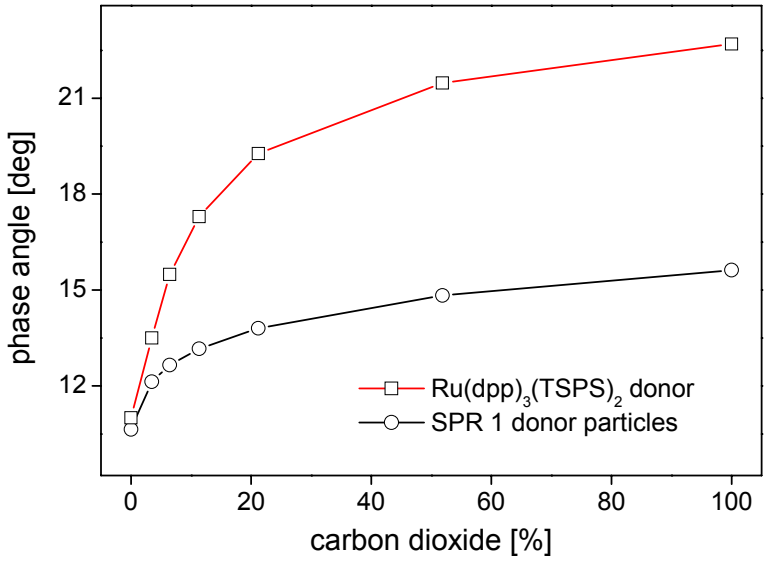

Fig. 2-21 *Phase calibration plots for FRET-based carbon dioxide sensor films using SPR 1 donor particles (black) and $Ru(dpp)_3(TSPS)_2$ (red).*

2.6. Conclusion

Although this FRET-based carbon dioxide sensor successfully introduced luminescence lifetime-based carbon dioxide sensing up to 100%, it suffers from several disadvantages which make it unsuitable for application in modified atmosphere packaging [32]. However, there was recently introduced a new method which can overcome the problems encountered by the energy transfer method. Dual luminophore referencing is the promising method of lifetime-based sensing without oxygen cross-sensitivity [29].

2.7. References

1 Lakowicz, J. *Principles of Fluorescence Spectroscopy*, **1983**, Plenum Press, New York / London, 257

2 Klimant, I.; Beiser, P.; Wolfbeis, O. *Talanta*, **1994**, *41*, 985

3 Holst, G.; Köster, T.; Voges, E.; Lübbers, D. *Sens. Actuators B*, **1995**, *29*,

4 McDonagh, C.; Kolle, C.; McEvoy, A.; Dowling, D.; Cafolla, A.; Cullen, S.; MacCraith, B. *Sens. Actuators B*, **2001**, *74*, 124231

5 Lippitsch, M.; Pusterhofer, J.; Leiner, M.; Wolfbeis, O. *Anal. Chim. Acta*, **1988**, *205*, 1

6 Sipior, J.; Randers-Eichhorn, L.; Lakowicz, J.; Carter, G.; Rao, G. *Biotechnol. Prog.*, **1996**, *12*, 266

7 Förster, T. *Ann. Phys.* **1948**, *2*, 55

8 Selvin, P. *Methods Enzymol.*, **1995**, *246*, 300

9 Lakowicz, J.; Szmacinski, H.; Karakelle, M. *Anal. Chim. Acta*, **1993**, *272*, 179

10 Thompson, R.; Frisoli, J.; Lakowicz, J. *Anal. Chem.* **1992**, *64*, 2075

11 Bambot, S.; Sipior, J.; Lakowicz, J.; Rao, G. *Sens. Actuators B*, **1994**, *22*, 181

12 Preininger, C.; Mohr, G. *Anal. Chim. Acta,* **1997**, *342*, 207

13 Kosch, U.; Klimant, I.; Werner, T.; Wolfbeis, O. *Anal. Chem.*, **1998**, *70*, 3892

14 Huber, C.; Werner, T.; Krause, C.; Klimant, I.; Wolfbeis, O. *Anal. Chim. Acta*, **1998**, *364*, 143

15 Krause, C.; Werner, T.; Huber, C.; Klimant, I.; Wolfbeis, O. *Anal. Chem.*, **1998**, *70*, 3983

16 Wolfbeis, O.; Klimant, I.; Werner, T.; Huber, C.; Kosch, U.; Krause, C.; Neurauter, G.; Dürkop, A. *Sens. Actuators B*, **1998**, *51*, 17

17 Mohr, G.; Draxler, S.; Trznadel, K.; Lehmann, F.; Lippitsch, M. *Anal. Chim. Acta,* **1998**, *360*, 119

18 Neurauter, G.; Klimant, I.; Wolfbeis, O. *Anal. Chim. Acta*, **1999**, *382*, 67

19 Green, F. *The Sigma-Aldrich Handbook of Stains, Dyes and Indicators*, Aldrich Chemical Company, Milwaukee, **1990**, 656

20 Mills, A.; Eaton, K. *Quimica Analitica*, **2000**, *19*, 75

21 Mills, A.; Chang, Q.; McMurray, N. *Anal. Chem.*, **1992**, *64*, 1383

22 Mills, A.; Chang, Q. *Anal. Chim. Acta*, **1994**, *285*, 113

23 Malins, C.; MacCraith, B. *Analyst*, **1998**, *123*, 2373

24 Wolfbeis, O.; Weis, L.; Leiner, M.; Ziegler, W. *Anal. Chem.*, **1988**, *60*, 2028

25 Chang, Q.; Randers-Eichhorn, L.; Lakowicz, J.; Rao, G. *Biotechnol. Prog.*, **1998**, *14*, 326

26 Raemer, D.; Walt, D.; Munkholm, C. *US Pat.*, 5005 572, **1991**

27 Mills, A.; Lepre, A.; Wild, L. *Sens. Actuators B*, **1997**, *419*, 38

28 McDonagh, C.; MacCraith, B.; McEvoy, A. *Anal. Chem.*, **1998**, *70*, 45

29 von Bültzingslöwen, C.; McEvoy, A.; McDonagh, C.; MacCraith, B.; Klimant, I.; Krause, C.; Wolfbeis, O. *Analyst*, **2002**, *127*, 1478

30 Kosch, U.; Klimant, I.; Wolfbeis, O. *Fresenius J. Anal. Chem.*, **1999**, *364* , 48

31 http://www.optosense.de/

32 von Bültzingslöwen, C.; McEvoy, A.; McDonagh, C.; MacCraith, B. *Anal. Chim. Acta*, **2003**, *480*, 275

3. Dual Luminophore Referencing

3.1. DLR-Introduction

Many luminescence intensity sensors for ionic species, oxygen, pH, carbon dioxide and other analyte gases have been published in the past [1-6]. Although this type of sensor provides good sensitivity and selectivity for analytes, intensity measurement is susceptible to a variety of interfering factors. Fluctuations in the optoelectronic system can cause a signal drift, while a damage or position change of the sensitive coating can equally cause signal alterations. Furthermore, measurement in scattered, coloured or turbid media and changes in the refractive index will lead to signal fluctuations. Leaching and photobleaching will also have an effect on the intensity reading.

One approach to overcome this problem, in the case of pH or CO_2 sensing, is the use of fluorophores with different emission spectra in protonated and deprotonated form, which allow ratiometric measurement at both emission wavelengths [7]. Another way is the use of fluorophores with different absorption spectra, but identical emission spectra in their acidic and alkaline forms [8]. These ratiometric luminescence intensity measurements solve problems associated with indicator leaching and photobleaching. However, drift referencing caused by the optoelectronic system or from changes in the detection path is not possible. Nevertheless, these problems occurring in intensity-based measurements are overcome to a large extent by fluorescence decay time measurements [9-11]

Most reported fluorescence-based optical carbon dioxide sensors rely on the intensity change of a luminescent pH-indicator such as 1-hydroxypyrene-3,6,8-trisulfonate (HPTS), but the very short decay times of such species cannot be measured by the low-cost phase modulation techniques used for oxygen sensors [5,12,13]. Ruthenium complexes with pH-sensitive ligands, which were used for the design of lifetime-based CO_2 sensors, have been reported [14]. However, their decay times are comparatively low, and their dynamic range is not high enough for the application targeted here. As reported in the previous chapter, Fluorescence Resonance Energy Transfer (FRET) from a long-lifetime donor to a pH-sensitive

acceptor has been employed to produce carbon dioxide sensor membranes that are compatible with existing oxygen sensor technology [15,16]. Limitations to this approach, however, include the lack of a suitable acceptor dye for achieving the desired dynamic range (0 – 100% CO_2), low signal to noise ratio and a susceptibility to signal drift.

Recently, however, a novel sensing scheme has been introduced that offers the possibility to overcome some of the problems normally associated with luminescence intensity-based sensors [17-23]. Dual Luminophore Referencing (DLR) is an internal ratiometric method whereby the analyte-sensitive fluorescence intensity signal is converted into the phase domain by co-immobilising an inert long-lifetime reference luminophore with similar spectral characteristics. Moreover, the detected phase signal provides an indirect referenced intensity measurement. Excitation and emission wavelengths of ruthenium complexes and the HPTS dye are sufficiently well matched to make them excellent candidates for a DLR-type carbon dioxide sensor that exhibits excellent compatibility with phase fluorometric oxygen sensor technology [20]. However suitable the ruthenium dyes are as reference luminophores, their extremely good quenchability by molecular oxygen creates a cross-sensitivity problem of the resulting membranes. This problem has been minimised by incorporation of the ruthenium dye in nano-beads of very low oxygen permeability [17,24].

In the DLR sensing scheme, two luminophores are incorporated into the sensing membrane. The indicator has a short decay time (τ_{ind}), whereas the reference dye has a long decay time (τ_{ref}) which is ideally unaffected by either carbon dioxide or oxygen, because it is contained in an impermeable polymer matrix. The two luminophores have overlapping excitation and emission spectra, so that they can be excited at the same wavelength, and their fluorescence can be detected using the same photodetector-filter combination. In this DLR referencing scheme, two different luminescence signals are generated in the sensing membrane, which can be represented as two single sine wave signals as indicated in Fig. 3-1. The total signal amplitude (total signal) is a superposition of the two signals generated by the analyte-sensitive fluorophore (indicator) and the inert reference luminophore (reference).

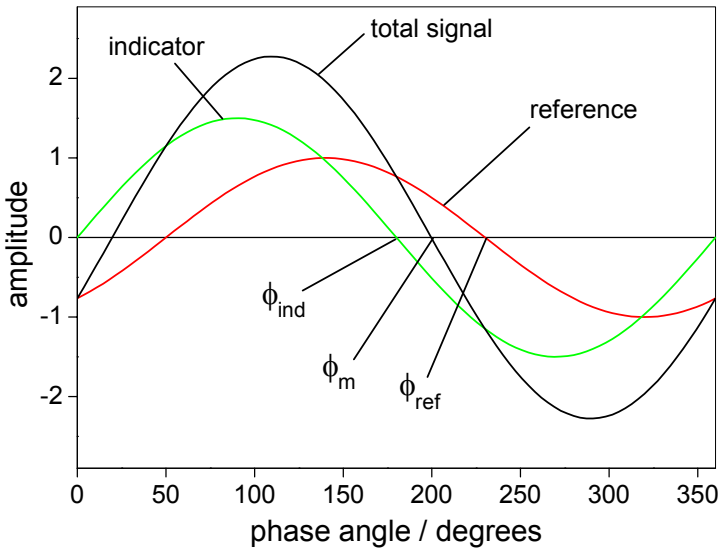

Fig. 3-1 *Single sine wave signals generated by the reference luminophore (red) and the analyte-sensitive luminophore (green). The superposition of the two signals represents the detected signal (black). The reference phase angle (ϕ_{ref}) and the indicator phase angle (ϕ_{ind} = 0) remain constant. The total luminescence phase angle (ϕ_m) is a function of the amplitude of the indicator signal in the presence and absence of CO_2.*

The indicator signal has a phase angle $\phi_{ind} \approx 0$ due to its very short lifetime, whereas, in the absence of oxygen quenching, the signal of the reference has a constant amplitude and phase angle ϕ_{ref}, determined by the modulation frequency f and its decay time τ. The superposition of the two signals will result in a non-zero phase angle ϕ_m of the total measured signal. When the indicator signal changes its amplitude in response to the concentration of carbon dioxide, the phase angle ϕ_m of the total signal will change accordingly. Thus, ϕ_m may be correlated with the indicator fluorescence intensity, and it can be calculated using

$$N_m = \sum A_i \cdot \sin \phi_i \qquad (3\text{-}1)$$

$$D_m = \sum A_i \cdot \cos \phi_i \qquad (3\text{-}2)$$

where N_m and D_m are the sine and cosine transforms of the intensity decays [19], A_i refers to the fractional amplitude and ϕ_i is the phase angle of each fluorophore. The phase ϕ_m for a multi-exponential decay is:

$$\tan \phi_m = N/D \tag{3-3}$$

Assuming a mono-exponential decay for both luminophores, the values of N and D are

$$N = A_m \cdot \sin \phi_m = A_{ref} \cdot \sin \phi_{ref} + A_{ind} \cdot \sin \phi_{ind} \tag{3-4}$$

$$D = A_m \cdot \cos \phi_m = A_{ref} \cdot \cos \phi_{ref} + A_{ind} \cdot \cos \phi_{ind} \tag{3-5}$$

where A_m is the measured amplitude at a given frequency, and the indices *ind* and *ref* stand for the short lifetime (τ_{ind}) and long lifetime (τ_{ref}) phase signals and their components.

Provided that both luminophores have very different decay times, only the long lived reference luminophore undergoes a phase modulation, whereby the short delayed analyte sensitive luminophore remains non-modulated.

This simplification yields:

$$\phi_{ind} = 0 \tag{3-6}$$

where τ and the modulation frequency are small.

When eq. (3-6) is introduced into eqs. 3-4 and 3-5 the sine and cosine transforms of intensity decays respectively become:

$$N = A_m \cdot \sin \phi_m = A_{ref} \cdot \sin \phi_{ref} \tag{3-7}$$

$$D = A_m \cdot \cos \phi_m = A_{ref} \cdot \cos \phi_{ref} + A_{ind} \tag{3-8}$$

Finally, converting tan ϕ_m in eq. 3-3 into cot ϕ_m and substituting N and D with eqs. 3-7 and 3-8, a relationship between the measured phase angle ϕ_m and the amplitude ratio A_{ind}/A_{ref} is obtained:

$$\cot\phi_m = \cot\phi_{ref} + \frac{1}{\sin\phi_{ref}} \cdot \frac{A_{ind}}{A_{ref}} \qquad (3\text{-}9)$$

Therefore, cot ϕ_m reflects the referenced intensity of the fluorescence indicator. If ϕ_{ref} is constant and known, there is a linear relationship between cot ϕ_m and A_{ind}/A_{ref}. Consequently cot ϕ_m does not relate to overall signal intensity. As depicted in eq. 3-9, it linearly depends on the *amplitude ratio* of the two signals A_{ind}/A_{ref}, thereby referencing out any drifts that might occur due to power fluctuations or temperature changes.

This DLR method has recently been used for the development of lifetime-based sensors for pH [19,20,23], ions [17,19,20,22], amines [21] and carbon dioxide [20]. However, the previously published optical CO_2 sensor based on DLR only offers good sensitivity in a very low concentration range (0-3%). Therefore the work presented in this chapter deals with the development of a DLR-based carbon dioxide sensor with a concentration range up to 100% CO_2 [25].

3.2. Experimental

3.2.1. pH-Indicator

The dynamic range of a carbon dioxide sensor depends on the type of buffer system used and on the pK_A-value of the pH-indicator. The development of a DLR-based carbon dioxide sensor, using a long-lifetime ruthenium complex and having a dynamic range up to 100% CO_2, requires a luminescent pH-indicator with excitation and emission spectral properties similar to the ruthenium complex, and a just over neutral pK_A-value. In order for the reference luminophore and the fluorescent pH-indicator to be compatible with the DLR sensing scheme, there are some requirements that need to be fulfilled. The emitters must have widely different decay times (e.g. in ns and μs range), so that

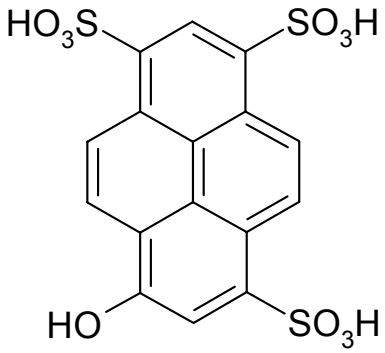

Fig. 3-2 *1-hydroxypyrene-3,6,8-trisulfonate (HPTS)*

only the long-lived luminophore shows a measurable phase shift with respect to the excitation LED signal. 1-Hydroxypyrene-3,6,8-trisulfonate (HPTS) is a pH-sensitive luminophore and thus is pCO_2-sensitive, which fulfils the criteria for the short-lived luminophore in the DLR sensing scheme (Fig. 3-2).

HPTS has been used extensively for optical chemical carbon dioxide and pH sensors due to its pK_A value (~7.3), a large Stokes shift, good photostability, high quantum yield and spectral compatibility with blue LEDs [5,12,13,26]. For the same reasons, it was chosen as the analyte-sensitive indicator for this carbon dioxide sensor. As is shown in Fig. 3-3, $Ru(dpp)_3^{2+}$ fluorescence is excitable in the same region as HPTS, and both match the blue LED emission spectrum excellently. The decay time of HPTS luminescence in a solid matrix is very short (~1 ns), so its application as a pH-indicator in DLR carbon dioxide sensing scheme is good, and eq. 3-9 is valid for it.

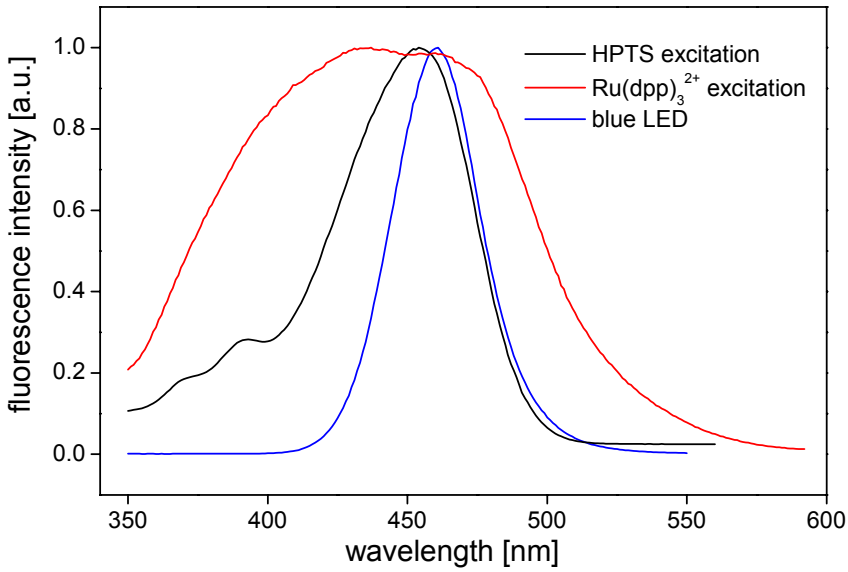

Fig. 3-3 *Fluorescence excitation spectra of $Ru(dpp)_3^{2+}$ immobilised in polymer nano-beads (red) and HPTS in MTEOS (black). Both luminophores can be excited by a single light source, represented by the blue LED emission spectrum (blue).*

The two emission peaks, however, are significantly separated (Fig. 3-4). Nonetheless, introduction of a suitable long-pass filter (LEE 135) provides enough of

the HPTS luminescence in the photodiode signal to ensure good functionality of the sensor, but at the same time prevents any blue light from reaching the detector.

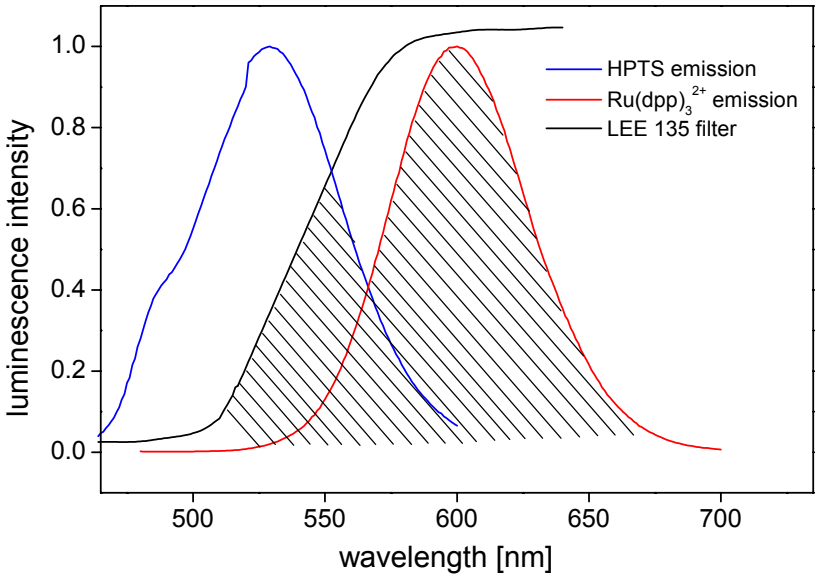

Fig. 3-4 *Fluorescence emission spectra of $Ru(dpp)_3^{2+}$-doped nano-beads (red) and HPTS in MTEOS (blue). Also shown is the transmission cut-off point of the LEE 135 long-pass filter (black). The hatched area corresponds to the total luminescence signal detected by the photodiode.*

3.2.2. Reference luminophore

The reference luminophore must have similar spectral properties to HPTS, apart from being chemically inert towards carbon dioxide and having a suitably long lifetime. The spectral compatibility of $Ru(dpp)_3^{2+}$ with HPTS (Figs. 3-3 & 3-4), as well as its long lifetime (~ 5 μs) and high quantum yield make it an excellent candidate for use as reference luminophore in the carbon dioxide sensor. In common with many ruthenium polypyridyl complexes, however, its fluorescence intensity and decay time are strongly quenched by molecular oxygen [27-29].

Due to the nature of the proposed application, it was therefore necessary to encapsulate the $Ru(dpp)_3^{2+}$ in a matrix that leaves its spectral characteristics largely unchanged, while protecting it from the effect of concentrations of molecular oxygen such as may be encountered inside food packages. Such encapsulation of $Ru(dpp)_3^{2+}$ in PD-1 nanoparticles of the oxygen-impermeable polymer poly(acrylonitrile) was performed by OptoSense [24]. Superior performance, however, was achieved by using doped sol-gel particles. These TEOS-based $Ru(dpp)_3^{2+}$-doped particles are fabricated by us, and their performance is compared with that of the polymer nanoparticles in Chapter 5.

3.2.3. Base

A second precondition for a carbon dioxide sensor for application in food packaging technology is that it provides sufficient sensitivity over the complete range of CO_2 concentrations that are encountered in MAP gases (0–100%). The majority of reported optical chemical carbon dioxide sensors, however, only provide sufficient sensitivity up to ca. 10% CO_2 [5,12-15]. The sensitivity of a carbon dioxide sensor is linked to the equilibrium constant of the pH indicator used (pK_A) and to the nature of the buffer that surrounds it [29]. The first generation of optical carbon dioxide sensors, which contained an aqueous hydrogen carbonate buffer, was later replaced by solid sensor membranes [30]. Solid-type carbon dioxide sensors do not contain a classic aqueous buffer system, but they contain a quaternary ammonium hydroxide, mostly tetraoctylammonium hydroxide (TOA-OH), in a hydrophobic membrane.

It is possible that the size and shape of the ammonium cation can affect the HPTS pH-indicator sensitivity by influencing how strongly the positive charge is shielded from the protonable group. Therefore, it seems possible to reduce the sensitivity of the sensor by replacing TOA-OH with a smaller or less spherical quaternary ammonium base. Tetrabutylammonium hydroxide (TBA-OH) represents a readily available candidate for a smaller, but still spherical ammonium base.

Next to TOA-OH, cetyltrimethylammonium hydroxide (CTA-OH) is, to our knowledge, the only other quaternary ammonium base that has been reported for solid carbon dioxide sensors [26,31]. In order to ensure a DLR-based CO_2 sensor with a high enough sensitivity, a range of five different available quaternary ammonium hydroxides was tested. Two easily accessible quaternary ammonium

hydroxides, tetradecyl-trimethylammonium hydroxide (TDTA-OH) and tetra-decylammonium hydroxide (TDA-OH), were included in this analysis. In this work, all four were tested as internal buffers in simple HPTS intensity-based membranes and compared to a classical TOA-OH membrane as can be seen in Fig. 3-5.

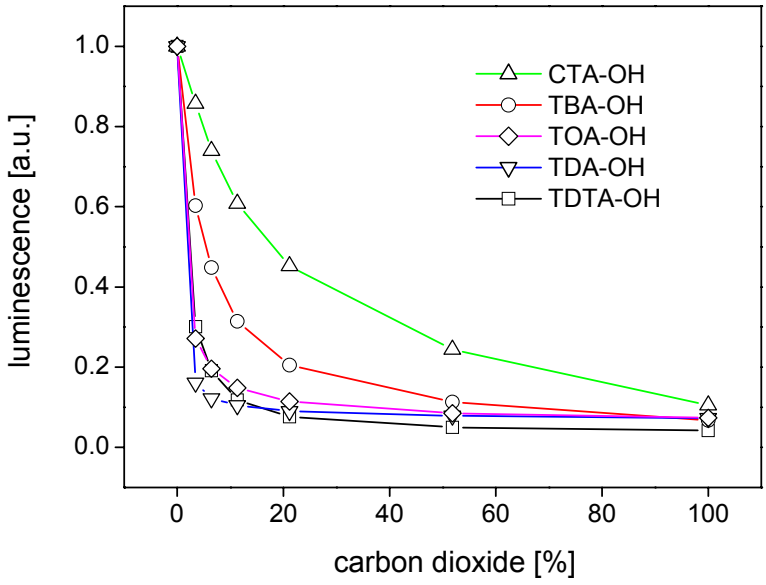

Fig. 3-5 *Calibration plots for FRET-based carbon dioxide sensor films using the five tested quaternary ammonium bases and the HPTS pH-indicator.*

There are clearly only two of these ammonium bases which provide a high enough carbon dioxide sensitivity for this sensor. The graph shows that TBA-OH indeed increased the dynamic range substantially, but response and recovery times were found to be more than twice as long than previously experienced with TOA-OH membranes. The CTA-OH membranes, surprisingly, showed not only an increased dynamic range compared to both TOA-OH and TBA-OH, but their response and recovery times were substantially shorter also. Because of these clear advantages, CTA-OH was chosen as the internal buffer for all the following sensor membranes. It has to be added, however, that this effect is probably restricted to HPTS and definitely cannot be duplicated by using phenolphthalein derivatives, which are the majority of pH-indicators used for colourimetric carbon dioxide sensors (thymol blue, cresol red, etc.) [29]. The absorption spectra recorded from the films containing CTA-OH as base, exhibited a bathochromic shift of 18 nm compared with that

measured in aqueous solution. This shift provides supporting evidence for the formation of closely associated ion-pairs between HPTS and CTA-OH.

3.2.4. Preparation

A solution of cetyltrimethylammonium hydroxide (CTA-OH) in methanol (0.66 $mol \cdot l^{-1}$) was prepared as reported elsewhere [31]. 75 mg of the doped nano-beads were suspended in 4.0 ml of MTEOS and stirred for 70 hours. Then, 1.45 ml of 0.1 N hydrochloric acid was added while stirring rapidly until the two phases mixed and hydrolysis and condensation reactions started. After further stirring for two hours, 30 mg HPTS (5.7×10^{-5} mol) dissolved in 5 ml CTA-OH solution were added, and the whole cocktail was saturated with carbon dioxide in order to delay the gelling process thus facilitating deposition onto the substrate.

A portion of 7% of the CTA-OH concentration is used to form the $HPTS(CTA)_4$ ion-pair, and a further 4% of it is used for neutralising the present amount of 0.1 N hydrochloric acid. The excess amount (89%) of base acts as a lipophilic bicarbonate buffer system and exists in the form of $CTA^+HCO_3^-$ x H_2O [32]. This cocktail was then spin-coated at 1000 rpm onto a polymer substrate and the resulting membrane was dried at 70ºC for four days. After drying, the membrane was stored in a sealed plastic bag under humid conditions.

3.2.5. Instrumentation

Fluorescence excitation and emission spectra were recorded with a Spex FluoroMax 2 spectrofluorometer (Jobin Yvon Inc., Edison, NJ, USA), and absorption spectra were acquired with a Cary 50 Scan UV-vis spectrometer (Varian Inc, USA). The flow cell used for the phase fluorometric measurements is described elsewhere [24], and the complete experimental set-up is illustrated in Fig. 2-11. A digital dual-phase lock-in amplifier (DSP 7225 Perkin Elmer Instruments, USA) was used for sinusoidal modulation of the LED (20 kHz / 5.0 V) and for phase-shift detection of the photodiode output signal.

The optical set-up consisted of a blue LED (λ_{max} = 470 nm, NSPB 500 Nichia, Germany) with a blue band-pass filter (BG-12, Schott, Mainz, Germany) and an integrated photodiode amplifier (IPL 10530 DAL, IPL Inc, Dorset, UK) with an orange

long-pass filter (LEE 135, LEE Filters, Hampshire, UK). The desired concentrations of carbon dioxide were achieved by mixing pure gases with computer-controlled mass flow controllers (UNIT Instruments, Dublin, Ireland). The gas mixture was humidified using two midget impingers and the flow rate was kept constant at 500 $cm^3 \cdot min^{-1}$. The reference method for determination of carbon dioxide levels was a Gascard II IR gas monitor (Edinburgh Sensors Ltd., UK).

3.3. Theory

3.3.1. Mathematical Description

It was described in early literature that linear calibration plots can be obtained for solid carbon dioxide sensors by plotting the ratio of protonated and deprotonated pH-indicator against pCO_2 [30]. Either absorption or fluorescence intensity does correlate with protonation levels of pH-indicators in a solid matrix. The linearisation of DLR-based carbon dioxide sensors was presented in a very similar manner [33]. The theory used in these cases always relied on solid sensor matrices which allow complete protonation of immobilised pH-indicators. However, the use of pH-indicators in an ormosil matrix requires changes to this DLR theory, because some parts of these dyes are unavailable for the sensing reaction with carbon dioxide. The emission spectrum of deprotonated HPTS remains present to some extent when it is chemically protonated as much as possible. Therefore, an important change to the present DLR theory has to be introduced in order to convert the measured phase angles into a parameter which can linearly reflect the concentration of protonated HPTS in these DLR-based sensors. This important change is based on the fact that in the *amplitude ratio* of the two signals A_{ind}/A_{ref} (eq. 3-9), the indicator amplitude A_{ind} can not be equal to zero, even when the dye is completely protonated. This change is presented in the following development of theory. A certain quantity of the immobilised pH-indicator cannot be protonated by carbon dioxide or even strong acids. That means that even when all protonable sites have been used, there is always a baseline level of indicator luminescence which cannot be quenched.

We call this baseline amplitude level A_{max}, and the corresponding phase angle ϕ_{max}. Therefore we have a relation between the deprotonated form of the pH-indicator $[D^-]$ and the indicator amplitude A_{ind} and A_{max}:

$$\left[D^-\right] \propto A_{Ind} - A_{\max} \qquad (3\text{-}10)$$

As mentioned above, the ratio of protonated to deprotonated pH-indicator dye (R_d) is linear to carbon dioxide partial pressure pCO_2:

$$R_d = \frac{[HD]}{\left[D^-\right]} = \frac{\left[HD_0\right] - \left[D^-\right]}{\left[D^-\right]} = K \cdot pCO_2 \qquad (3\text{-}11)$$

$[HD_0]$ corresponds to the total amount of the pH-indicator dye in the sensing membrane, [HD] reflects the protonated and $[D^-]$ the deprotonated form of it. The combination of equations 3-10 and 3-11 leads to a linear correlation of the lifetime data and the corresponding pCO_2:

$$\frac{\left(A_{ind}^0 - A_{\max}\right) - \left(A_{ind} - A_{\max}\right)}{\left(A_{ind} - A_{\max}\right)} = K \cdot pCO_2 \qquad (3\text{-}12)$$

where A_{ind}^0 is the high intensity measured in absence of carbon dioxide. After simplifying the equation and including the reference amplitude, this equation changes to:

$$\frac{\left(\frac{A_{ind}^0}{A_{ref}}\right) - \left(\frac{A_{ind}}{A_{ref}}\right)}{\left(\frac{A_{ind}}{A_{ref}}\right) - \left(\frac{A_{\max}}{A_{ref}}\right)} = K \cdot pCO_2 \qquad (3\text{-}13)$$

This equation can be changed and simplified using equation 3-9 in order to represent the measured phase angles of these lifetimes. Equation 3-14 represents this final version of theory for DLR-based pCO_2 sensors:

$$\frac{\cot\phi_0 - \cot\phi}{\cot\phi - \cot\phi_{\max}} = K \cdot pCO_2 \qquad (3\text{-}14)$$

where ϕ_0 is the phase angle measured in absence of carbon dioxide, and ϕ_{max} is the baseline amplitude phase angle. Following equation 3-14 a straight line plot for the calibration data can be achieved if K, ϕ_0 and ϕ_{max} are known. ϕ_0 is the measured phase angle at 0% CO_2. However by reforming equation 3-14 we can reach a fit

function for the phase response of the sensor and use this fit to determine K and ϕ_{max}. The fit function for the calibration function in the form cot ϕ = f(pCO_2) is:

$$\cot\phi = \cot\phi_{max} + \frac{\cot\phi_0 - \cot\phi_{max}}{1 + K \cdot pCO_2} \qquad (3\text{-}15)$$

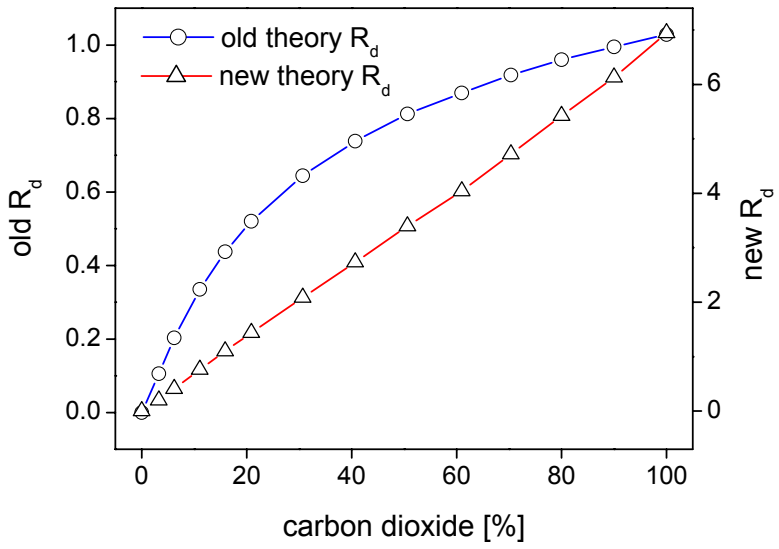

Fig. 3-6 *Phase angles were linearised using the published old theory and the newly developed theory (Eq. 3-14) of calculating the ratio of protonated to deprotonated pH-indicator dye (R_d).*

3.3.2. Simulation

The theoretical description of DLR sensors offers the opportunity to simulate different influences on sensor performance. There are three parameters in equation 3-15 which can be used for that purpose: ϕ_0, ϕ_{max} and K. Figs. 3-7 to 3-9 show the effect of changes made to each of these parameters while the other two are kept constant.

Figure 3-7 shows how the shape of phase calibration functions is influenced by the value of ϕ_{max}. The closer ϕ_{max} comes to ϕ_{ref} (~38 degrees in this case), the more the sensor dynamic range is shifted towards higher values. The only way this is

achieved, is by reducing the fraction of sites in the sensor matrix which are unavailable for protonation.

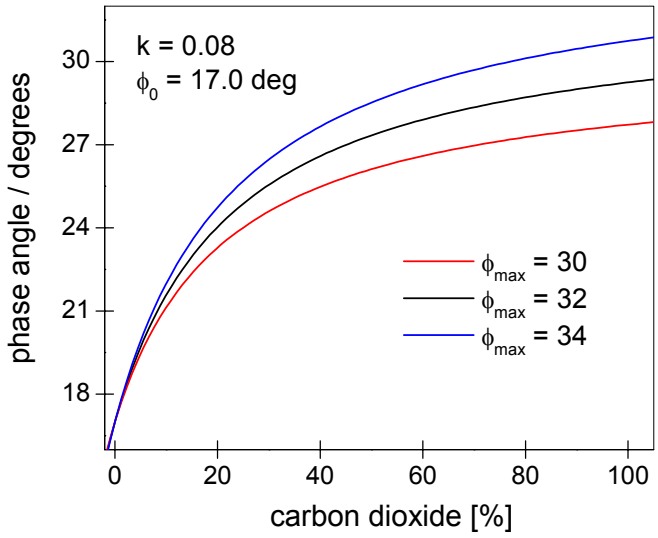

Fig. 3-7 *Effect of different ϕ_{max} on the shape of the response curve.*

It is, however, not clear how this can be achieved in reality. However, this result explains why the dynamic range of some sensors decreased after the membranes were kept in humid conditions. The ongoing hydrolysis and condensation of the sol-gel matrix reduced the average pore-size and therefore the accessibility of the dye molecules.

The second parameter which significantly influences the sensitivity of the sensor, is the equilibrium constant K. Fig. 3-8 shows that the response function is less hyperbolic for lower values of K. This effect is the easiest to understand in terms of the sensing chemistry, because it is mainly linked to the pK_A-value of the indicator dye and the strength (basicity) of the lipophilic buffer. The fact, that the dynamic range of the sensor can be altered by these parameters is clearly understandable. The current sensor membranes have mainly been optimised along this line.

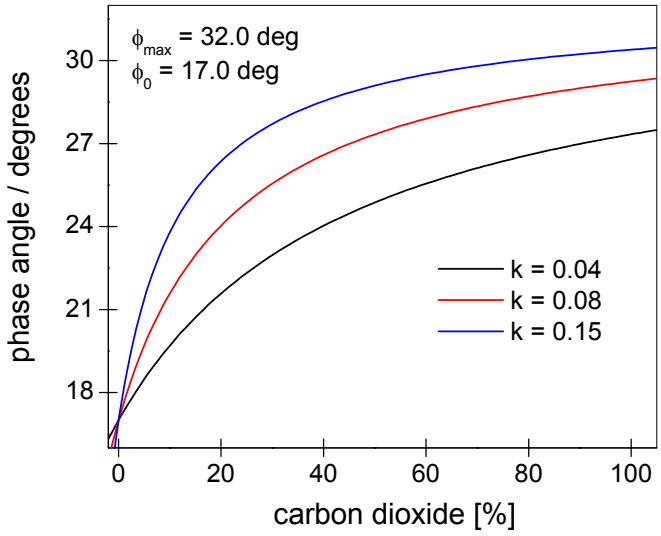

Fig. 3-8 *Effect of different equilibrium constants K on the shape of the response curve.*

The last parameter to be investigated is ϕ_0. This is the phase angle in the absence of carbon dioxide, and is mainly associated with the concentration ratio of indicator and reference luminophore, as well as the type of filter used at the photodetector. The effect which this parameter has on the shape of the phase calibration function is presented in Fig. 3-9, where it can be seen that the lower the value of ϕ_0, the more linear the response function gets. In order to achieve a higher dynamic range for the sensor membrane, one can either increase the concentration of indicator dye or reduce the amount of reference luminophore in the matrix. The effect that these concentration changes have on the calibration curve were indeed observed with our membranes in the past.

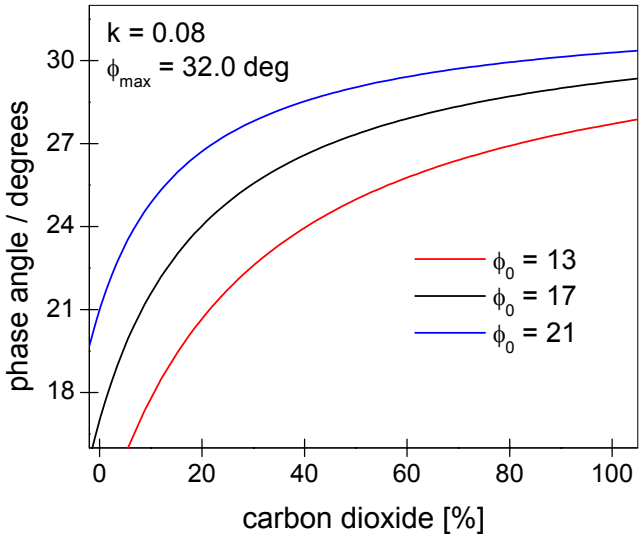

Fig. 3-9 *Effect of different ϕ_0 on the shape of the response curve.*

Another possibility to achieve the same effect without having to make changes in the actual sensing chemistry, is to modulate the amount of indicator luminescence reaching the photodetector. The fact that the luminescence emission spectra of reference and pH-indicator are shifted by ~70 nm offers the opportunity to change the ratio of the two signal intensities by simply changing the optical filter used in front of the photodiode. However, this method is not recommended in our case, due to the restrictions placed on the set-up by the intended MAP application (same filters as O_2-probe). It has to be said that the effect which ϕ_0 has on the response function, cannot be translated into the real world as readily as in the case of K and ϕ_{max}. The simulations presented here have assumed that a change in one parameter leaves the other two unchanged, but by changing the intensity ratio of the two luminophores, not only ϕ_0 is altered, but a change in ϕ_{max} has to be assumed as well.

3.4. Characterisation

3.4.1. Sensitivity

The donor concentration in a DLR-based sensor matrix has almost no effect on the sensitivity [15]. The only effect that a concentration increase of the donor offers is improvement of signal-to-noise ratio by increasing the fluorescence signal intensity. The concentration of the analyte-sensitive luminophore has little effect on calibration curves, but can be essential for fine tuning of DLR sensors. However, chemical methods can adjust the sensitivity of DLR-based sensor membranes by three different methods:

- Matrix material
- pK_A of the analyte-sensitive luminophore
- Concentration of lipophilic base

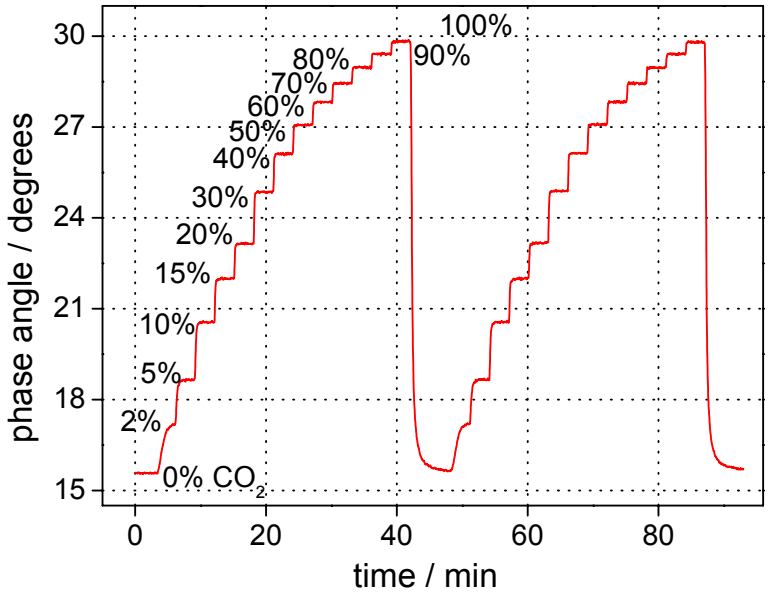

Fig. 3-12 *Phase response of the DLR-based sensor membrane to 0, 2, 5, 10, 15, 20, 30, 40, 50, 60, 70, 80, 90 and 100% carbon dioxide.*

The matrix material and the type of analyte-sensitive luminophore are already fixed in this case and therefore do not offer further influence on sensitivity. However, the concentration of the CTA-OH base presents an important influence on the sensitivity. Although the sensitivity increase for higher base concentrations seems to be a positive step, it is important to limit the base concentration in the sol-gel matrix. If there is too much base present, the sol-gel material will lose much of its stability and chemical neutrality. Therefore it was decided to compromise between good chemical matrix stability and high enough sensitivity by choosing the same base concentration as the presented Energy Transfer-based sensor, described in Chapter 2.

The sensor displays a fast response and a fully reversible phase difference (Fig. 3-12) of 13.5 degrees between 100% N_2 and 100% CO_2. The response time, which lies in the order of 20 – 30 seconds, is determined by the equilibration time of the midget impingers and the dead volume of the gas tubes, rather than the true response time of the sensor membrane. The dynamic range is sufficiently high to guarantee a resolution of ± 0.5% up to 50% CO_2 and ± 1% above that level. A conservative estimate for the limit of detection (LOD) was found to 0.08% CO_2, calculated as three times the standard deviation (3σ). A preliminary spot reproducibility test for the spin-coated sensor membrane yielded a maximum standard deviation of ±1.8% of the total phase signal. The resulting phase calibration plot was linearised using equation 3-14 and is shown in Fig. 3-13.

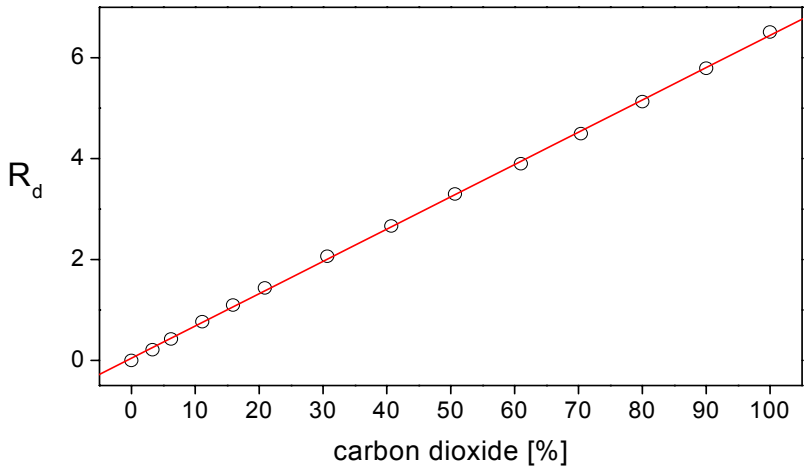

Fig. 3-13 *Linearised phase calibration plot for the DLR-based membrane.*

3.4.2. Stability

A drawback of sol-gel materials is the structural evolution that they can undergo over time in the case of incomplete hydrolysis. This is particularly evident in high humidity conditions. During the time the glass matrix takes to stabilise, its microstructure is varying, and consequently so too will the calibration function. In order to monitor the temporal stabilisation of the sensor, the membranes were stored in moist conditions and scanned approximately once every week.

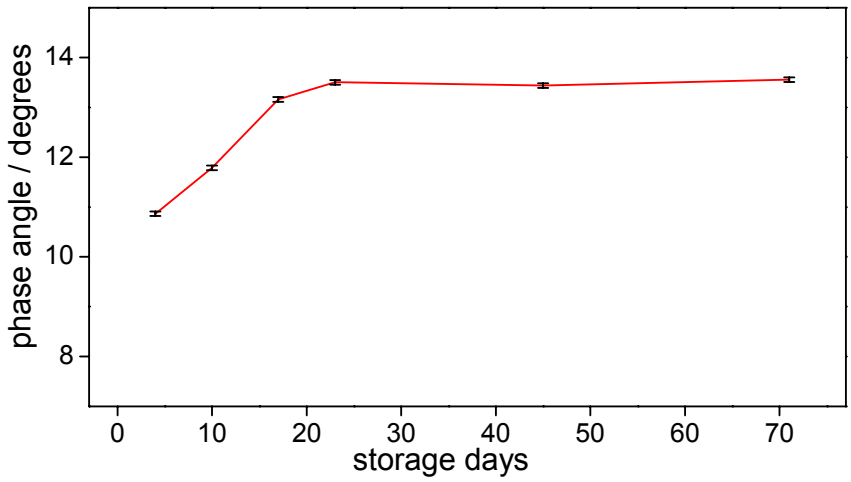

Fig. 3-10 *Temporal evolution of the total phase signal change between 100% N_2 and 100% CO_2. Note that the first data point is recorded after four days at 70°C. The membranes have reached equilibrium three weeks after sensor production.*

The total signal change $\Delta\phi$ between 100% N_2 and 100% CO_2 was recorded and plotted against the storage time (Fig. 3-10). It is clear that the membranes require about three weeks stabilisation time before they can be employed in their designated application. The reason for this long stabilisation time is unclear, but it may be due to a combination of a hydration effect and a structural evolution of the sol-gel matrix. The stabilised membranes were further stored and their performance in pre-set calibration cycles was tested for a further 32 weeks (Fig. 3-11).

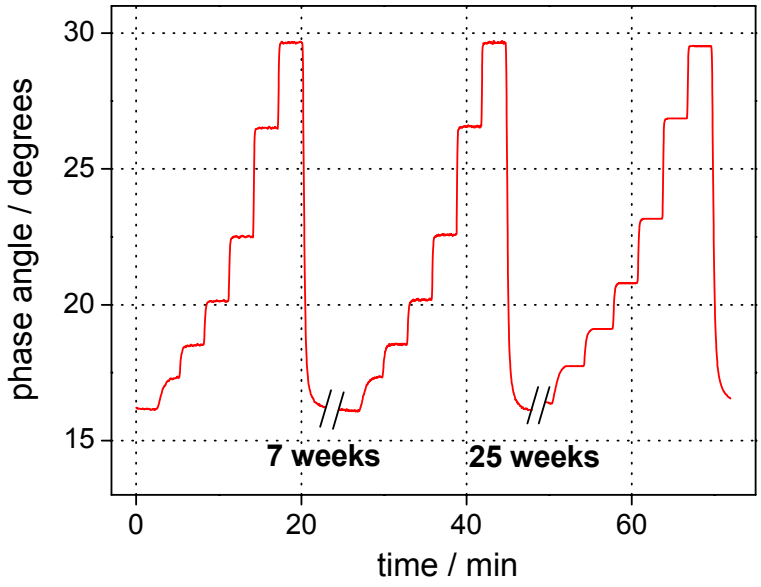

Fig. 3-11 *Phase response of the sensor to various CO_2 concentrations. Note the excellent repeatability and stability over the time of 32 weeks.*

An important feature of the response is its excellent long-time stability and repeatability over a time of more than 32 weeks. The shelf life of the membranes, if kept in humid conditions, in the dark, and away from detrimental influences like SO_2 or HCl, is longer than seven months.

3.4.3. Temperature

It is well known that temperature has a pronounced influence on the sensitivity of solid-type carbon dioxide sensors [34]. It was therefore necessary to establish how strongly the sensor material is influenced by temperature changes. In Fig. 3-14, linearised calibration functions are presented which were recorded between 10ºC and 35ºC in steps of five degrees. The data were linearised according to equation 3-14 in order to obtain a set of straight lines, from which the equilibrium constants K of the sensing reaction could be determined.

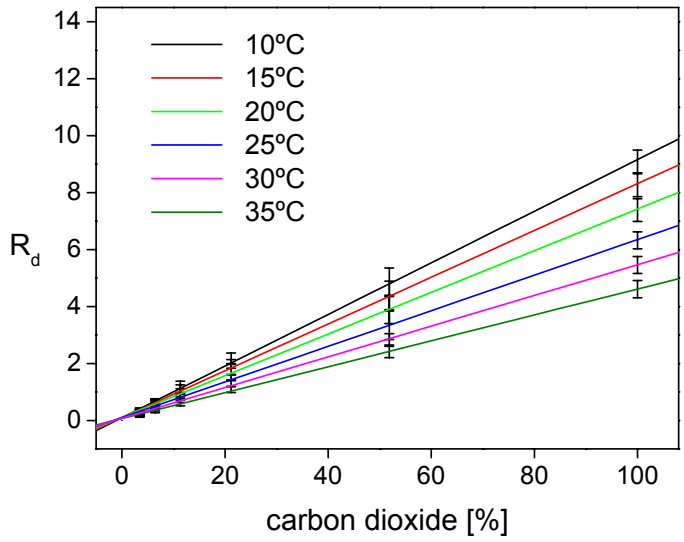

Fig. 3-14 *Calibration plots for the DLR-based membrane showing its behaviour over a range of different temperatures between 10°C and 35°C in steps of five degrees.*

Fig. 3-15 shows the linear correlation between 1/T and ln K (R^2 = 0,98718), and the analysis according to the Arrhenius equation (Eq. 2-11). Use of this equation and Eq. 2-12, yielded the activation enthalpy ΔH = -21.9±1.2 kJ mol^{-1} and an entropy term ΔS of -57.4±4.2 J K^{-1} mol^{-1}.

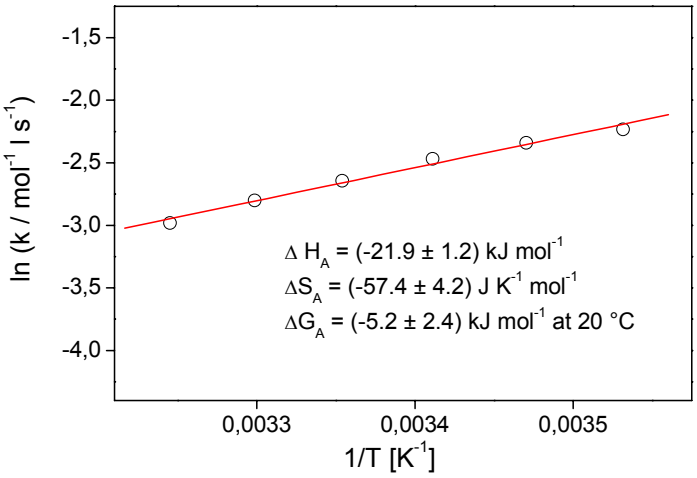

Fig. 3-15 *Arrhenius plot for the DLR-based membrane with fitting parameters.*

The negative value for ΔH indicates that the sensitivity of the membranes is greater at lower temperatures, which is apparent from Fig. 3-14 as well. This fact can be explained by the higher solubility of carbon dioxide in the matrix at lower temperatures [15]. However, both enthalpy and entropy are significantly smaller than in the case of Energy Transfer-based carbon dioxide sensors (Section 2.4.2). It is also worth noting that the sensor signal in the absence of CO_2 is almost completely independent of temperature, thereby showing the effectiveness of the DLR sensing scheme as an internal referencing technique.

3.4.4. Humidity

Protective gas mixtures that contain carbon dioxide are typically used for food items that maintain humidity levels close to 100% [35]. Therefore, in order to simulate those conditions as closely as possible, all experimental and storage conditions had to constantly maintain a high humidity level. The films still exhibit a reversible response to CO_2 at 90%, 60% and even 0% humidity indicating that there is sufficient water of crystallisation within the membranes (Fig. 3-16). However, it is clear that the sensitivity varies as a function of humidity.

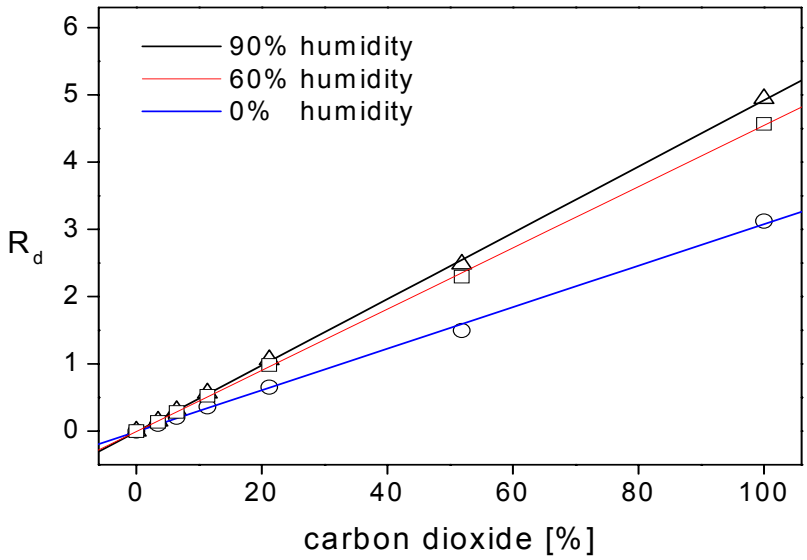

Fig. 3-16 *Linearised phase calibration plots for the DLR-based membrane at three different humidity levels.*

3.4.5. Oxygen

As was pointed out above, oxygen cross-sensitivity is a crucial factor for the sensor in the context of its application in MAP technology. The encapsulation of the reference luminophore $Ru(dpp)_3^{2+}$ in polymer nano-beads of very low oxygen permeability was designed to remove its susceptibility to dynamic quenching by molecular oxygen. In order to test the success of this approach, a comparison was made between calibration cycles, which were recorded with nitrogen and air, respectively, as carrier gases (Fig. 3-17).

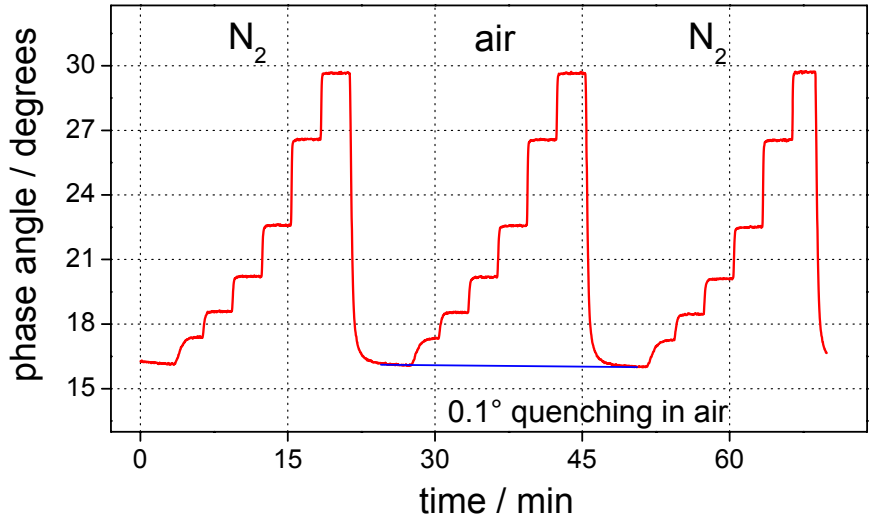

Fig. 3-17 *The phase response of the DLR-sensor membrane using nitrogen and air (21% O_2) as carrier gases for carbon dioxide experiments.*

The two calibration functions, which are generated by plotting cot ϕ against the CO_2 concentration, are plotted in Fig. 3-18. It is clear that the two curves almost completely overlay. In fact, the only visible difference is due to quenching of 0.10 degrees at 100% air, which represents a decrease of only 0.6% for 21% oxygen. Given the very high susceptibility of $Ru(dpp)_3^{2+}$ to quenching by molecular oxygen (>40% at 21% oxygen in MTEOS), this represents a substantial improvement, and reduces oxygen cross-sensitivity to an acceptable level.

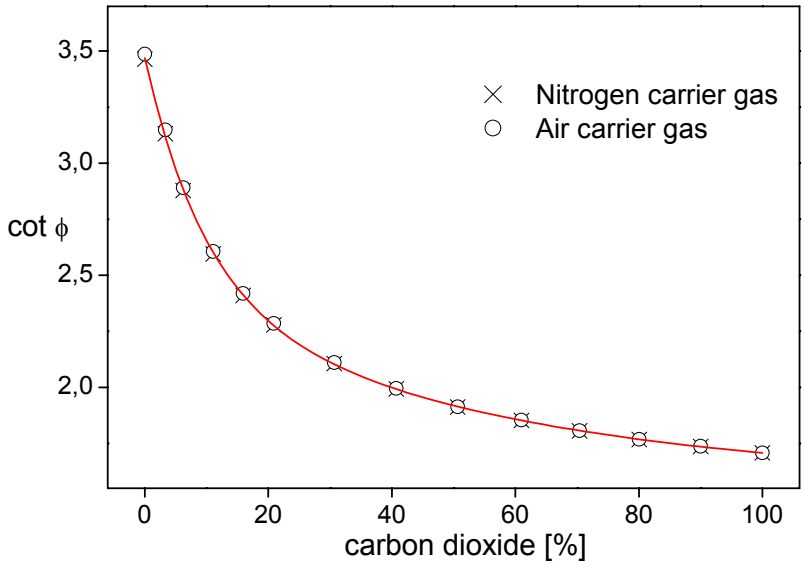

Fig. 3-18 *Calibration functions for the sensor using nitrogen and air as carrier gases. The presence of 21% oxygen only leads to quenching of 0.10 degrees (0.6%).*

In light of its intended application in the food industry, cross-sensitivity towards chloride ions and pH was also examined. The membrane showed no measurable quenching on exposure to a 0.3 M sodium chloride solution in pH 5 buffer for 1½ hours. Treatment of the sensor with 0.01 M hydrochloric acid resulted in quenching of only 0.06 degrees over the same time. The sensor membrane only exhibited a significant response (0.48 degrees) when a concentration of 0.1 M hydrochloric acid was applied. Equilibrium was reached after 25 minutes, after which no further quenching occurred. Considering the fact that pH conditions found in food packaging generally do not go below pH 4, it can safely be said that chloride and pH do not represent a cross-sensitivity problem for this sensor.

3.4.6. Results

The performance of the sensor was evaluated in comparison to a standard reference method for carbon dioxide measurement. Infrared absorption spectroscopy is such a reference method and represents the type of carbon dioxide sensor, which is most widely used in MAP technology at present [36]. A number of randomly set carbon dioxide concentrations was first measured in the optical flow-cell, using the calibration function presented in Fig. 3-18. Then the gas stream was dried using a Nafion® gas dryer tube and it was sampled by the Gascard II IR gas monitor designed and calibrated for carbon dioxide gas analysis. The optical sensor membrane output and the output of the reference method were then plotted against each other, ideally leading to a 45° straight line. A linear regression of the resulting plot, which is presented in Fig. 3-19, yielded a correlation coefficient R^2 = 0.99994, indicating an excellent agreement of the two sensor outputs.

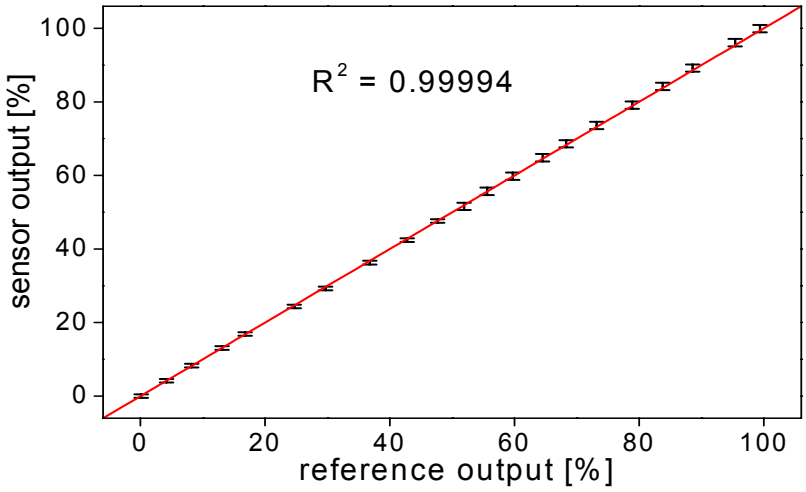

Fig. 3-19 *Comparison of the sensor membrane to a standard infrared absorption-based reference method for carbon dioxide measurement (correlation coefficient R^2 = 0.99994).*

Although printability of sensor films on food packaging material is an objective of this research work, only preliminary investigations have been carried out. Figure 3.20 shows the performance of the DLR sensor films as an

insert in a food package filled with various concentrations of CO_2 gas. These data show excellent correlation with the calibration (χ^2 = 0.034397).

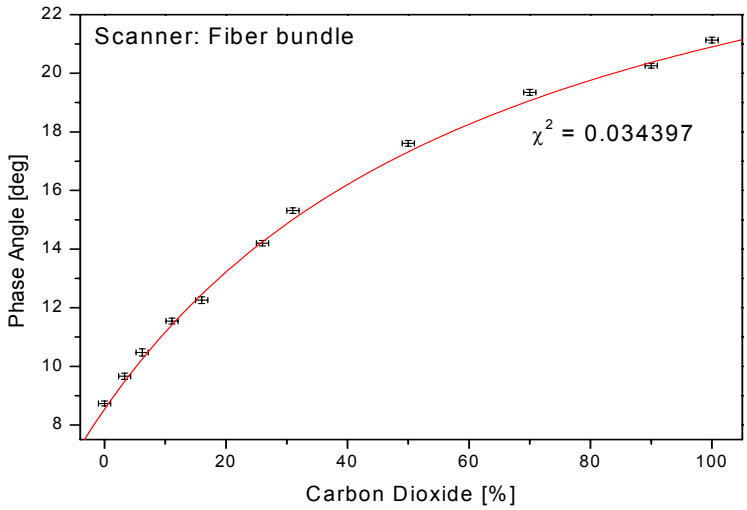

Fig. 3-20 *Performance of the DLR sensor films as an insert in a food package filled with various concentrations of CO_2 gas*.

3.5. Conclusion

The sensor presented here exhibits a fast and reversible response to carbon dioxide over a wide range of concentrations. The replacement of the commonly used base TOA-OH by CTA-OH has dramatically increased its dynamic range up to 100% CO_2 with a resolution of ±1%. However, it is capable of detecting concentrations as low as 0.08% CO_2. The use of Dual Luminophore Referencing has enabled the sensor to be interrogated using the same phase fluorometric measurement technology that is currently employed in lifetime-based oxygen sensing. Furthermore, it has removed many of the sources of drift commonly encountered in fluorescence intensity-based sensors, and provided the sensor with excellent repeatability and stability of the resulting calibration function. The problem of oxygen cross-sensitivity, which is introduced by the use of $Ru(dpp)_3^{2+}$ as a long-lifetime reference luminophore has been minimised by encapsulating the dye in oxygen-impermeable polymer nano-beads. Cross-sensitivity towards chloride and pH has been shown to be negligible.

The sensor output is in excellent agreement with a standard method of carbon dioxide detection. All of the above points support the application of the sensor as an on-pack sensor strip in modified atmosphere packaging technology.

3.6. References

1 Demas, J.; DeGraff, B. *Sens. Actuators B*, **1993**, *11*, 35

2 Malins, C.; Glever, H.; Keyes, T.; Vos, J.; Dressick, W.; MacCraith, B. *Sens. Actuators B*, **2000**, *67*, 89

3 Mohr, G.; Draxler, S.; Trznadel, K.; Lehmann, F.; Lippitsch, M. *Anal. Chim. Acta*, **1998**, *360*, 119

4 Krause, C.; Werner, T.; Huber, C.; Wolfbeis, O.; Leiner, M. *Anal. Chem.*, **1999**, *71*, 1544

5 Mills, A.; Chang, Q. *Analyst*, **1993**, *118*, 839

6 McDonagh, C.; Kolle, C.; McEvoy, A.; Dowling, D.; Cafolla, A.; Cullen, S.-J.; MacCraith, B. *Sens. Actuators B*, **2001**, *74*, 124

7 Ferguson, J.; Healy, B.; Bronk, K.; Barnard, S.; Walt, D. *Anal. Chim. Acta*, **1997**, *340*, 123

8 Parker, J.; Laksin, O.; Yu, C.; Lau, M.; Klima, S.; Fisher, R.; Scott, I.; Atwater, B. *Anal. Chem.*, **1993**, *65*, 2329

9 Lakowicz, J. *Principles of Fluorescence Spectroscopy*, **1983**, Plenum Press, New York / London, 257

10 McEvoy, A.; McDonagh, C.; MacCraith, B. *Analyst*, **1996**, *121*, 785

11 Klimant, I.; Wolfbeis, O. *Anal. Chem.*, **1995**, *67*, 3160

12 Wolfbeis, O.; Weis, L.; Leiner, M.; Ziegler, W. *Anal. Chem.*, **1988**, *60*, 2028

13 Malins, C.; MacCraith, B. *Analyst*, **1998**, *123*, 2373

14 Marazuela, M.; Moreno-Bondi, M.; Orellana, G. *Appl. Spectrosc.*, **1998**, *52*, 1314

15 Neurauter, G.; Klimant, I.; Wolfbeis, O. *Anal. Chim. Acta*, **1999**, *382*, 67

16 von Bültzingslöwen, C.; McEvoy, A.; McDonagh, C.; MacCraith, B. *Anal. Chim. Acta*, **2003**, *480*, 275

17 Huber, C.; Klimant, I.; Krause, C.; Werner, T.; Mayr, T.; Wolfbeis, O. *Fresenius J. Anal. Chem.*, **2000**, *368*, 196

18 Klimant, I. *Ger. Pat. Appl.*, **1997**, DE 198.29.657

19 Lakowicz, J.; Castellano, F.; Dattelbaum, J.; Tolosa, L.; Rao, G.; Gryczynski, I. *Anal. Chem.*, **1998**, *70*, 5115

20 Klimant, I.; Huber, C.; Liebsch, G.; Neurauter, G.; Stangelmayer, A.; Wolfbeis, O. In: Valeur, B.; Brochon, C. (Eds), *Fluorescence Spectroscopy: New Methods and Applications*, **2001**, Springer, Berlin

21 Mohr, G.; Klimant, I.; Spichiger-Keller, U.; Wolfbeis, O. *Anal. Chem.*, **2001**, *73*, 1053

22 Huber, C.; Klimant, I.; Krause, C.; Wolfbeis, O. *Anal. Chem.*, **2001**, *73*, 2097

23 Liebsch, G.; Klimant, I.; Krause, C.; Wolfbeis, O. *Anal. Chem.*, **2001**, *73*, 4354

24 http://www.optosense.de/

25 von Bultzingslowen, C.; McEvoy, A.; McDonagh, C.; MacCraith, B.; Klimant, I.; Krause, C.; Wolfbeis, O. *Analyst*, **2002**, *127*, 1478

26 Ge, X.; Kostov, Y.; Rao, G. *Biosens. Bioelectr.*, **2002**, *00*, 1

27 McDonagh, C.; MacCraith, B. D.; McEvoy, A. *Anal. Chem.*, **1998**, *70*, 45

28 Wolfbeis, O.; Klimant, I.; Werner, T.; Huber, C.; Kosch, U.; Krause, C.; Neurauter, G.; Dürkop, A. *Sens. Actuators B*, **1998**, *51*, 17

29 Mills, A.; Chang, Q. *Anal. Chim. Acta*, **1994**, *285*, 113

30 Mills, A.; Chang, Q.; McMurray, N. *Anal. Chem.*, **1992**, *64*, 1383

31 Chang, Q.; Randers-Eichhorn, L.; Lakowicz, J.; Rao, G. *Biotechnol. Prog.*, **1998**, *14*, 326

32 Mills, A.; Eaton, K. *Quimica Analitica*, **2000**, *19*, 75

33 Neurauter, G. *Dissertation*, Univ. Regensburg, **2000**, 40

34 Mills, A.; Monaf, L. *Analyst*, **1996**, *121*, 535

35 Air Products PLC, *The FRESHLINE guide to Modified Atmosphere Packaging (MAP)*, **1995**, 32

36 Smolander, M.; Hurme, E.; Ahvenainen, R. *Trends in Food Sci. and Technol.*, **1997**, *4*, 101

4. Materials and Characteriation

4.1. Introduction

The nature of the proposed application of the carbon dioxide sensor in food technology demands that the immobilisation matrix must fulfil a set of strict conditions. The harsh surroundings inside of food packages can lead to the detachment of sensor membranes [1]. Due to the water-mediated sensing chemistry, humidity has a potentially strong influence on the sensor performance. The use of relatively hydrophobic membranes can minimise this effect, but makes ion-pairing necessary [2].

4.1.1. Polymers

Many polymers that have previously been employed for carbon dioxide sensing do not offer sufficient chemical and mechanical stability under the conditions of food packaging. Polymers typically chosen for encapsulation are ethyl cellulose, polyvinyl butyral or poly(HEMA) which provide good sensor performance, but they are still somewhat ion-permeable. Furthermore, they can swell when placed in contact with liquids, which can easily happen in a food package. This not only aggravates the problem of cross-sensitivity to chloride ions or pH, for example, but can also lead to leaching of the sensor chemistry into the food product, or even to the membrane completely falling off. A completely ion-impermeable material such as silicone, however, does not offer enough mechanical resistance to be considered for this application.

4.1.2. Organically modified silica glasses

Organically modified silicates (ormosils), produced via the sol-gel process, offer a good solution to these problems. Sol-gel-derived materials are chemically inert and mechanically very resistant, and properties such as polarity and porosity can be specifically adjusted [1,3-5]. During hydrolysis and condensation, the conditions in the sol are sufficiently hydrophilic to facilitate dye doping, but after drying and curing, the surface is much more hydrophobic than that of ethyl cellulose for example. Therefore, the ion-permeability of an ormosil such as MTEOS is substantially lower than that of the latter, although it is not completely impermeable. Additionally, the mechanical strength and chemical inertness that is achievable with sol-gels even under very moist conditions is very high. Malins *et al* first successfully used organically modified silica sol-gel (ormosil) materials to fabricate solid pCO_2 sensor films [6]. The spectroscopic and chemical properties of some indicator dyes, however, can be restricted by immobilisation in some sol-gel glasses, due to interactions with the inner surface of the pores [4,7]. The use of ormosils and polymer / sol-gel hybrid materials can overcome this restriction.

Other advantages of sol-gel-derived materials include their optical transparency, the possibility to tailor properties such as polarity and porosity and the fact that they can be printed or moulded in industrial-scale processes. One disadvantage of ormosil-based carbon dioxide sensors is their higher susceptibility to changes in humidity levels as compared to silicone or plasticised ethyl cellulose [8]. However, protective gas mixtures that contain carbon dioxide are typically used for food items that maintain humidity levels close to 100% [9]. Therefore, in order to simulate those conditions as closely as possible, all experimental and storage conditions had to constantly maintain a high humidity level. The films still exhibit a reversible sensitivity towards CO_2 at 0% humidity, however, indicating that there is sufficient water of crystallisation within the membranes. A drawback of sol-gel materials is the structural evolution that they can undergo over time in the case of incomplete hydrolysis. This is particularly evident in high humidity conditions. During the time the glass matrix takes to stabilise, its microstructure is varying, and consequently so too will the calibration function.

4.2. Experimental

4.2.1. Energy Transfer Sensor

A solution of tetraoctylammonium hydroxide (TOA-OH) in methanol was prepared by stirring 10.0 g silver(I)oxide and 23.1 g tetraoctylammonium bromide in 50.0 ml methanol for 2 h. The methanolic free base was filtered and stored in a refrigerator. Ethyl cellulose (5.0 g) was dissolved in 100 ml of a toluene/ethanol mixture (80/20 v/v). Sol-gel solutions were prepared by adding 4.35 ml of 0.1 N hydrochloric acid to 12.0 ml of MTEOS while stirring rapidly until the two phases mixed, and hydrolysis and condensation started. The sol-gel was then stirred for a further two hours before mixing into the sensor cocktails. Stock solution I was prepared by dissolving 58.0 mg of the $Ru(dpp)_3(TSPS)_2$ ion-pair in 20.0 ml of the methanolic TOA-OH solution. Stock solution II was prepared by dissolving 60.0 mg Sudan III in 10.0 ml of the TOA-OH solution. Cocktails for making films with different quantities of ethyl cellulose (E0 – E5) were made by mixing different quantities of stock solution I and II, the methanolic base solution, the ethyl cellulose solution and the sol-gel solution (Table 4-1). The cocktails were saturated with carbon dioxide before spin coating at 700 RPM onto dustfree polymer substrates. The resulting membranes were dried at 70ºC for 22 hours and then stored in sealed plastic bags under ambient conditions.

Table 4-1 *Composition of sensor membranes E0 to E5*

membrane	E0	E1	E2	E3	E4	E5
sol-gel [ml]	4.725	3.365	2.725	1.775	0.790	-
ethyl cellulose [ml]	-	1.360	2.0	2.950	3.935	4.725
TOA-OH [ml]	0.625	0.625	0.625	0.625	0.625	0.625
solution I [ml]	1.0	1.0	1.0	1.0	1.0	1.0
solution II [ml]	0.375	0.375	0.375	0.375	0.375	0.375
ethyl cellulose in the matrix [%]	0	7	12	23	48	100

4.2.2. Dual Luminophore Referencing Sensor

A solution of cetyltrimethylammonium hydroxide (CTA-OH) in methanol was prepared by stirring 10.0 g silver(I)oxide and 15.7 g cetyltrimethylammonium bromide in 50.0 ml methanol for 2 h. The methanolic free base was filtered and stored in a refrigerator. Ethyl cellulose (5.0 g) was dissolved in 100 ml of a toluene/ethanol mixture (80/20 v/v). Sol-gel solutions were prepared by adding 4.35 ml of 0.1 N hydrochloric acid to 12.0 ml of MTEOS while stirring rapidly until the two phases mix, and hydrolysis and condensation starts. The sol-gel was then stirred for a further two hours before mixing into the sensor cocktails. The basic stock solution was prepared by suspending 525 mg of the $Ru(dpp)_3^{2+}$ doped PD-1 nano-beads [10], and dissolving 210 mg 1-hydroxypyrene-3,6,8-trisulfonate (HPTS) in 35.0 ml CTA-OH solution. Cocktails for making films with different quantities of ethyl cellulose (F0 – F5) were made by mixing different quantities of the base solution, the ethyl cellulose solution and the sol-gel solution (Table 4-2). The cocktails were saturated with carbon dioxide before spin coating at 700 RPM onto dustfree polymer substrates. The resulting membranes were dried at 70ºC for 22 hours and then stored in sealed plastic bags under ambient conditions.

Table 4-2 *Composition of sensor membranes F0 to F5*

membrane	F0	F1	F2	F3	F4	F5
sol-gel [ml]	4.725	3.365	2.725	1.775	0.790	-
ethyl cellulose [ml]	-	1.360	2.0	2.950	3.935	4.725
base solution [ml]	5.0	5.0	5.0	5.0	5.0	5.0
ethyl cellulose in the matrix [%]	0	7	12	23	48	100

4.2.3. Instrumentation

The flow cell used for the phase fluorometric measurements is described elsewhere [11], and the complete experimental set-up is illustrated in Fig. 2-11. A digital dual-phase lock-in amplifier (DSP 7225 Perkin Elmer Instruments, USA) was used for sinusoidal modulation of the LED (20 kHz / 5.0 V) and for phase-shift

detection of the photodiode output signal. The optical set-up consisted of a blue LED (λ_{max} = 470 nm, NSPB 500 Nichia, Germany) with a blue band-pass filter (BG-12, Schott, Mainz, Germany) and an integrated photodiode amplifier (IPL 10530 DAL, IPL Inc, Dorset, UK) with an orange long-pass filter (LEE 135, LEE Filters, Hampshire, UK). The desired concentrations of carbon dioxide were adjusted by mixing pure nitrogen and carbon dioxide using computer-controlled mass flow controllers (UNIT Instruments, Dublin, Ireland).

4.3. Characterisation

4.3.1. Energy Transfer Sensor

The phase response of this sensor in a pure MTEOS membrane showed only limited sensitivity to carbon dioxide when compared to the sensitivity achievable in an ethyl cellulose matrix. Therefore, the possibility of a hybrid material between MTEOS and ethyl cellulose, which would combine the excellent mechanical and chemical stability of the sol-gel with the superior sensitivity of the polymer, was investigated.

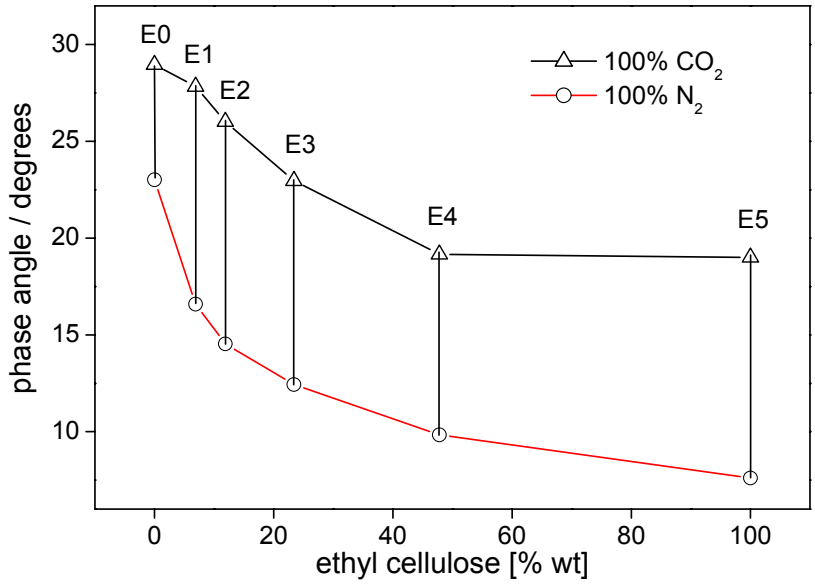

Fig. 4-1 *Absolute phase response of ET-based sensor membranes E0 – E5 in the absence (red) and presence (black) of carbon dioxide (100%).*

In order to maintain the mechanical and chemical characteristics of MTEOS films, the proportion of ethyl cellulose in the mixture needed to be kept relatively low. The correlation between ethyl cellulose content in the matrix and the absolute phase signal change between 100% nitrogen and 100% carbon dioxide is shown in Fig. 4-1 (membranes E0 – E5). It was found that a fraction of only 7% (m/m) of ethyl cellulose in MTEOS increased the absolute phase response from 6.0 degrees to 11.2 degrees.

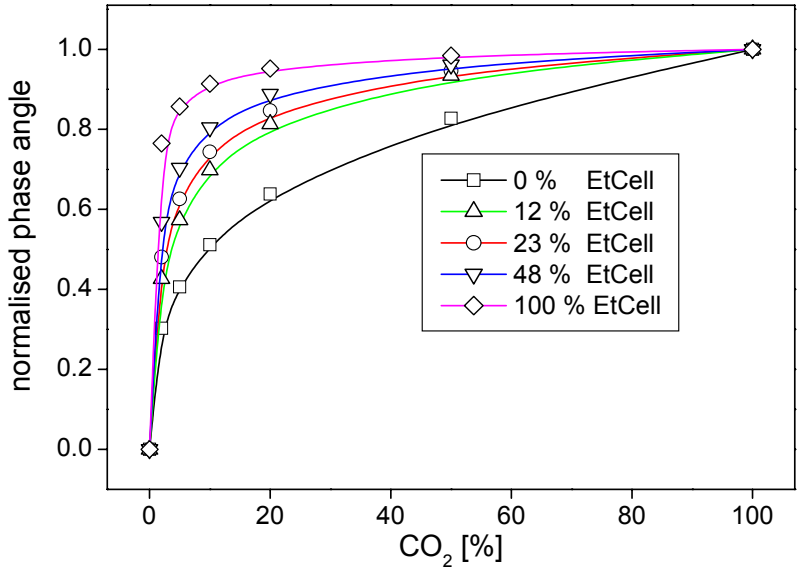

Fig. 4-2 *Normalised calibrations of energy-transfer-based membranes for different mass fractions of ethyl cellulose in MTEOS.*

Any further increase in the content of ethyl cellulose improved only minutely the absolute phase response, but decreased the useful measurement range of the sensor to lower carbon dioxide concentrations at the same time (Fig. 4-2).

An increase in the content of ethyl cellulose resulted in a decrease of the recorded phase angle in both nitrogen and carbon dioxide. It seems likely that the rigid cage structure of the silica sol-gel offers less opportunity for vibrational deactivation of the excited ruthenium complex than the more flexible structure of the ethyl cellulose polymer. Therefore, average fluorescence decay times are longer, and measured phase signals are higher in MTEOS. So sol-gel materials appear to be better suited for fluorescence-based sensors than ethyl cellulose.

4.3.2. Dual Luminophore Referencing Sensor

The reduced phase response of the FRET-based sensor in pure MTEOS resulted in the use of a sol-gel/polymer hybrid material for the sensor membrane. Therefore, the same experiment was carried out for the HPTS-based DLR sensors. The phase signal of carbon dioxide sensors in the pure MTEOS membrane showed an almost equal response as compared to the pure EtCell layer (Fig. 4-3).

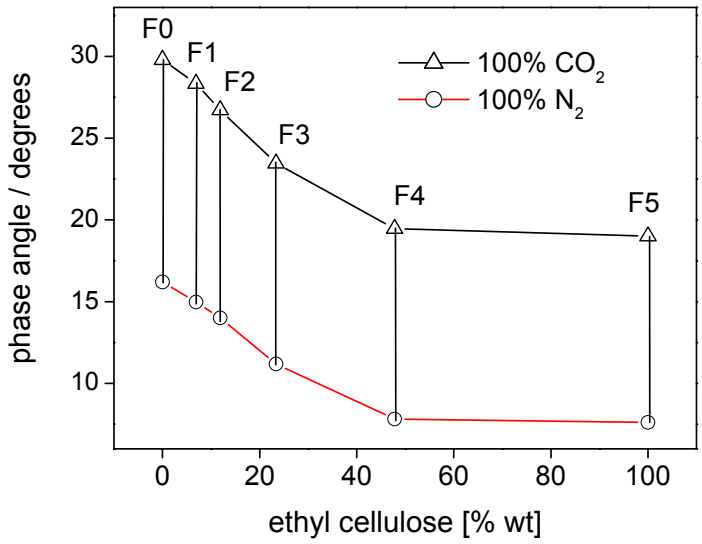

Fig. 4-3 *Absolute phase response of DLR-based sensor membranes F0 – F5 in the absence (red) and presence (black) of carbon dioxide (100%).*

This graph shows that the use of a hybrid material is not necessary for the DLR-based sensors. Consequently, two main disadvantages connected to the EtCell polymer are therefore prevented:

- As shown in Fig. 4-2, the content of EtCell decreased the useful measurement range of the sensor to lower carbon dioxide partial pressure.
- Figs. 4-1 and 4-3 clearly show the decrease of fluorescence lifetime due to the vibrational deactivation of the excited ruthenium complex by EtCell membranes.

The use of polymers for the sensor membranes is therefore not necessary, thereby providing additional evidence that the DLR-sensors are better suited for luminescence-based CO_2 sensors than ones based on energy transfer.

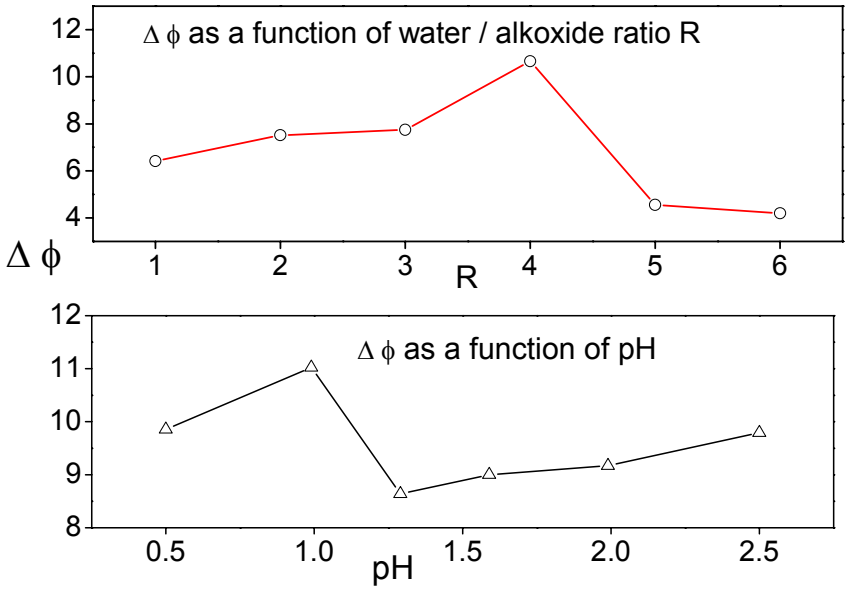

Fig. 4-4 *Optimisation of the phase response as a function of pH (black) and water to alkoxide ratio R (red) of the MTEOS membranes.*

The use of a sol-gel membrane should be optimised with regards to its water/alkoxide ratio R and the pH of the water used for the sol-gel reaction [12]. Fig. 4-4 shows the results of this study, which found the same optimum settings as the well-described oxygen sensors which have been developed for the MAP application [13]. A water/alkoxide ratio R=4 and a sol-gel pH 1 were found to be the best settings for the DLR-based sensor material.

4.4. Conclusion

In this chapter, the two different sensing schemes were compared with respect to the immobilisation matrix material under the restrictions made by the planned application in Modified Atmosphere Packaging. The sensor using Fluorescence Resonance Energy Transfer (FRET) can not be used in a 100% sol-gel membrane due to its limited sensitivity to carbon dioxide when compared to the sensitivity achievable in a pure ethyl cellulose matrix. However it was found that a

fraction of only 7% (m/m) of ethyl cellulose in MTEOS increased the absolute phase response from 6.0 degrees to 11.2 degrees. This low mass fraction of ethyl cellulose restricted the sensitivity change of the sensor to lower pCO_2, as well as minimised the decrease of fluorescence lifetime.

In contrast to the FRET-membranes, the DLR-based sensor showed no response restriction by using a pure sol-gel matrix material. Therefore, the reduction of the measurement range and the decrease of fluorescence lifetime, which is caused by a ethyl cellulose matrix, were avoided. The MTEOS-based matrix was optimised using its water/alkoxide ratio R and the pH of the water used for the sol-gel reaction.

4.5. References

1 von Bültzingslöwen, C.; McEvoy, A.; McDonagh, C.; MacCraith, B.; Klimant, I.; Krause, C.; Wolfbeis, O. *Analyst*, **2002**, *127*, 1478

2 Mills, A.; Chang, Q. *Analyst*, **1993**, *118*, 839

3 McDonagh, C.; MacCraith, B.; McEvoy, A. *Anal. Chem.*, **1998**, *70*, 45

4 Lin, J.; Brown, C. *Trends in Anal. Chem.*, **1997**, *16*, 200

5 Collinson, M. *Crit. Rev. Anal. Chem.*, **1999**, *29*, 289

6 Malins, C.; MacCraith, B. *Analyst*, **1998**, *123*, 2373

7 von Bültzingslöwen, C.; McEvoy, A.; McDonagh, C.; MacCraith, B. *Anal. Chim. Acta*, **2003**, *480*, 27

8 Mills, A.; Eaton, K. *Quimica Analitica*, **2000**, *19*, 75

9 Air Products PLC, *The FRESHLINE guide to Modified Atmosphere Packaging (MAP)*, **1995**, 32

10 http://www.optosense.de/

11 McDonagh, C.; MacCraith, B. D.; McEvoy, A. *Anal. Chem.*, **1998**, *70*, 45

12 Brinker, C.; Scherer, G. *Sol-Gel Science*, **1990**, Academic Press Ltd., London

13 McDonagh, C.; Kolle, C.; McEvoy, A.; Dowling, D.; Cafolla, A.; Cullen, S.; MacCraith, B. *Sens. Actuators B*, **2001**, *74*, 124

5. Sol-Gel Reference Particles

5.1. Introduction

Ruthenium(II)-diimine complexes are widely used as attractive reference standards. In this case, $Ru(dpp)_3^{2+}$ was selected as a long-lived luminophore due to its lifetime in the microsecond range, which facilitates phase modulation techniques at frequencies of 20 kHz, for example. This ruthenium dye has a high luminescence quantum yield of ~0.5, as well as a good photostability and absorption in the visible range. Using the $Ru(dpp)_3^{2+}$ complex as a DLR-based reference luminophore doped into oxygen impermeable micro- or nano-particles offers the solution to some well known problems. Primarily, dynamic luminescence quenching caused by oxygen and other species will lead to signal fluctuations. Furthermore the reactive singlet oxygen produced will be able to oxidise and therefore destroy the indicator dyes. However, as known from published temperature and carbon dioxide sensors, encapsulation of the ruthenium dye into materials with low oxygen permeability allows the manufacturing of sensors with no oxygen cross-sensitivity [1-3].

5.1.1. PAN-Particles

So far $Ru(dpp)_3^{2+}$ immobilised into PAN-nanoparticles has been used for the production of DLR-based carbon dioxide sensors [2-4]. However, although these particles almost completely remove cross-sensitivity problems with oxygen, they create a new problem for the sensor membranes. These nano-particles usually solidly agglomerate to particle groups in the scale of about 100 μm.

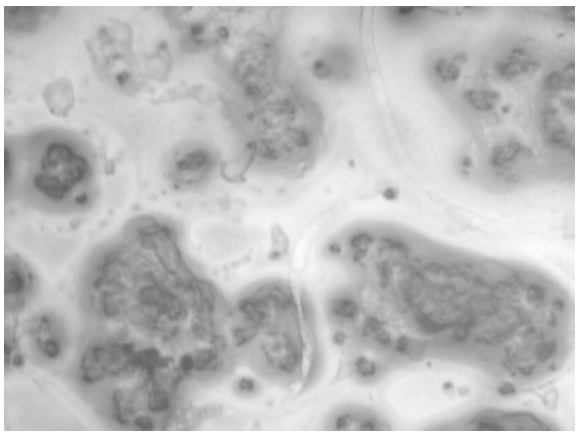

Fig. 5-1 *Microscopic picture of the surface of DLR sensor made using PD-1 nano-particles*

Fig. 5-1 is a microscopy picture of the surface of the DLR sensor made with the PD-1 nanoparticles and clearly shows these agglomerated particles in the sensor membrane. This rough and irregular accumulation of reference particles results in a poor repeatability for these DLR-membranes.

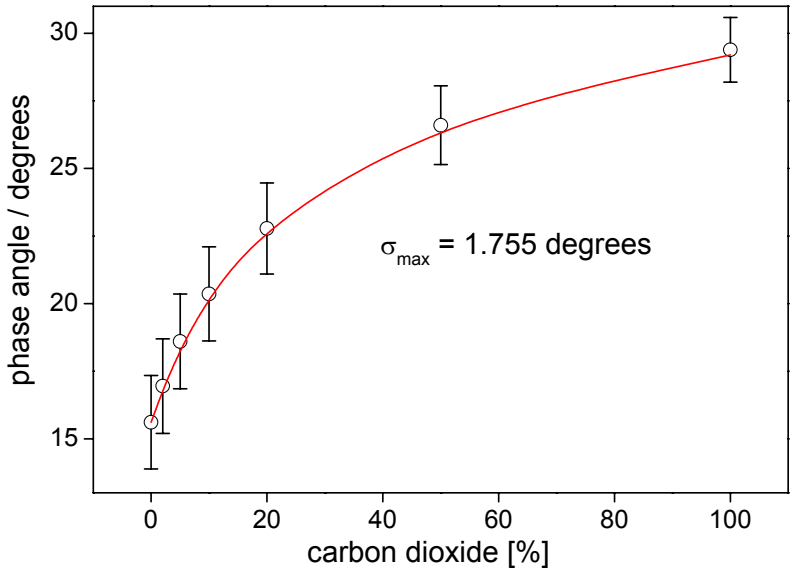

Fig. 5-2 *Poor repeatability (n=10) of DLR-based carbon dioxide sensor membranes made of PAN PD-1 nanoparticles.*

A spot-test was carried out for this membrane and yielded an average standard deviation of ±1.76 degrees (n = 10) for the phase angle calibration (Fig. 5-2). Therefore, an alternative approach for reference particles was carried out in order to improve the reproducibility of the CO_2 sensor.

5.1.2. Sol-gel particles

In the following sensor membrane, the reference luminophore $Ru(dpp)_3^{2+}$ was separately encapsulated into sol-gel based μ-particles [3]. This type of sol-gel is a preferable material because it is a chemically similar material to the MTEOS-based membranes. Unfortunately, in a standard sol-gel glass formation process, the matrix formed is rather porous and permeable to oxygen. Therefore, in an adapted manufacturing and sensor production process, these sol-gel particles were densified.

The TEOS particles, which are shown in Fig. 5-3, have an average diameter of around 2 μm and can be prepared in a straightforward manner. They have a relatively non-porous, dense structure, and therefore encapsulate the $Ru(dpp)_3^{2+}$ dye effectively. These particles were fabricated according to the procedure detailed by De *et al* [5].

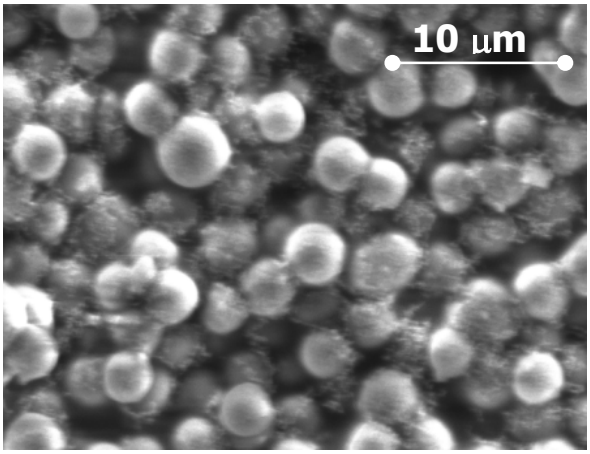

Fig. 5-3 *$Ru(dpp)_3$-doped sol-gel μ-particles*

The concentration of TEOS-based reference μ-particles used in the carbon dioxide sensor matrices has a considerable influence on the sensor performance. Although luminescence intensity can be a bit higher for sensors using more reference dye, the useful measurement range of the sensor is decreased to lower carbon dioxide concentrations (Fig. 5-4). Therefore, these carbon dioxide sensors were made with a low amount of reference particles to guarantee a similarly low sensitivity range as previously described (Chap. 3), while the signal intensity remains high enough for easy measurement.

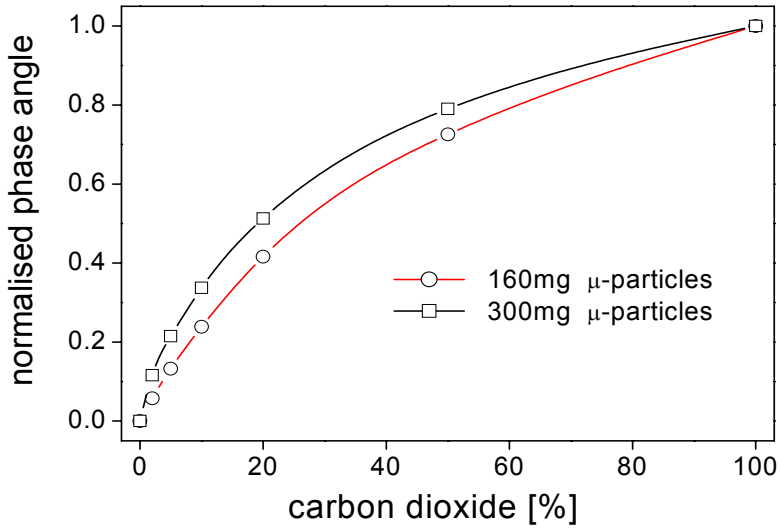

Fig. 5-4 *Normalised calibrations of DLR based membranes using different amounts of TEOS sol-gel reference particles.*

5.2. Experimental

5.2.1. Preparation

The preparation of a solution of cetyltrimethylammonium hydroxide (CTA-OH) in methanol (0.66 $mol \cdot l^{-1}$) was reported elsewhere [6]. 160 mg of the doped TEOS μ-particles were suspended in 4.0 ml of MTEOS and 1.45 ml of 0.1 N hydrochloric acid was added while stirring rapidly until the two phases mixed and hydrolysis and condensation reactions started. After further stirring for two hours, 30 mg HPTS (5.7×10^{-5} mol) dissolved in 5 ml CTA-OH solution were added, and the whole cocktail was saturated with carbon dioxide.

A portion of 7% of the CTA-OH concentration is used to form the $HPTS(CTA)_4$ ion-pair, and further 4% of it are used for neutralising the present amount of 0.1 N hydrochloric acid. The excess amount (89%) of base acts as a lipophilic bicarbonate buffer system and exists in the form of $CTA^+HCO_3^-$ x H_2O [7]. This cocktail was then spincoated at 1000 rpm onto a polymer substrate and the resulting membrane **Bef-1** was dried at 70ºC for three days. After drying, the membrane was stored in a sealed plastic bag under humid conditions.

5.2.2. Instrumentation

Fluorescence excitation and emission spectra were recorded with a Spex FluoroMax 2 spectrofluorometer (Jobin Yvon Inc., Edison, NJ, USA), and absorption spectra were acquired with a Cary 50 Scan UV-vis spectrometer (Varian Inc, USA). The flow cell used for the phase fluorometric measurements is described elsewhere [8], and the complete experimental set-up is illustrated in Fig. 2-11. A digital dual-phase lock-in amplifier (DSP 7225 Perkin Elmer Instruments, USA) was used for sinusoidal modulation of the LED (20 kHz / 5.0 V) and for phase-shift detection of the photodiode output signal. The optical set-up consisted of a blue LED (λ_{max} = 470 nm, NSPB 500 Nichia, Germany) with a blue band-pass filter (BG-12, Schott, Mainz,

Germany) and an integrated photodiode amplifier (IPL 10530 DAL, IPL Inc, Dorset, UK) with an orange long-pass filter (LEE 135, LEE Filters, Hampshire, UK). Temperature was controlled using Lauda Ecoline Thermostat RE 104 with control unit E 100.

The desired concentrations of carbon dioxide were adjusted by mixing pure gases with computer-controlled mass flow controllers (UNIT Instruments, Dublin, Ireland). The gas mixture was humidified using two midget impingers and the flow rate was kept constant at 500 $cm^3 \cdot min^{-1}$. The reference method for determination of carbon dioxide levels was a Gascard II IR gas monitor (Edinburgh Sensors Ltd., UK).

5.3. Characterisation

5.3.1. Sensitivity

The matrix material, the type of analyte-sensitive luminophore and the concentration of the CTA-OH base are already fixed and therefore do not offer further influence on sensitivity. However, the different particle type doped with $Ru(dpp)_3^{2+}$ will influence the sensor phase signals. The performance of the membranes with fixed concentrations of HPTS pH-indicator, TEOS-based reference μ-particles and CTA-OH was therefore tested. Fig. 5-5 displays the phase response and recovery behaviour of sensor membrane **Bef-1**. The resulting phase calibration plot was linearised using equation (3-14) and this is shown in Fig. 5-6.

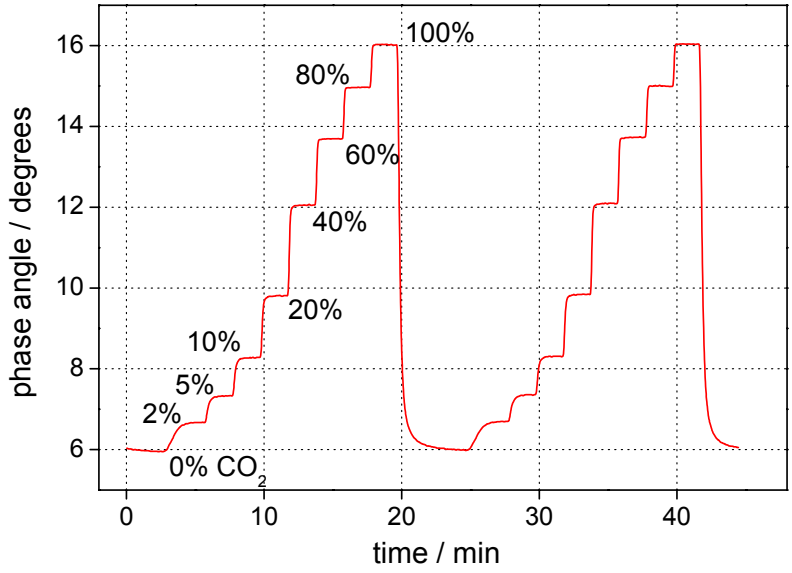

Fig. 5-5 *Phase response of the DLR sensor membrane **Bef-1** to 0, 2, 5, 10, 20, 40, 60, 80 and 100% carbon dioxide (20°C).*

The sensor displays a fast response and a fully reversible phase difference of 10.08 degrees at 20°C between 100% N_2 and 100% CO_2. The measured response time, which lies in the order of 20 – 30 seconds, is determined by the equilibration time of the midget impingers and the dead volume of the gas tubes, rather than the true response time of the sensor membrane.

The dynamic range is sufficiently high to guarantee a resolution of ± 1% up to 50% CO_2 and ± 2% above that level. A conservative estimate for the limit of detection (LOD) was found to be 0.04% CO_2, calculated as three times the standard deviation (3σ).

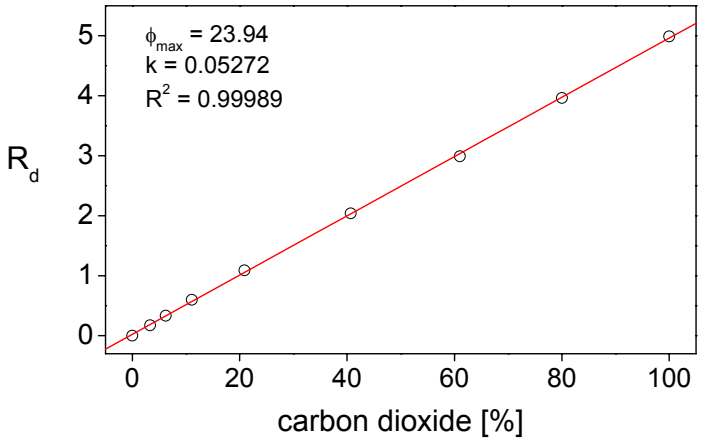

Fig. 5-6 *Linearised phase calibration plot for the DLR-based* ***Bef-1*** *membrane (20°C).*

5.3.2. Repeatability

The main reason for replacing the reference nano-particles with sol-gel-based μ-particles is the poor statistical repeatability exhibited by carbon dioxide sensor membranes fabricated using PAN-particles. As shown in Fig. 5-1, these PAN-particles have the tendency to agglomerate into particle groups in the scale of about 100 μm, which impairs the reproducibility of these membranes. Two main conditions for choosing TEOS-based sol-gel glass as a material for these new μ-particles, are the formation of a smoother surface of the sensor films without amassed particle piles, and obviously retaining very low oxygen cross-sensitivity.

The repeatability of DLR-based carbon dioxide sensor membranes made using PAN PD-1 nanoparticles was presented in Fig. 5-2, which has an average standard deviation of ±1.76 degrees (n = 10) for the phase angle calibration. The performance of the new sensor membrane **Bef-1** based on the use of TEOS μ-particles is presented in Fig. 5-7, and its reproducibility is more than five times better than the previous PAN-particles with a standard deviation of ±0.33 degrees (n = 10) for the phase angle calibration.

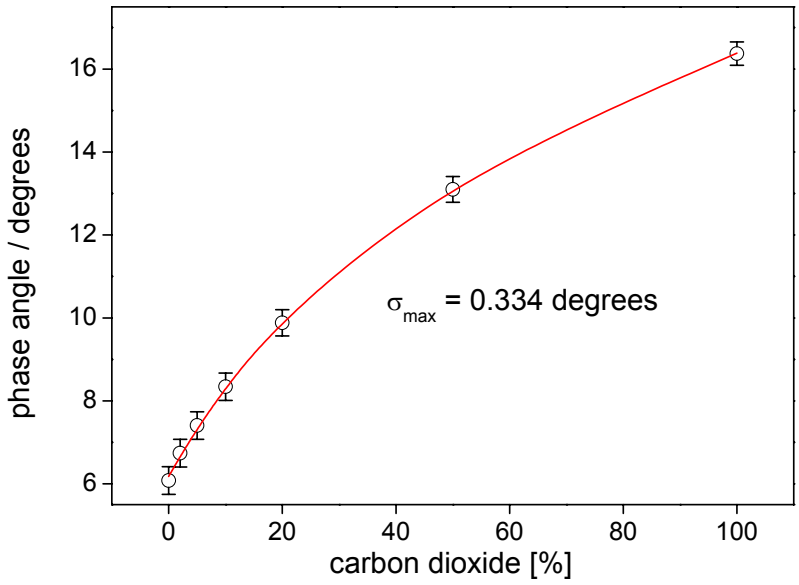

Fig. 5-7 *Good repeatability (n=10) of DLR-based **Bef-1** carbon dioxide sensor membranes made with TEOS-based microparticles (20°C).*

A drawback of sol-gel materials is the structural evolution that they can undergo over time in the case of incomplete hydrolysis. This is particularly evident in high humidity conditions. In order to monitor the temporal stability of the sol-gel reference particles in the sensor, the membranes were stored in moist conditions and scanned approximately once every week. The stabilised membranes were stored and their performance in pre-set calibration cycles was tested for a further 5 weeks (Fig. 5-8).

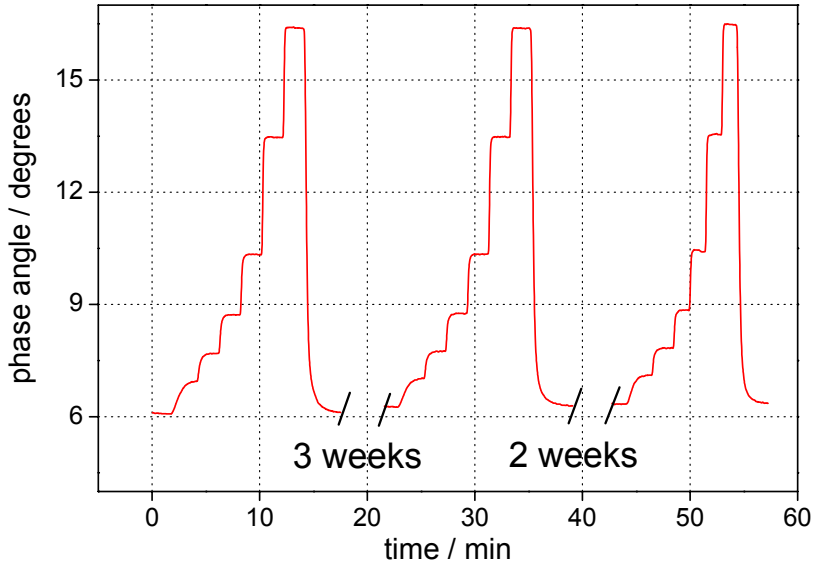

Fig. 5-8 *Phase response of the **Bef-1** sensor membrane to various CO_2 concentrations at fixed temperature (20°C). Note the good repeatability and stability over the time of 5 weeks.*

An important feature of the response is its excellent long-time stability and repeatability over a time of more than 5 weeks. The shelf life of the membranes, if kept in ambient conditions, in the dark, and away from detrimental influences like SO_2 or HCl, is longer than three months, during which a slight drift in sensitivity was observed (< 5%). However, there is no need for the presence of sodium carbonate or similar sinks for volatile acidic compounds in the storage bags, as was reported for previous pCO_2 sensors [2].

5.3.3. Oxygen

As was pointed out before, the main condition for these new TEOS μ-particles is the retaining of very low oxygen cross-sensitivity as provided by the PAN-based PD-1 nanoparticles. Therefore the membrane **Bef-1** was examined using a similar experiment as all other carbon dioxide sensors were tested before. However, the experiment was not conducted using nitrogen and air (21% O_2) as the two different carrier gases as before (Figs. 2-19 & 3-17), but it was nitrogen and pure oxygen this time (Fig. 5-9).

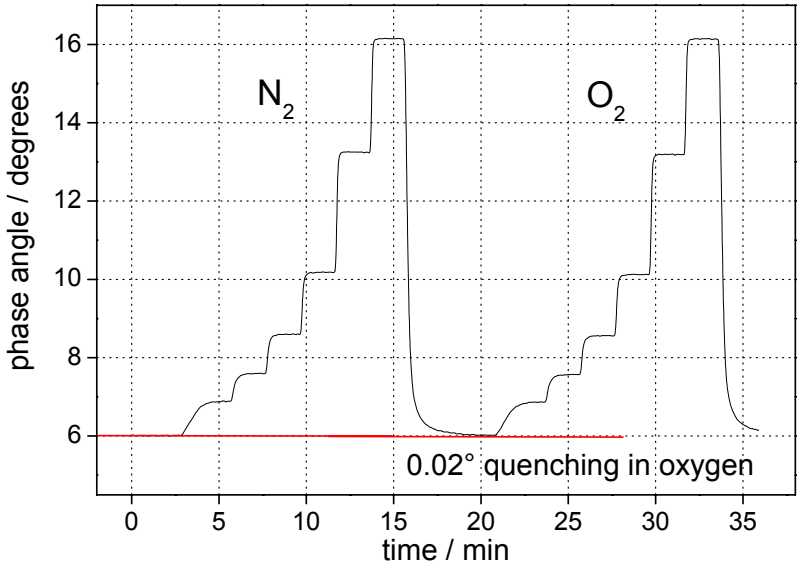

Fig. 5-9 *The phase response of the **Bef-1** DLR-sensor membrane using nitrogen and oxygen (100% O_2) as carrier gases for carbon dioxide experiments (20°C).*

Although the oxygen concentration is a lot higher this time, the cross sensitivity which the **Bef-1** membrane demonstrates, is less than half the percentage shown by the previous sensor in 21% oxygen. In fact, the only visible difference is 0.02 degrees at 100% oxygen, which represents a decrease of only 0.2%. Given the very high susceptibility of $Ru(dpp)_3^{2+}$ to quenching by molecular oxygen, this represents a substantial improvement, and almost completely removes oxygen cross-sensitivity.

The two calibration functions of the sensors based on PD-1 nanoparticles, which were generated by plotting cot ϕ against the CO_2 concentration, were plotted in Fig. 3-18. It was clear that these two curves almost completely overlay each other, and the only visible difference was due to quenching of 0.10 degrees at 21% oxygen. The new **Bef-1** membrane shows an even lower cross-sensitivity to pure oxygen than before, so these two calibration functions would be fully identical, and therefore do not have to be presented again.

5.3.4. Temperature

The solubility of carbon dioxide in liquid and solid materials decreases with increasing temperature. This goes in parallel with a signal decrease caused by the temperature dependence of the equilibrium constants of the bicarbonate system. Moreover, temperature decreases the pK_A-value of the indicator, resulting in a signal decrease as described before [7,9,10]. It was therefore necessary to re-establish how strongly our sensor is influenced by this parameter, so phase calibration curves were recorded between 10ºC and 35ºC in steps of five degrees.

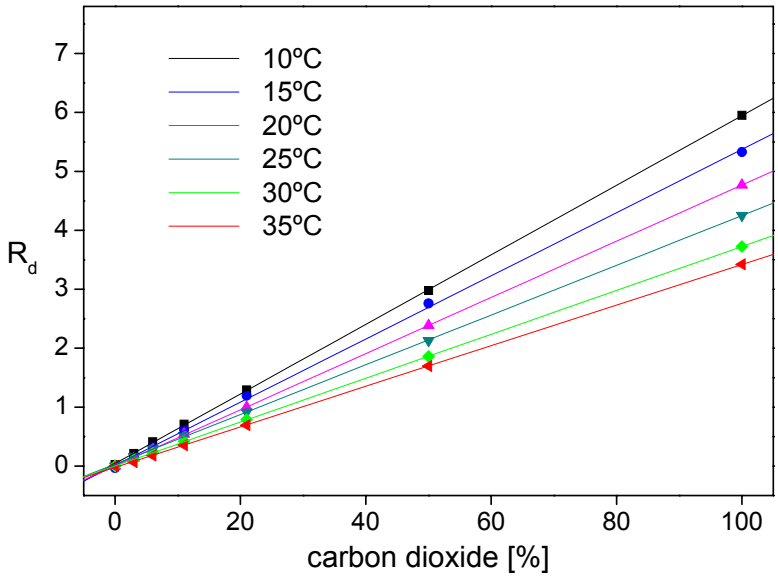

Fig. 5-10 *Calibration plots for the* ***Bef-1*** *DLR sensor using TEOS microparticles doped with* $Ru(dpp)_3^{2+}$ *showing its behaviour over a range of different temperatures between 10ºC and 35ºC in steps of five degrees.*

These data were linearised according to equation 3-14 in order to obtain a set of straight lines, from which the equilibrium constants K of the sensing reaction could be determined (Fig. 5-10). Fig. 5-11 shows the linear correlation between 1/T and ln K (R^2 = 0.99654), and the analysis according to the Arrhenius equation (Eq. 2-11) and following thermodynamics (Eq. 2-12) yielded the activation enthalpy ΔH = -16.2±0.5 kJ mol^{-1} and an entropy term ΔS of -42.4±1.6 J K^{-1} mol^{-1}. Negative values for ΔH indicate that membrane sensitivity is greater at lower temperatures, which is apparent from Fig. 5-10 as well.

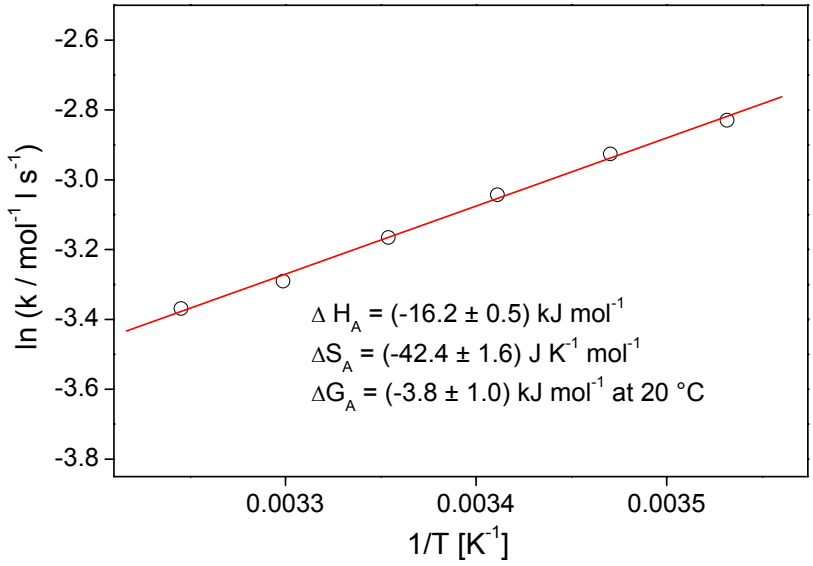

Fig. 5-11 *Arrhenius plot for the **Bef-1** DLR sensor using TEOS microparticles doped with $Ru(dpp)_3^{2+}$ showing the thermodynamic fitting parameters.*

This fact is explained by the higher solubility of carbon dioxide in the matrix at lower temperatures [2]. Both enthalpy and entropy of the **Bef-1** sensor are significantly smaller than in the case of Energy Transfer based sensors (Section 2.4.2), and slightly lower than the sensors based on PD-1 nanoparticles.

5.3.5. Results

The sensor presented exhibits a fast and reversible response to carbon dioxide over a wide range of concentrations. The exhibited phase response between 0 and 100% pCO_2 is slightly lower for this new sensor (10.08 degrees at 20°C), but the dynamic range remained equally high as before. It is sufficiently high to guarantee a resolution of ± 1% up to 50% CO_2 and ± 2% above that level. A conservative estimate for the limit of detection (LOD) was found to be 0.04% CO_2.

The **Bef-1** membrane has a standard deviation of ±0.33 degrees (n = 10) for the phase angle calibration. The sensor shows excellent long-time stability and repeatability over a time of more than 5 weeks, and the shelf-life of the membrane is longer than three months, during which a slight drift in sensitivity can be observed (< 5%).

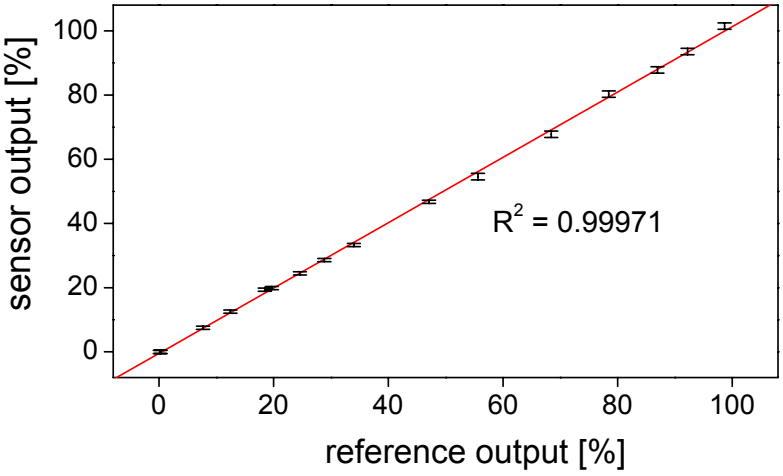

Fig. 5-12 *Comparison of the sensor membrane to a standard infrared absorption-based reference method for carbon dioxide measurement (correlation coefficient R^2 = 0.99971).*

Oxygen cross-sensitivity, which can be introduced by the use of $Ru(dpp)_3^{2+}$ as a long-lifetime reference luminophore, has been minimised by encapsulating the dye in oxygen-impermeable μ-beads made of TEOS. In fact, the only visible difference is 0.02 degrees at 100% oxygen, which represents a decrease of only 0.2%. Given the very high susceptibility of $Ru(dpp)_3^{2+}$ to quenching by molecular oxygen [8], this represents a substantial improvement, and almost completely removes oxygen cross-sensitivity. This sensor showed a slightly lower temperature dependence than the previously described DLR-based sensors.

The performance of the sensor was evaluated in comparison to the infrared absorption spectroscopy standard reference method for carbon dioxide measurement. [11]. A number of randomly set carbon dioxide concentrations was first measured in the optical flow-cell, using the calibration function presented in Fig. 5-7. Then the gas stream was dried using a Nafion® gas dryer tube and it was sampled by the Gascard II IR gas monitor designed and calibrated for carbon dioxide gas analysis. The optical sensor membrane output and the output of the reference method were then plotted against each other, ideally leading to a 45° straight line. A linear regression of the resulting plot, which is presented in Fig. 5-12, yielded a correlation coefficient R^2 = 0.99971, indicating an excellent agreement of the two sensor outputs.

All of the above points support the application of these TEOS based reference particles in carbon dioxide sensors as an on-pack sensor strips in modified atmosphere packaging technology.

5.4. Conclusion

The main problem of pCO_2 sensors based on PAN nano-particles was poor measurement repeatability. These particles usually form agglomerate particle groups around the size of 100 μm. Therefore, a set of sol-gel based micro-particles was investigated in order to improve the chemical setting inside an MTEOS-based membrane. The DLR-sensor using novel TEOS-based reference particles was tested and found to be better in most studies. Although the response is about 10% lower than before, oxygen cross-sensitivity and measurement repeatability are better than presented before. Fig. 5-13 shows a microscopy picture of the surface of the DLR sensor made with TEOS-based μ-particles and clearly shows that these membranes do not show a strong agglomeration as the PAN-particles did before. The removal of this rough and irregular accumulation increased the repeatability of the DLR-based sensors.

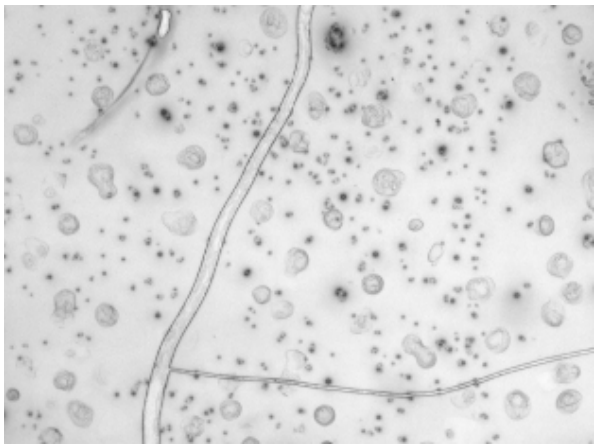

Fig. 5-13 *Surface scan of the **Bef-1** DLR sensor made using TEOS μ-particles*

Therefore, it seems that all the main necessities for a useful lifetime-based carbon dioxide sensor have been obtained, and the development of realistic MAP-sensing optodes can be realised.

5.5. References

1 Liebsch, G.; Klimant, I.; Wolfbeis, O. *Adv. Mat.*, **1999**, *11*, 1292

2 Neurauter, G.; Klimant, I.; Wolfbeis, O. *Anal. Chim. Acta*, **1999**, *382*, 67

3 von Bültzingslöwen, C.; McEvoy, A.; McDonagh, C.; MacCraith, B.; Klimant, I.; Krause, C.; Wolfbeis, O. *Analyst*, **2002**, *127*, 1478

4 http://www.optosense.de/

5 De, G.; Karmakar, B., Ganguli, D., *J. Mater. Chem.*, **2000**, *10*, 2289

6 Chang, Q.; Randers-Eichhorn, L.; Lakowicz, J.; Rao, G. *Biotechnol. Prog.*, **1998**, *14*, 326

7 Mills, A.; Eaton, K. *Quimica Analitica*, **2000**, *19*, 75

8 McDonagh, C.; MacCraith, B.; McEvoy, A. *Anal. Chem.*, **1998**, *70*, 45

9 Kosch, U.; Klimant, I.; Wolfbeis,O. *Fresenius J. Anal. Chem.* **1999**, *364*, 48

10 Mills, A.; Chang, Q.; McMurray, N. *Anal. Chem.*, **1992**, *64*, 1383

11 Smolander, M.; Hurme, E.; Ahvenainen, R. *Trends in Food Sci. and Technol.*, **1997**, *4*, 101

Summary

This thesis reports on the development of new optical sensors (often referred to as *optodes*) for carbon dioxide. The motivation for this work derives from the need for such sensors in modified atmosphere packaging (MAP) of food products. Apart from the performance characteristics (e.g. broad operational range up to 100% CO_2, long-term stability, reversibility), a key requirement was that the developed sensor materials be compatible with existing optical sensing instrumentation for oxygen monitoring. This instrumentation is based on measurement of the fluorescence decay time of immobilised ruthenium phenanthroline complexes via the technique of phase fluorimetry. These complexes have absorption maxima around 450 nm which makes them compatible with blue light emitting diodes (LED's), which can act as low-cost excitation sources. The resultant emission peaks at around 620 nm which also facilitates the use of low-cost photodiode detection. Moreover, the phase fluorimetric approach may be implemented with moderate modulation frequencies (typically in the range 20-100 kHz) which are also compatible with the optoelectronic components used.

Although the oxygen-sensitive ruthenium complexes have properties which are attractive from both spectroscopic and instrumental perspectives, no such optode materials are routinely available for carbon dioxide sensing. The main challenge in this work was the development of such materials. Optodes for CO_2 are generally based on a different analytic approach to that used for oxygen. CO_2 is a weakly acidic gas that change the pH of an immobilised buffer. The acidification of such a buffer resulting from exposure to CO_2 is indicated by the change in the optical properties (absorbance or fluorescence) of a co-immobilised pH indicator. Although this effect in itself could be used for CO_2 sensing purposes, it is not possible via this method to achieve instrumental consistency with the oxygen sensing scheme. For example, most of the luminescent pH-indicator dyes, such as 1-hydroxypyrene-3,6,8-trisulfonate (HPTS) and fluorescein, which have been used in optical CO_2 sensors, have lifetimes which are largely independent of CO_2. In order to overcome this problem, I have investigated and developed two alternative approaches both of which have the desired instrumental compatibility. The first of these employs the Fluorescence Resonance Energy Transfer (FRET) technique, in which a colourimetric

pH indicator and an "inert" ruthenium complex are co-immobilised. In this manner carbon dioxide sensing is achieved by converting pH-dependent colour changes into decay time information. Instead of using the traditional approach of an actual buffer retained inside a gas-permeable membrane, I have employed the hydrated ion-pair concept, which provides the sensing chemistry with the necessary water of crystallisation. This approach offers a number of advantages, including an all-solid sensor material. Chapter 2 details the development of this sensing material.

The second sensing scheme investigated was Dual Luminophore Referencing (DLR). DLR is an internal ratiometric method whereby an analyte-sensitive fluorescence intensity signal is converted into the phase domain by co-immobilising an inert long-lifetime reference luminophore with similar spectral characteristics. The developed DLR-based sensor makes use of the HPTS pH indicator dye and $Ru(dpp)_3^{2+}$ as a referencing dye to create a lifetime-based CO_2 sensor. A key feature here was an encapsulation strategy to remove the oxygen cross-sensitivity of the ruthenium complex. The development of this sensor is detailed in Chapter 3.

A critical element common to the development of both sensor materials was the selection of immobilisation matrix. This matrix has not only to be compatible with the sensing chemistry but must also withstand the conditions present in modern day food packages. The principal material system used in this context is *or*ganically *mo*dified *sil*ica glass (ormosil) as well as polymer hybrids in some cases. The development of these materials is described in Chapter 4.

The last experimental chapter (Chapter 5) refers to the use of microparticles and nanoparticles which are shown to be useful reference particles in optical sensors. These are made from sol-gels and modified sol-gels and have unique properties including narrow particle distribution and high luminescent brightness. Particles of that kind have a large potential, not only in sensor technology, but in micro- and nanotechnology in general, and therefore were characterised in this work with respect to the repeatability of their preparation, temperature effects and quenching by molecular oxygen.

All sensor types developed in this work were tested for the parameters and properties that are of relevance in the context of MAP. These include sensitivity to

humidity, varying temperature, and aging effects (over periods of months in some cases).

In conclusion, it can be said that the two types of optical sensors presented here represent a novel type of sensor for MAP applications, with several advantages over existing sensor types. In particular, the cost of sensor preparation, the ease of depositing the sensor material on flexible packaging materials, and the possibility of reading the signal through an optically transparent package material (usually colourless plastic), are substantial advantages that make the results of this work highly promising. I am confident that further studies (to be performed in the respective industry) will demonstrate the enormous potential of this new method.

Zusammenfassung

In der vorliegenden Arbeit wird die Entwicklung von neuen optischen Sensoren (auch als *Optoden* bezeichnet) für Kohlendioxid beschrieben. Die Motivation für diese Arbeit besteht in der Nachfrage für solche Sensoren in Lebensmittelverpackungen (*modified atmospheric packaging, MAP*). Neben den generellen Sensoreigenschaften (z. B. hinsichtlich einer Einsatzmöglichkeit bis zu einem CO_2-Gehalt von 100%, einem langzeitstabilen Verhalten und der Reversibilität der Messung) war ein Hauptkriterium, dass die zu entwickelnden Sensormaterialien mit einem der bestehenden sensorischen Verfahren für die Sauerstoffbestimmung kompatibel sein mussten. Das Hauptverfahren beruht auf der Messung der Fluoreszenzabklingzeit immobilisierter Ruthenium-phenanthrolin-Komplexe mit Hilfe der Phasenfluorometrie. Diese Komplexe haben ein Absorptionsmaximum bei etwa 450 nm, was sie mit blauen Leuchtdioden, welche als billige Lichtquellen zur Fluoreszenzanregung verwendet werden können, kompatibel macht. Die entstehende Emission hat bei etwa 620 nm ein Maximum, was die Detektion über kostengünstige Photodioden ermöglicht. Darüber hinaus kann bei der phasenfluorometrischen Analyse mit moderaten Frequenzen (typischerweise 20-100 kHz) gearbeitet werden, was das System mit etablierten optoelektronischen Komponenten bzw. Systemen kompatibel macht.

Während mehrere Sauerstoff-empfindliche Ruthenium-Komplexe (bzw. deren Polymerlösungen) bekannt sind, die in Hinblick auf spektroskopische als auch instrumentelle Aspekte zur Sensorik geeignet sind, stehen solche Materialien für Optoden zur Kohlendioxidmessung nicht zur Verfügung. Die Hauptaufgabe in dieser Arbeit war demnach die Entwicklung solcher Materialien. Optoden für CO_2 basieren im Gegensatz zu Sauerstoffsensoren generell auf einem anderen analytischen Ansatz. CO_2 ist ein schwach saures Gas, welches den pH-Wert eines immobilisierten Puffers verändert. Die Protonierung eines solchen Puffers nach CO_2-Exposition wird durch die Veränderung der optischer Eigenschaften (Absorption oder Fluoreszenz) eines co-immobilisierten pH-Indikators angezeigt. Obwohl dieser Effekt bereits für die CO_2-Sensorik verwendet werden könnte, ist es bei dieser Methode nicht möglich, eine instrumentelle Konsistenz mit dem Verfahren zur Sauerstoffsensorik zu erreichen. Zum Beispiel besitzen die meisten der lumineszenten pH-Indikatoren, wie etwa das

1-Hyrdoxypyren-3,6,8-trisulfonat (HTPS) oder das Fluorescein (die bereits in CO_2-Sensoren verwendet wurden), Abklingzeiten, welche in der Hauptsache von CO_2 unabhängig sind. Um dieses Problem zu umgehen, wurden zwei alternative Ansätze untersucht und weiter entwickelt. Beide Verfahren besitzen die gewünschte instrumentelle Kompatibilität. In dem ersten Ansatz wurde die Methode des "Fluorescence Resonance Energy Transfers" (FRET) implementiert, bei welcher ein kolorimetrischer pH-Indikator eingesetzt wird, der seine Energie auf einen gegenüber CO_2 inerten, stark fluoreszierenden Ruthenium-Komplex überträgt, der ebenfalls in der Sensormembran co-immobilisiert vorliegt. Eine CO_2-Sensorik wird dadurch erzielt, dass wegen der pH-induzierten Farbveränderung eine Änderung des Effizienz des FRET und damit eine Änderung der entsprechenden Abklingzeit eintritt. An Stelle des traditionellen Ansatzes über einen Puffer in einer gas-permeablen Membran wurde das Konzept der hydratisierten Ionen-Paare verwendet, welches der in der Sensormembran ablaufenden Chemie das notwendige Kristallwasser zur Verfügung stellt. Dies hat den Vorteil, dass alle verwendeten Sensormaterialien Feststoffe sind. Kapitel 2 erklärt die Entwicklung dieses Sensormaterials im Einzelnen.

Der zweite Ansatz war das sog. "*Dual Luminophore Referencing*" (DLR). DLR ist eine interne ratiometrische Methode, bei der ein auf den Analyten sensitives Fluoreszenzintensitäts-Signal in die Phasenabhängigkeit überführt wird, indem ein inerter langsam abklingender Referenzfarbstoff mit ähnlichen spektralen Eigenschaften co-immobilisiert wird. Bei dem DLR-Sensor wurde HTPS als pH-Indikator-Farbstoff und $Ru(dpp)_3^{2+}$ als Referenzfarbstoff verwendet um einen Lebenszeit-basierten CO_2-Sensor herzustellen. Das Wichtigste dabei war die Abschirmung des Rutheniumfarbstoffes, um eine Beeinflussung der Messung durch eine Löschung durch Sauerstoff zu verhindern. Die Entwicklung dieses Sensors wird in Kapitel 3 beschrieben.

Bei der Entwicklung beider Methoden war die Wahl der geeigneten Matrix zur Immobilisierung der Komponenten ein wichtiges Kriterium. Diese Matrix muss nicht nur chemisch mit der Methode kompatibel sein, sondern muss auch die bei modernen Lebensmittelverpackungen herrschenden Bedingungen überdauern. Das zugrunde liegende Material, welches in diesem Zusammenhang zum Einsatz kam, war ein „*or*ganically *mo*dified *sil*ica glass" (Ormosil), in einigen Fällen auch organische Polymere. Die Entwicklung dieser Materialien wird in Kapitel 4 erläutert.

Das letzte experimentelle Kapitel (Kap. 5) bezieht sich auf die Verwendung von Mikro- und Nanopartikeln, welche sich als nützliche Referenzpartikel in optischen Sensoren erwiesen haben. Sie werden aus Sol-Gelen und modifizierten Sol-Gelen gewonnen und besitzen so einzigartige Eigenschaften (wie z. B. eine kleine Größenverteilung und eine helle Lumineszenz). Partikel dieser Art haben großes Potenzial, nicht nur in der Sensortechnologie, sondern auch ganz allgemein in der Mikro- und Nanotechnologie. Deswegen wurden sie in dieser Arbeit im Hinblick auf die Reproduzierbarkeit ihrer Herstellung, den Einfluss der Temperatur und die Löschung durch molekularen Sauerstoff charakterisiert.

Alle im Zuge dieser Arbeit entwickelten Arten von Sensoren wurden auf die im Zusammenhang mit Lebensmittelverpackungen relevanten Parameter und Eigenschaften hin untersucht. Dies beinhaltet deren Empfindlichkeit gegenüber Feuchtigkeit und verschiedenen Temperaturen, sowie die Untersuchung von Alterungseffekten (in einigen Fällen über Monate hinweg).

Zusammenfassend kann gesagt werden, dass die beiden hier vorgestellten Sensoren, einen neuen Sensortyp für die Anwendung in der Lebensmittelverpackung darstellen und gegenüber bestehenden Sensoren einige Vorteile bieten. Insbesondere die Herstellungskosten und die Möglichkeit, das Sensormaterial einfach auf flexiblen Verpackungen anzubringen und das Signal durch optisch transparente Materialien (normalerweise farblose Kunststofffolien) auslesen zu können, stellen grundsätzliche Vorteile dar, welche die Ergebnisse dieser Arbeit viel versprechend machen. Ich bin überzeugt, dass zukünftige Studien (welche in der entsprechenden industriellen Forschung durchzuführen sind) das enorme Potenzial dieser Methode unterstreichen werden.

Curriculum Vitae

Name: Christoph Alexander Johannes von Bültzingslöwen

Address: 2 Bushfield Square, Philipsburgh Avenue,
Fairview, Dublin 3, Ireland.
Tel: +353-1-8570843
Email: cvb@dcu.ie

Date of birth: 28.04.1970

Place of birth: Simbach am Inn, Germany

Marital status: Single

Nationality: German

Education:

1976-1980	Elementary school in Regensburg, Germany
1980-1990	Grammar school in Regensburg; leaving certificate (Abitur)
1990-1993	Educational travels in Asia, South America and Australia
1993-1999	Study of chemistry at the University of Regensburg
1996-1997	M.Sc. course in Materials Chemistry at the University of Kent Thesis: *A new gas dosimeter for ozone*
Since 1999	Ph.D. studies at Dublin City University Thesis: *Development of Optical Sensors ("Optodes") for Carbon Dioxide and their Application to Modified Atmosphere Packaging (MAP).*

Work Experience:

1987-1996	Part-time jobs in construction and restaurant businesses
1991-1993	Military service at long range reconnaissance patrol unit in Weingarten and Regensburg, Germany
1997	Research student at PiezOptic Ltd., Ashford, UK (5 months)
1998	Research study for Eppendorf, Hamburg, Germany (2 months)
Since 1999	Research assistant at the National Centre for Sensor Research (4 years)

Special skills:

Languages:	Fluent German and English; basic Spanish and French
Software:	LabView, TurboPascal, MSOffice, Origin, Maple

Hobbies and Interests:

Since 1980	Mountaineering, hiking, skiing and free climbing
1985-1999	Voluntary service in German Red Cross (mountain rescue)
Since 1987	Shotokan Karate (2nd Dan)

Dublin, 01/04/2003

Publications and Presentations

M.Sc. and Diploma Thesis

A new Gas Dosimeter for Ozone, University of Kent at Canterbury and University of Regensburg (1997)

Publications

John Wright, Christoph von Bültzingslöwen, Timothy Carter, Florence Colin, Paul Shepherd, Jennifer Oliver, Simon Holder, Roeland Nolte, **Optical transduction of chemical sensing by thin films of colour reagents and molecular receptors using piezo-optical and surface plasmon resonance methods**, *J. Mater. Chem.*, **2000**, *10*, 175

Aisling McEvoy, Christoph von Bültzingslöwen, Brian MacCraith, Colette McDonagh, Ingo Klimant, Otto Wolfbeis, **Optical sensors for application in intelligent food packaging technology**, *Proc. SPIE,* **2002**, *4876*

Christoph von Bültzingslöwen, Aisling McEvoy, Colette McDonagh, Brian MacCraith, Ingo Klimant, Christian Krause, Otto Wolfbeis, **Sol-gel based optical carbon dioxide sensor employing dual luminophore referencing for application in food packaging technology**, *Analyst*, **2002**, *127*, 1478

Christoph von Bültzingslöwen, Aisling McEvoy, Colette McDonagh, Brian MacCraith, **Lifetime-based optical sensor for wide range pCO_2 detection employing fluorescence resonance energy transfer**, *Anal. Chim. Acta*, **2003**, *480*, 275

Séverine Aubonnet, Henry F. Barry, Christoph von Bültzingslöwen, Jean-Marc Sabattié, Brian MacCraith, **Photo-patternable optical chemical sensors based on hybrid sol-gel materials**, Submitted to *Electronics Letters*.

Oral Presentations

Christoph von Bültzingslöwen, Timothy Carter, Florence Colin, Ceri Gibson, Paul Shepherd, **Piezo-Optical Occupational and Environmental Monitoring - A New Way of Using Colourimetric Reagents**, *4th International Symposium on Functional Dyes*, Osaka, Japan (1999)

Brian MacCraith, Christoph von Bültzingslöwen, Aisling McEvoy, Colette McDonagh, Lubos Polerecky, **Sol-Gel Waveguide Fluorescence Sensors for Food Packaging**, *PITTCON 2000*, New Orleans, USA (2000)

Christoph von Bültzingslöwen, Aisling McEvoy, Brian MacCraith, Colette McDonagh, **Optical carbon dioxide sensing for Modified Atmosphere Packaged (MAP) food**, *Europt(r)ode V*, Lyon, France (2000)

Severine Aubonnet, Brian MacCraith, Henry Barry, Christoph von Bültzingslöwen, **UV-patternable Sol-Gel Material for Chemical Sensor Applications**, *4th UK - Ireland Sol-Gel Group Meeting* , Nottingham, England (2000)

Brian MacCraith, Christoph von Bültzingslöwen, Aisling McEvoy, Colette McDonagh, Lubos Polerecky, **Sol-Gel Waveguide Fluorescence Sensors for Food Packaging**, *Photonics East*, Boston, USA (2000)

Christoph von Bültzingslöwen, Aisling McEvoy, Brian MacCraith, Colette McDonagh, Ingo Klimant, Otto Wolfbeis, **DLR-based Optical Carbon Dioxide Sensor for Application in Food Packaging Technology**, *Europt(r)ode VI*, Manchester, England (2002)

Aisling McEvoy, Christoph von Bültzingslöwen, Brian MacCraith, Colette McDonagh, Ingo Klimant, Otto Wolfbeis, **Optical sensors for application in intelligent food packaging technology**, SPIE Opto Ireland conference, Galway, Ireland (2002)

Aisling McEvoy, Christoph von Bültzingslöwen, Brian MacCraith, Colette McDonagh, Ingo Klimant, Otto Wolfbeis, **Intelligent food packaging technology,** Remote Autonomous Monitoring Systems (RAMS) II workshop, Dublin, Ireland (2002)

Poster Presentations

Chris Malins, Christoph von Bültzingslöwen, Brian MacCraith, **Ion-pair approach for fluorescence-based carbon dioxide detection in an Ormosil glass**, *3rd UK - Ireland Sol-Gel Group Meeting* , Loughborough, England (1999)

Christoph von Bültzingslöwen, Aisling McEvoy, Brian MacCraith Colette McDonagh, **ORMOSIL-based Optical Sensor for Carbon Dioxide employing Fluorescence Resonance Energy Transfer (FRET)**, *4th UK - Ireland Sol-Gel Group Meeting*, Nottingham, England (2000)

Christoph von Bültzingslöwen, Aisling McEvoy, Colette McDonagh, Brian MacCraith, **Sol-Gel-based Optical Carbon Dioxide Sensing for Modified Atmosphere Packaged Food (MAP) Application**, *XI International Workshop on Glasses, Ceramics, Hybrids and Nanocomposites from Gels*, Padova, Italy (2001)

Brian MacCraith, Severine Aubonnet, Henry Barry, Christoph von Bültzingslöwen, Jean-Marc Sabattié, Conor Burke, **Optical Chemical Sensor Systems based on Photosensitive Hybrid Sol-Gel Glass**, *XI International Workshop on Glasses, Ceramics, Hybrids and Nanocomposites from Gels*, Padova, Italy (2001)